ABSTRACT

Title of Dissertation:	CHANGES OF CLIMATE ZONES AND THEIR IMPLICATIONS FOR BIODIVERSITY
	Diyang Cui, Doctor of Philosophy, 2022
Dissertation directed by:	Dr. Dongdong Wang, Associate Professor, Department of Geographical Sciences

Climate change is driving biodiversity redistribution on Earth, undermining the effectiveness of protected areas (PAs) in conserving global biodiversity. Managing the consequences of biodiversity redistribution and promoting effective conservation necessitates a better understanding of climate shift patterns and species' ability to track changing climate. Recent studies assessing the effects of climate change on biodiversity have increasingly used velocity metrics to represent climate shifts over space and time. Velocity based on a single climate variable or climate space identified using statistically combined multivariate indices may not be related to biomes or ecosystems and lacks potential to conduct risk evaluation for biodiversity. The widely used Köppen–Geiger classification scheme provides an effective way to characterize bioclimatic conditions by incorporating multiple climatic indicators and biological information, thus can be a new direction for developing velocity metrics and supporting the development of species distribution models (SDMs). To identify research gaps, this dissertation research first reviews recent detection and assessment studies on past and future projected climate zone changes. Previous studies have shown that accelerated global warming since the 1980s has resulted in changes in climate zones that have been observed over 5% of the global land area. Tropical and arid climate zones are expected to expand into mid and high latitudes, while polar climates are shifting poleward and upward, leading to significant area shrinkage. Given the need for improved historical and future global climate maps with long-term temporal coverage and

accurate depiction of fine-grained bioclimatic conditions in climate change studies, the study creates a set of 1 km Köppen-Geiger climate classification maps (KGClim) for six historical periods in 1979–2013 and four future periods in 2020–2099 under RCP2.6, 4.5, 6.0, and 8.5. The new maps offer higher classification accuracy than existing datasets and demonstrate the ability to capture recent and future projected changes in distribution of climate zones. Using the new KGClim dataset, this dissertation calculates the velocity of climate zone shifts to assess exposure risks of global PAs and examines the spatial patterns of near-, mid- and long-term climate shifts projected based on different emission pathways. Based on the findings, under RCP8.5, 38% of global protected land could undergo climate zone shifts at accelerating rates for the remainder of this century. Furthermore, global protected lands are experiencing novel (8% of global protected land) and disappearing (7%) climates, shifts of climates outside current PA networks (8%), and transition to human dominated land use (6%). The fine-scale velocity metrics reveal spatiotemporal patterns of climate shifts and biodiversity redistribution, which can inform adaptive conservation planning to address the ongoing biodiversity crisis and achieve future conservation goals.

CHANGES OF CLIMATE ZONES AND THEIR IMPLICATIONS FOR BIODIVERSITY

by

Diyang Cui

Dissertation submitted to the Faculty of the Graduate School of the
University of Maryland, College Park, in partial fulfillment
of the requirements for the degree of
Doctor of Philosophy
2022

Dissertation Advisory Committee
Dr. Dongdong Wang, Chair
Dr. Shunlin Liang
Dr. George Hurtt
Dr. Tatiana V. Loboda
Dr. Zhiliang Zhu
Dr. Joseph H. Sullivan

Dedication

To my beloved parents,

Zhu Peng and Sheng Cui

and my grandparents

for their unconditional love and support along the journey

To the memory of my grandma,

Tianxiu Zhu

Acknowledgements

First, I would like to express my deep gratitude to my advisors, Prof. Shunlin Liang, and Prof. Dongdong Wang, for their advice, guidance, and mentorship over the years. Thanks for providing me constructive feedback and continuous support in both my study and life. I could not have undertaken this journey without your help.

I would also like to thank my committee members, Prof. George Hurtt, Prof. Tatiana Loboda, Dr. Zhiliang Zhu, Prof. Joseph Sullivan, who have generously provided valuable insights and expertise to improve this dissertation from a variety of perspectives. Thanks for my funding support from the School of Public Policy, Center for Global Sustainability and the project leader, Dr. Ryna Cui.

I am also grateful to my colleagues and friends, Aolin Jia, Dr. Yao Li, Jiaming Lu, Xueyuan Gao, Shuo Xu, Ruohan Li, Jiena He, Dr. Yuan Zhou, Dr. Yuhan Rao, Xiuxia Li, Guimin Zhu, Yunting Song, and many others, who helped me a lot and made this journey so joyful and memorable.

Lastly, I would like to thank my parents, Zhu Peng and Sheng Cui, and my grandparents, Xiuying An and Junsheng Peng. Their endless love has always been the largest source of encouragement and motivations for me during my PhD years. I would also like to express my thanks to my boyfriend, Liu Zheng, for all his love and care for me. Thank you for being part of my life. And many thanks to our adorable cats, Wuhua and Rou, for bringing so much joy and emotional support during the pandemic. I am truly grateful to have so many wonderful people and memories in my life.

Table of Contents

List of Figures

List of Tables

List of Abbreviations

Atmosphere-Ocean General Circulation Models (AOGCMs)

Convention on Biological Diversity (CBD)

Program on Climate Change, Agriculture and Food Security (CCAFS)

Climatologies at High resolution for the earth's Land Surface Areas (CHELSA)

Climate Hazards Center's Precipitation Climatology (CHPclim)

Coupled Model Intercomparison Project Phase 5 (CMIP5)

Climatic Research Unit (CRU)

Global Forest Resources Assessment (FRA)

Food and Agriculture Organization (FAO)

Global Climate Model (GCM)

Global Summary of the Day (GSOD)

Global Historical Climatology Network (GHCN)

Global Mean Surface Temperature (GMST)

Global Precipitation Climatology Centre (GPCC)

Intergovernmental Panel on Climate Change (IPCC)

Köppen Climate Classification (KCC)

Köppen-Geiger Classification (KGC)

Köppen-Trewartha Classification (KTC)

Land-Use Harmonization2 (LUH2)

Mean Annual Precipitation (MAP)

Mean Annual Temperature (MAT)

Protected Areas (PAs)

PRECipitation REConstruction over Land (PREC/L)

Representative Concentration Pathway (RCP)

Surface Air Temperature (SAT)

Species Distribution Modeling (SDM)

Special Report on Emissions Scenario (SRES)

Shuttle Radar Topography Mission (SRTM)

World Database on Protected Area (WDPA)

World Wildlife Federation (WWF)

Chapter 1: Introduction

1.1 Background and motivations

1.1.1 Climate-driven redistribution of Earth's species

Driven by anthropogenic climate change, distribution of species on the Earth are changing at accelerating rates, with far-reaching impacts on ecosystem functioning and human well-being (I.-C. Chen et al., 2011; Parmesan & Yohe, 2003; Pecl et al., 2017). Climate, as a key driver of the ecological interactions and biological processes, shape global patterns of biomes and biodiversity (Kreft & Jetz, 2007; Woodward et al., 2004). In response to current climate change, species are undergoing evolutionary adaptation (Merilä & Hendry, 2014; Parmesan, 2006), changing phenology and abundance (Parmesan & Yohe, 2003; Scheffers et al., 2016), and shifting their distribution to track changing climates (I.-C. Chen et al., 2011). Changes in availability and positions of climatically suitable areas have resulted in many latitudinal and elevational shifts in species distribution (Garcia et al., 2014; Scheffers et al., 2016). Consequently, the climate-driven redistribution of Earth's species has led to restructured biotic community compositions (Williams & Jackson, 2007), loss of ecosystem services, and increased threats to human welfare across the globe (Kreft & Jetz, 2007; Pecl et al., 2017). However, consideration of these climate-driven changes in biodiversity is critical yet lacking in most conservation strategies (Dobrowski et al., 2021; Pecl et al., 2017; Watson et al., 2013). Strategic and adaptive conservation planning that explicitly incorporates climate change impacts on biodiversity is critical to addressing the ongoing biodiversity crisis and achieving future conservation goals.

1.1.2 Undermined effectiveness of protected areas (PA) under climate change

Protected areas (PAs) are widely recognized as a core of modern biodiversity conservation strategies (Arafeh-Dalmau et al., 2021; Dobrowski et al., 2021) and have demonstrated their importance in protecting the earth's biodiversity by reducing rates of habitat loss (Geldmann et al., 2013) and enhancing species diversity within their boundaries (Gray et al., 2016). PAs also provide a variety of social and economic benefits by preserving natural resources, delivering ecosystem services, and supporting human livelihoods (J. E. M. Watson et al., 2014). Expanding global PA coverage while maintaining the effectiveness of the PA networks are key conservation targets agreed upon in the Convention on Biological Diversity post-2020 framework (CBD) (OECD, 2019; Visconti et al., 2019). However, changes in climate and land use greatly undermine the effectiveness of current PA networks (Arafeh-Dalmau et al., 2021; Batllori et al., 2017; Elsen et al., 2020; Hoffmann et al., 2019). As climate shifts, suitable climates for species may become less accessible and species may track their preferred climatic conditions and migrate into unprotected and human-dominated areas (Batllori et al., 2017; Hoffmann et al., 2019; Wessely et al., 2017). Current static boundaries, low connectivity of PAs (Asamoah et al., 2021; Batllori et al., 2017; Lawler et al., 2015), biased PA locations towards areas of low human influence(Joppa & Pfaff, 2009; Venter et al., 2018), and close alignment with existing biodiversity patterns with inadequate consideration of future changes (Lawler et al., 2015; Loucks et al., 2008; Myers et al., 2000), could further diminish the capacity of PA networks in protecting future biodiversity, thereby impeding the achievement of global conservation goals. Conservation planners must incorporate climate shifts and biodiversity redistribution into PA conservation planning to improve the effectiveness of global PAs and develop more strategic and

adaptive PA conservation approaches (Dobrowski et al., 2021; Pecl et al., 2017; J. E. M. Watson et al., 2013).

1.1.3 Assessments of biodiversity exposure to climate change using climate change metrics

Managing the consequences of biodiversity redistribution and promoting effective conservation requires better understanding of patterns of climate shifts and capacity of species to track the shifting climate (Garcia et al., 2014; Lenoir et al., 2020). Most assessments of the impact of climate change on biodiversity have largely relied on simple climatic indicators, with some commonly used measures such as change magnitude of climate variables (Giorgi, 2006), extreme values (Beaumont et al., 2011; Jiménez et al., 2011), and timing shifts of climatic events (Burrows et al., 2011). These univariate metrics depict local temporal change in climates. Recent studies assessing exposure risks of biodiversity increasingly used metrics of climate change to represent spatiotemporal shifts of climates (Garcia et al., 2014), such as climate velocity (Brito-Morales et al., 2018; Loarie et al., 2009), climate analogs (Ordonez & Williams, 2013; Williams & Jackson, 2007), climate stability (Watson et al., 2013), novel and disappearing climates (Garcia et al., 2014; Hoffmann et al., 2019; Williams et al., 2007). These metrics are based on either one climate variable or climate space identified using statistically combined multivariate indices, and may not be related to properties and functions of biomes or ecosystems and lack potential to conduct risk assessments for biodiversity (Brito-Morales et al., 2018; Cui et al., 2021).

1.1.4 Köppen-Geiger climate classification and climate zone shifts

To examine shifts in climate zones and potential changes in biomes, researchers applied the Köppen-Geiger climate classification scheme (Chan & Wu, 2015; Mahlstein et al., 2013; Rubel & Kottek, 2010). Climate has direct impacts on the processes and functioning of the ecosystem as well as on the distribution of species. (I.-C. Chen et al., 2011; Ordonez & Williams, 2013; Pinsky et al., 2013; Thuiller et al., 2005). The spatial patterns of climates have been often identified using the Köppen climate classification system. Köppen-Geiger classification (KGC), the most widely used bioclimatic classification scheme in biology, earth, and environmental sciences (Rubel & Kottek, 2011), was first introduced by Wladimir Köppen to map the world's biomes based on the amplitude and seasonal phase of annual cycles of surface air temperature and precipitation (Köppen, 1936). KGC classifies five major climate classes and 30 subtypes globally and shows strong correlations with biome distribution (Cui, Liang, & Wang, 2021; Rohli, Joyner, et al., 2015). It has been used in a variety of climate change studies, including assessments of climate change impacts on ecosystem (Roderfeld et al., 2008), biome distribution (Leemans et al., 1996; Rohli, Joyner, et al., 2015) and biodiversity (Garcia et al., 2014). KGC adds a new direction to the development of climate change metrics by providing an ecologically relevant and effective method for characterizing climate conditions, and it can support the development of species distribution modeling (SDM).

The increased availability of globally gridded datasets of climatic variables allowed for the generation of maps for the global distribution of Köppen climate zones. To fulfill the current needs of climate change research, there is an urgent need for improved historical and future global maps of the Köppen climate classification with long-term temporal coverage and more accurate depiction of fine-grained climatic conditions. Most previously published Köppen

climate classification maps have a relatively low resolution of 0.5° (Belda et al., 2014; Grieser et al., 2006; Kottek et al., 2006; Kriticos et al., 2012; Rubel & Kottek, 2010). Several map products used interpolation methods to achieve a higher resolution of ~0.1° (Kriticos et al., 2012; Peel et al., 2007; Rubel et al., 2017). Fine resolutions of at least 1-km are required to detect climate refugia and promote effective conservation. Another existing issue with future climate maps was the large discrepancy in GCMs, with possible uncertainty sources in model resolution, biases, deficiencies in model physics, and reference data selection (Hanf et al., 2012; Tapiador et al., 2019; Zhang & Yan, 2014). Systematic methods for assessing uncertainty and optimizing the model performance for future climate zone distribution projections are required.

Significant shifts in Koppen climate zone boundaries have been observed and projected in the recent two centuries (Belda et al., 2014; Chan & Wu, 2015; D. Chen & Chen, 2013; Rohli, Andrew, et al., 2015; Yoo & Rohli, 2016). Studies have shown that under climate change, Köppen-Geiger climate zones are shifting poleward and upward into warmer and drier climates, with significant area expansion in tropical (A) and arid (B) climate zones and area shrinkage of polar (E) climates (Chan & Wu, 2015; Cui, Liang, & Wang, 2021; Mahlstein et al., 2013; Rohli, Andrew, et al., 2015). However, large discrepancies and different levels of details in patterns of climate zone shifts exist in previous studies. It is unclear whether significant climate zone changes can be detected in climate observations, and if so, at what rate and time. Furthermore, while model simulations are increasingly being used to investigate the future climate shifts, the uncertainties in the projected climate zone changes remain largely unknown.

1.2 Research questions and dissertation structure

The overarching question of the dissertation is what impacts that climate zone changes have on biodiversity and what can be informed for biodiversity conservation? This dissertation sets out to answer four research questions:

1) How the global climate zones are changing over time and space, driven by past and future projected climate change, in terms of area changes, latitudinal and elevational shifts?

2) How can we improve the global climate classification data at 1-km for historical (1979-2013) and future periods (2020-2100), with the use of data integration, bias correction and data downscaling based on observational climatology datasets and model projections?

3) How climate zone shifts, stratified by velocity and displacement patterns, can imply for biodiversity, and affect conservation capacity of global PAs, and how can it benefit from fine spatial and temporal scales and considerations of topographic paths?

This dissertation presents five chapters. Chapter 1 introduces the background and motivation of the research, as well as the research questions and dissertation structure.

Chapter 2 provides a review of the literature on recent and future changes in global climate zones. This chapter begins by discussing the development and applications of the Köppen classification system as well as its association with the global biome distribution and other climate classification schemes. A summary of all available map products of the Köppen climate classification is provided with future product development directions. The results of a large body of literature on the detection and assessment of climate zone changes are then synthesized in this chapter. To identify knowledge gaps and guide future research, consolidated summaries of recent

studies are performed for both observed and projected climate zone changes. Chapter 2 has been published in Wiley Interdisciplinary Reviews: Climate Change (Cui, Liang, & Wang, 2021).

Chapter 3 presents a 1-km global dataset of Köppen–Geiger climate classification maps of historical (1979-2013) and future (2020-2100) periods for different emission scenarios (RCP2.6, RCP4.5, RCP6.0 and RCP8.5), based on multiple downscaled observational datasets, and an ensemble of bias-corrected downscaled CMIP5 model projections. This chapter describes in detail the methods used for statistical downscaling, data integration, and validation, and demonstrates the new climate classification maps' improved classification accuracy, good correspondence with topographic features and vegetation distribution. This chapter also provides an example of how the new dataset can be used to detect long-term global area changes in climate zones. Chapter 3 has been published in Earth System Science Data (Cui, Liang, Wang, et al., 2021).

Chapter 4 examines the spatiotemporal patterns of climate zone shifts in the global terrestrial PAs by calculating fine-scale (1-km) climate zone velocity for four future periods (2020-2049, 2040-2069, 2060-2089, 2070-2099) using four RCPs (RCP2.6, RCP4.5, RCP6.0 and RCP8.5) with a baseline period of 1971-2000. The climate classification data used in Chapter 4 is from the dataset generated in Chapter 3. Furthermore, this chapter assesses exposure risks of global PAs and the spatial patterns of near, mid, and long-term future climate zone shifts. By presenting a case study applying the climate zone velocity for spatial PA prioritization, this chapter investigates the potential of climate zone velocity to inform biodiversity conservation.

Chapter 5 concludes with a summary of the major findings from all chapters and explores potential directions for future research.

Chapter 2: Observed and projected changes in global climate zones

2.1 Abstract

In recent years, there has been a growing body of literature applying the Köppen classification scheme to investigate the changes in the distribution of bioclimatic conditions. Area changes and latitude and elevation shifts of Köppen climate zones have been examined based on the observed and projected datasets. This review article provides a comprehensive insight into the changes in global Köppen climate zones. First, we summarize the advancements and limitations of different climate zone definitions and assess the available climate classification map products. We then review recent detection and assessment studies on observed and projected climate zone changes. Finally, we summarize the findings of the previous studies. It has been proven that changes in climate zones under global warming can have far-reaching impacts on ecological systems. Since the 1980s, anthropogenic accelerated global warming has already led to shifts in climatic conditions over a large land area. Hot tropics and arid climates are projected to expand into large areas of middle and high latitudes, an expansion that is potentially linked to the intensification of the global hydrologic cycle. Driven by increased warming in the Arctic, high-latitude climates will shift poleward and upward, leading to a significant area shrinkage of the polar climate zones. However, due to the large model uncertainties, the detectability of significant climate zone changes through observations and projections, the rate and time of the changes, and their causes remain unclear. In this paper, we identify the research gaps and propose directions for future research.

2.2 Introduction

Human activities have caused significant and far-reaching changes in the world's climate systems. For example, an increase in the global mean surface temperature (GMST) has resulted in more intense and frequent heavy precipitation events (IPCC, 2018). The warming signal is not homogeneously distributed. Greater warming beyond the global average is being experienced in some land areas and seasons, including the Arctic and boreal zones during winter (IPCC, 2018). Water cycle intensification is also expected, suggesting a larger contrast between wet and dry regions (Hartmann et al., 2013). As a result of the global climate change with unequal spatial and seasonal patterns, large portions of the Earth's surface are expected to experience changes in the average climatic conditions.

Climate has a direct impact on the world's ecosystems and the distribution of various plant and animal species. The rearrangement of the current distribution of plants and animals can lead to serious and irreversible impacts on ecological systems, posing a severe threat to biodiversity. As a result, there is an increasing need to quantify the impacts of climate change on the Earth's terrestrial ecosystems. Most research has focused more on identifying local changes and less on the spatial shifts in the distribution of climatic conditions at broader spatial extents. To represent the spatial shifts in climatic conditions and highlight the linkages between climate and ecological systems, some recent studies applied Köppen classification schemes to estimate the magnitude of the observed and projected shifts between different climate classes.

The Köppen climate classification demonstrates a good correlation with major biome distribution and can incorporate the amplitude and seasonal phase of temperature and precipitation annual cycles. Moreover, the Köppen classification scheme has proved to be a useful tool for detecting

the first-order bioclimatic influence of the past (Belda et al., 2014; Chan & Wu, 2015; D. Chen & Chen, 2013; Rohli, Andrew, et al., 2015) or future projections of climate change based on climate model simulations under diverse emission scenarios (Belda et al., 2016; Hanf et al., 2012; Mahlstein et al., 2013).

Significant changes in major Köppen climate zones have been observed in the 20th century and projected for the 21st century. However, large discrepancies and different levels of details in terms of the description of climate shifts exist in previous studies. It remains unclear whether significant climate zone changes are detectable in observations, and at what rate and time that these changes take place. Moreover, while model simulations are increasingly used to investigate the future climate shifts, the uncertainties in the projected climate zone changes remain largely unknown. In addition, it is not clear whether the changes can be attributed to external anthropogenic forcing components or natural variations, or how the changes in temperature and precipitation are associated with the changes in climate zone distribution.

To offer a comprehensive insight into the changes in global climate zones, this chapter first examines the climate zone definitions by discussing the development and applications of the Köppen classification system as well as its association with the global biome distribution and other climate classification schemes. A summary of all available map products of the Köppen climate classification is provided with a suggested direction for future product development. Then this chapter synthesizes the results from a large body of literature on the detection, and assessment of climate zone changes. Consolidated summaries of recent studies are performed for both observed and projected climate zone changes to identify the knowledge gaps and guide future research. Finally, this chapter concludes with a summary and future research scope.

2.3 Definitions of climate zones

Climate, defined as a comprehensive statistical description of climatic conditions over a sufficiently long period at a wide range of temporal scales (D. Chen & Chen, 2013), is one of the most critical determinants of Earth's ecosystems (Zhou & Wang, 2000). As a source of water and energy, climate acts as the primary control for ecosystem distribution (James, 1966). Controlled by the dominant climatic conditions and prevailing vegetation formations, major ecosystems are distributed on land in a predictable pattern. Major ecosystem regions are largely defined based on the climate zones following the Köppen climate classification system (Köppen, 1931). This land climate classification delineates the climate-controlled ecosystem regions of the world by integrating and arranging ecological climatic information on land units. It is a highly effective means to simplify spatial variability and aggregate climate gradients into simple but ecologically meaningful classes (H. E. Beck et al., 2018).

(a)
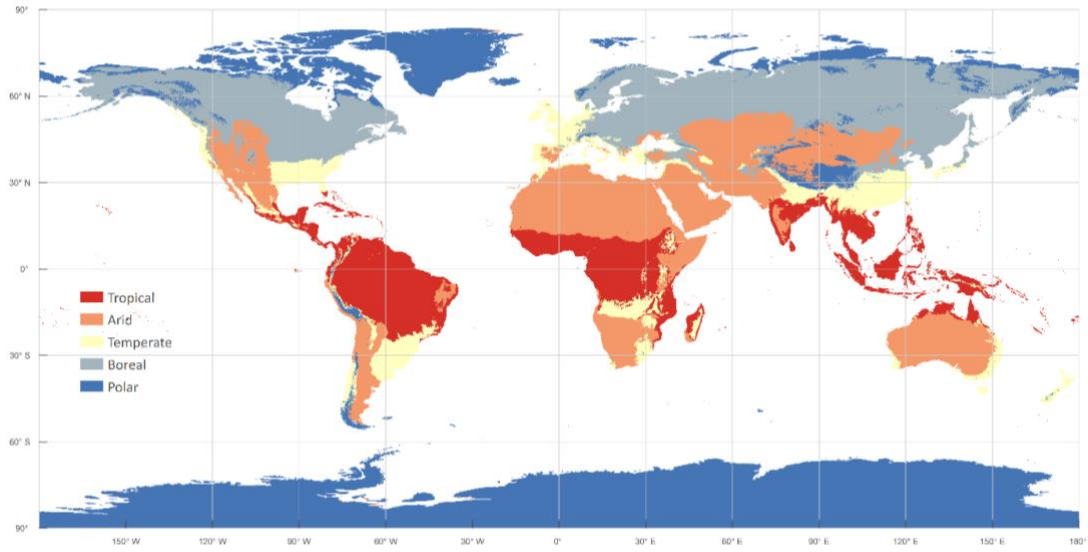
(b)
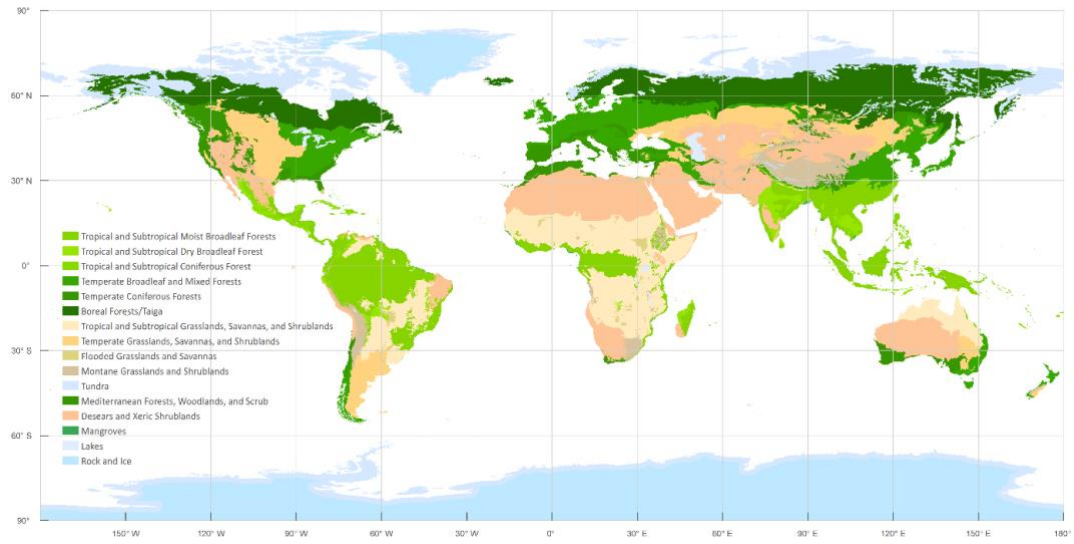
(c)
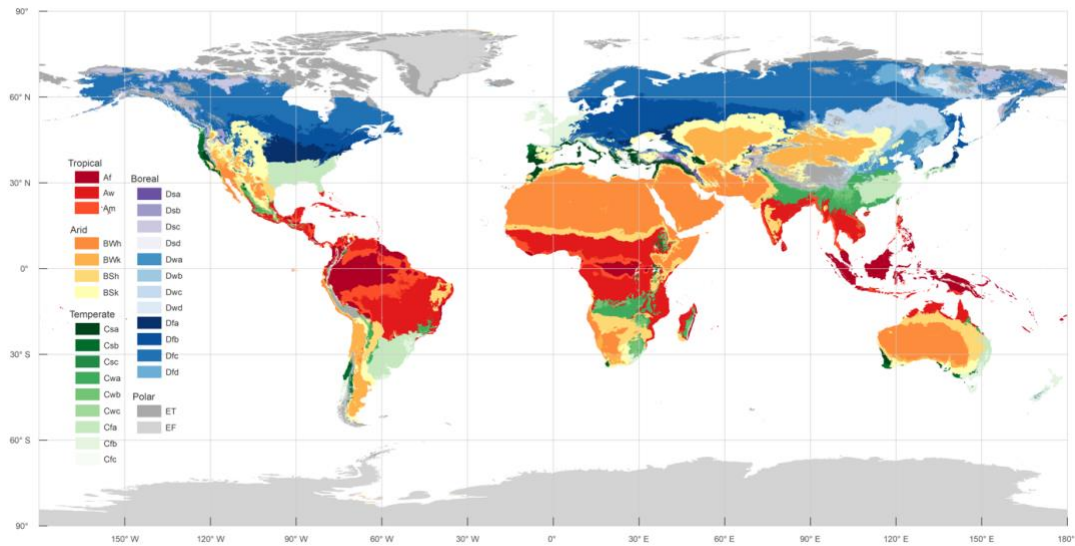
(d)
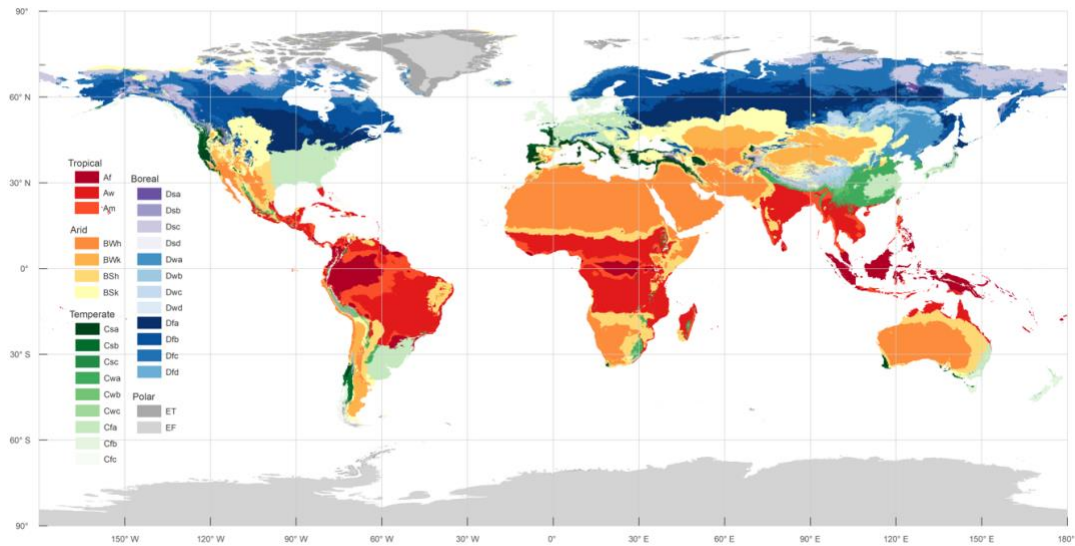
Figure 2-1 Present-day and future global distribution of climate zones and biomes. Global distribution of (a) major climate zones based on data from present day (1980–2016) Köppen-Geiger climate classification map (Beck et al., 2018), and (b) biomes with data from Terrestrial Ecoregions of the World (TEOW) (Olson et al., 2001). (c) and (d) present-day (1980-2016) and future (2071-2100) climate subtypes based on data from (Beck et al., 2018).

The Köppen classification is based on the annual cycle of monthly air temperature and

precipitation data, aiming to empirically map the world's biome distribution (Köppen, 1936).

13

The global distribution of climate zones and biomes are shown in Figure 2-1. With few exceptions, the classifications largely correspond to the distribution of zonal vegetation (Belda et al., 2014; Köppen, 1936; Trewartha, 1954) as well as soil type (Bockheim et al., 2005). As an integrated and convenient tool to unveil the spatial patterns of climatic variables and identify the relationships between climate and the Earth's physical and biological systems, the Köppen classification has been widely applied in biological sciences, earth and planetary sciences, and environmental sciences (Rubel & Kottek, 2011). It has been used in the evaluation of precipitation (Kim et al., 2017; Miró et al., 2017; Serra et al., 2014; Sharifi et al., 2018; Tang & Hossain, 2012; Wen et al., 2017) and temperature products (Peña-Angulo et al., 2016), the validation of climate models (Elguindi et al., 2014; Gnanadesikan & Stouffer, 2006; Kleidon et al., 2000; Lohmann et al., 1993), the assessment of climate change impacts (Bacon et al., 2014; A. Berg et al., 2013; Webber et al., 2011), and the analysis of simulated future climate change (Belda et al., 2016; T. Chen et al., 2017; Feng et al., 2014; Hanf et al., 2012; Mahlstein et al., 2013; Rohli, Andrew, et al., 2015; Rubel & Kottek, 2010; Tapiador et al., 2019).

The Köppen classification has been found useful for a variety of problems associated with climate change, such as in hydrological cycle studies (Manabe & Holloway, 1975; Peel et al., 2001), arctic climate change (Feng et al., 2012; Wang & Overland, 2004), assessment of climate change impacts on ecosystems (Roderfeld et al., 2008), biome distribution (Leemans et al., 1996; Rohli, Joyner, et al., 2015), and biodiversity (Garcia et al., 2014). The Köppen climate classification system experienced a resurgence in popularity as researchers sought to reveal the climatic component of global change and investigate the bioclimatic patterns in global climate. As climate is considered the primary factor to explain the species ranges at a large spatial extent (Heikkinen et al., 2016; Luoto et al., 2007; Pearson & Dawson, 2003), the Köppen climate

14

classification is often used as an input to analyze the species range distribution (Brugger &

Rubel, 2013; Tererai & Wood, 2014; Webber et al., 2011) and growth behavior of species

(Tarkan & Vilizzi, 2015), and to set up dynamic global vegetation models (Poulter et al., 2011).

Besides its application in impact studies, the Köppen classification has also been used to

illustrate global climate change in terms of shifting geographical boundaries of major climate

types (Belda et al., 2014, 2016; Chan & Wu, 2015; D. Chen & Chen, 2013; Feng et al., 2014;

Mahlstein et al., 2013; Zhang & Yan, 2014).

The widely applied Köppen climate classification, as the first quantitative classification of

Earth's climate, was first introduced by Wladimir Köppen in 1900. Even though various

classifications have been developed since then, those based on Köppen's original approach

(Köppen, 1923, 1931, 1936), especially its modifications, Köppen-Geiger classification (KGC)

(Köppen, 1936) and Köppen-Trewartha classification (KTC) (Trewartha, 1954), are still among

the most frequently used systems. KGC identifies the climate in similarity to their effects on

plant growth, which rely mainly on aridity and warmth (Rubel & Kottek, 2011). Developed by

Wladimir Köppen and Rudolf Geiger, and first published in 1936 (Köppen, 1936), KGC

classifies climate into five main classes and distinguishes the vegetation groups of the tropical

zone (A), arid zone (B), temperate zone (C), snow zone (D), and polar zone (E), referring to five

major climate zones (Sanderson, 1999) (Table 2-1).

Table 2-1 Definitions of major climate zones by Köppen climate classification schemes

KGC[*]			KTC[**]		
A Tropical	$T_{cold} \geq 18$		A Tropical	$T_{cold} \geq 18$	
B Arid (Dry)	$P_{ann} < P_{th}$		B Arid (Dry)	$P_{ann} < P_{th}$	
$P_{th} = 2 \times T_{ann}$	For rainfall concentrated in winter		Aridity threshold	$P_{th} = 2 \times A = 2 \times T_{ann} + 0.6 \times p_{hot} - 20$	
	Original KGC	$p_{win} > 2/3$	Patton's threshold	$P_{th} = R = 2.3 \times T_{ann} - 0.64 \times p_{win} + 41$	
	Updated KGC	$p_{win} > 70.0\%$	C Subtropical	$8 \leq n\,(T_{mon} > 10) \leq 12$ & $T_{cold} < 18$	

		2 × T$_{ann}$ + 28	For rainfall concentrated in summer			
		2 × T$_{ann}$ + 14	Otherwise			
C	Temperate	Original KGC	T$_{hot}$ > 10 & -3 < T$_{cold}$ < 18			
		Updated KGC	T$_{hot}$ > 10 & 0 < T$_{cold}$ < 18	D	Temperate	4 ≤ n (T$_{mon}$ > 10) ≤ 7 & T$_{cold}$ < 18
D	Cold (Snow/ Continental)	Original KGC	T$_{hot}$ > 10 & T$_{cold}$ ≤ -3			
		Updated KGC	T$_{hot}$ > 10 & T$_{cold}$ ≤ 0	E	Boreal (Subpolar)	1 ≤ n (T$_{mon}$ > 10) ≤ 3 & T$_{cold}$ < 18
E	Polar		T$_{hot}$ ≤ 10	F	Polar	T$_{hot}$ ≤ 10

Temperature in °C and precipitation in cm. The table is organized to represent the correspondence of climate zones defined by the KGC and KTC.

[*]Original KGC was used and cited in Kottek, Grieser, Beck, Rudolf, and Rubel (2006) and Rubel and Kottek (2010). Updated KGC was used and cited in Peel, Finlayson, and McMahon (2007), Kriticos et al. (2012) and Beck et al. (2018); p$_{win}$ is the percentage of annual precipitation occurring in winter (the coldest three months).

[**]Aridity threshold was used and cited in Feng et al. (2014). Patton's precipitation threshold was used and cited in Belda et al. (2016) and Belda et al. (2014). R is the Patton's precipitation threshold and p$_{win}$ is the percentage of annual precipitation occurring in winter (the coldest three months). A is the aridity threshold and p$_{hot}$ is the percentage of total precipitation received in the six high-sun months (in Northern Hemisphere, April to September and in Southern Hemisphere, October to March); n (T$_{mon}$ > 10) indicates the number of the months which monthly temperature is larger than 10°C.

The modification of the Köppen climate classification proposed by Trewartha (1954) redefines subtropical (C), temperature (D), and boreal (E) climates (Table 2-1). KTC adjusts the original temperature criteria and wet/dry climate thresholds for a stronger correlation between climate types and observed boundaries of natural landscapes (Belda et al., 2014; Castro et al., 2007). The simplification of the wet/dry climate threshold used in KTC was proposed by Patton (1962) to manage the inexplicit explanation of "rainfall concentration in summer/winter" by combining the three criteria into one equation. Even though the designations in both KGC and KTC are basically the same, the definitions of the types might be different in many aspects. A large part of temperate (C) and cold (D) climate zones classified using KGC are redistributed and designated into subtropical (C), temperate (D), and boreal (E) climate zones by KTC (Table 2-2). Compared with KGC, despite being less popular, KTC has the advantage of presenting a more detailed depiction of climate types. The Global Forest Resources Assessment (FRA) led by the Food and Agriculture Organization (FAO) utilized KTC to map global ecological zones and concluded that

there is a strong relationship between KTC climatic types and the natural climax vegetation types and soils (FAO, 2001).

Table 2-2 Percentage of land area comparison of climate zones defined by Köppen climate classification and other classification methods

		Climate zones defined by Köppen climate classification					
		A	B	C	D	E	Total
1) Comparison with Köppen-Trewartha climate classification with Patton's boundaries of arid (B) climate zone (Belda et al., 2014)	A	20.31	0.02				20.33
	B	2.09	26.72	2.03	1.51		32.35
	C		1	9.06			10.06
	D		0.62	5.02	9.13		14.77
	E		0.02	0.24	14.73		14.99
	F		0.24			7.26	7.5
	Total	22.4	28.62	16.35	25.37	7.26	
2) Comparison with climate types classified by K-means cluster analysis (Zhang & Yan, 2014)	A	21.34	3.03	3.32			27.70
	B	0.24	16.95	2.29			19.48
	C	0.01	6.54	9.93	3.84	0.46	20.78
	D		1.52	0.03	18.05	2.63	22.22
	E				0.96	4.08	5.03
	Total	21.59	28.04	15.57	22.85	7.16	
3) Comparison with biome classification from a merger of categories of Scott (1996) and the World Wildlife Federation (Rohli, Joyner et al., 2015)	TRF[*]	10.35	0.11	3.03			13.48
	Grassland	5.58	9.13	5.18	3.67		23.56
	Desert		14.96	0.79	0.54		16.29
	SSW[**]	1.57	2.04	2.05			5.67
	SMF[***]	0.38	0.14	5.74	3.01		9.27
	Boreal			0.13	11.02	0.47	11.61
	Tundra		0.16	0.47	2.23	5.60	8.47
	Ice Cap/ Highland	0.53	0.84	2.10	0.57	7.53	11.57
	Total	18.41	27.38	19.48	21.04	13.61	

[*]TRF is short for Tropical Rain Forest.

[**]SSW for Subtropical Scrub and Woodland.

[***]SMF for Subtropical and Mid-latitude Forest.

In addition to the Köppen classification systems, other bioclimatic methods based on human expertise have been used for mapping the global climate zones (Holdridge, 1947; Thornthwaite, 1931; Walter & Elwood, 1975). Meanwhile, various clustering-based methods using different choices of climatic variables and clustering algorithms (Bunkers et al., 1996; Degaetano, 1996; Fovell & Fovell, 1993; Hoffman et al., 2005; Mahlstein & Knutti, 2010; Metzger et al., 2013; Netzel & Stepinski, 2016; Stooksbury & Michaels, 1991; Unal et al., 2003; Zscheischler et al., 2012) have been proposed to complement human expertise and provide a natural approach to

climate classification. Based on the comparison results, about half of the climate types detected by clustering can be matched to the KGC classes, and the rest differ in climatic character and spatial distribution (Netzel & Stepinski, 2016). The area of five major climate zones defined by Köppen classification and K-mean clustering method coincides well with each other (Zhang & Yan, 2014) (Table 2-2). Unlike Köppen classifications, cluster analyses produce extensively objective boundaries, which are difficult to interpret (Rubel & Kottek, 2011). According to the principles that should be satisfied by climate classification (Essenwanger & Landsberg, 2001), a meteorological basis is requisite, which is not sufficiently fulfilled by statistical classification methods. Compared with the clustering methods built upon empirical relationships with vegetation distribution, the Köppen classification has advantages to perform dimensionality reduction of climatic variables into one class more related to biota (Tapiador et al., 2019). It is therefore not surprising that today, almost 120 years after Köppen began to develop this climate classification system, it is still the most widely used climate classification method, evidenced by a literature search revealing that 85% of references using climate classification chose the Köppen classification (Larson & Lohrengel, 2011).

Despite its popularity, the Köppen classification has a few limitations. First, it does not account for the possibility of the emergence of novel climate types, so under global change there is a need to develop a new classification scheme of the world climate (Sanderson, 1999). Updated based on recent and future high-resolution climate data and applied to climate model predictions, the Köppen classification will still be applicable in the future (Kottek et al., 2006). Another problem with the Köppen classification is that there exist large uncertainties to equate climate zones directly with actual biome distribution. Despite the agreement between the Köppen climates and major biomes, cautions should be taken when relating classification results to the

biome distribution: first, vegetation changes may lag the change in climate zones; second, factors not accounted for in the Köppen classification, such as atmospheric CO_2 level, may alter the relationship between climate classes and vegetation. Therefore, the Köppen classification should be interpreted as a description of macro climatic conditions, which are closely related to the biome distribution. Moreover, the Köppen classification system is threshold-based and lacks the notion to quantitatively measure similarities and differences between local climates beyond organizing them into a hierarchy. Despite these, it demonstrates a relatively good correlation with the biome distribution and still has competitive advantages of simplicity and integrating climatic variables.

2.4 Global climate classification maps

The availability of globally gridded datasets of climatic variables allowed for the generation of maps for the global distribution of Köppen climate types. Observed global temperature and precipitation datasets collected over the last two centuries, as well as global climate model simulations of past and future climate, offer the possibility to compile long-term time series of global maps of the Köppen climate classification. There exist eight versions of recent world maps of the Köppen climate classification systems (Table 2-S1).

Most of the existing Köppen climate classification world maps have a relatively low resolution of 0.5° (Belda et al., 2014; Grieser et al., 2006; Kottek et al., 2006; Kriticos et al., 2012; Rubel & Kottek, 2010), mainly because of the limited availability of high-resolution global climatology data. One of the first KGC world maps was published by Kottek et al. (2006). They produced a comprehensive map based on the Climatic Research Unit (CRU) TS 2.1 (Mitchell & Jones, 2005) for temperature, and the Global Precipitation Climatology Centre (GPCC) VASClimO

V1.1 (C. Beck, Grieser, Rudolf, et al., 2005) for precipitation at a resolution of 0.5° for 1951–2000. In the same year as Kottek et al. (2006), Grieser et al. (2006) produced a series of historical and present maps for multiple time periods within 1951–2000 using temperature and precipitation data from the CRU TS 2.1 (Mitchell & Jones, 2005) dataset, GPCC VASClimO V1.1 and GPCC Full Data Reanalysis (C. Beck, Grieser, Rudolf, et al., 2005). Following up on the work of Kottek et al. (2006), Rubel and Kottek (2010) generated a series of KGC world maps covering the extended period 1901–2100. These maps are based on CRU TS 2.1 and GPCC Full Data Reanalysis V4 for 1901–2002, and Global Climate Model (GCM) outputs for 2003–2100 were taken from the TYN SC 2.0 (Mitchell et al., 2004) dataset. Based on the ensemble projections of global climate models, the series of world maps of KGC produced by Rubel and Kottek (2010) depicts the shift in the climate zones within the 21st century by considering different Intergovernmental Panel on Climate Change (IPCC) scenarios.

Only a few map products applied interpolation methods to achieve a resolution better than 0.1° (Kriticos et al., 2012; Peel et al., 2007; Rubel et al., 2017). As a follow-up work of Kottek et al. (2006), the reanalyzed KGC map had a higher resolution of 0.083° and 0.167° using the downscaling algorithms described by Rubel et al. (2017). This high-resolution map product is representative of the more recent 25-year period of 1986–2010 rather than the historical 50-year period of 1951–2000 provided by Kottek et al. (2006). Peel et al. (2007) was also among the first to publish a terrestrial world map of KGC using a digitally gridded dataset but at a much finer resolution of 0.1°. Climate classifications were derived from the long-term station records of monthly precipitation and temperature from the Global Historical Climatology Network (GHCN) version 2.0 dataset (Peterson & Vose, 1997) and interpolated onto a 0.1° grid using a three-dimensional tension spline interpolation. Since elevation is an important variable in the

interpolation of temperature fields, one potential improvement of the methodology would be to apply a three-dimensional spline, using elevation as the third dimension (Daly, 2006). Moreover, the KGC scheme applied in Peel et al. (2007) was modified following Russell (1931) (Table 1). The first departure point from Geiger (1961) is the use of the temperature of the coldest month > 0 °C, rather than >-3 °C to define the boundary between the temperate (C) and cold (D) climate zones. Another modification is the use of a 70% precipitation criterion to distinguish the arid (B) climates. Kriticos et al. (2012) and Beck et al. (2018) followed the same KGC scheme described in Peel et al. (2007). The historical KGC map of Kriticos et al. (2012) was based on WorldClim V1 (Hijmans et al., 2005) temperature and precipitation datasets with resolutions of 0.167° and 0.083° for 1961–1990. The future 30-year KGC maps covering the period from 2001 to 2100 for A1B and A2 scenarios were derived from two GCMs, CSIRO-MK 3.0 and MIROC-H. Unlike Peel et al. (2007), Kriticos et al. (2012) applied the classification algorithm to gridded climate surfaces instead of kriging the classified climate stations, which would result in underrepresented topo-climatic patterns. In addition, using a limited number of data sources, these climate maps were generated based on a comparatively small number of ground stations with uneven distribution, inducing accuracy concerns. The limitations of the input data often lead to widespread misclassifications, particularly in regions with low station density and strong climatic gradients such as mountain ranges (Karger et al., 2017).

Focus has been on the improvement of data incorporation to maximize the accuracy with the current observational climatology datasets and future model projections. The most recent KGC map was presented by Beck et al. (2018), with an unprecedented resolution of 0.0083° (1km), for both present-day (1980–2016) and projected future conditions (2071–2100) under climate change. The present-day map was generated by combining the high-resolution climatic air

temperature and precipitation data from multiple independent sources, including WorldClim V1 (Hijmans et al., 2005) and V2 (Fick & Hijmans, 2017), CHELSA V1.2 (Karger et al., 2017) (Karger et al., 2017), and CHPclim V1 (Funk et al., 2015). The future map was derived from an ensemble of 32 Coupled Model Intercomparison Project - Phase 5 (CMIP5) (Taylor et al., 2012) model projections under the RCP8.5 scenario. The use of multiple data sources to generate the global climate maps maximizes the accuracy and allows for an evaluation of the classification uncertainty, which was estimated using the agreement in derived classes using different data input combinations. Further technical validation was completed using station observations compiled from the Global Historical Climatology Network-Daily (GHCN-D) database (Menne et al., 2012) and the Global Summary of the Day (GSOD) database. Beck et al. (2018) was the first to provide corresponding classification evaluation and uncertainty estimates. Their newly published KGC present-day map exhibited high classification accuracy of 80% (Table 2-S1). However, single-period coverage or non-comparable periods covered in Beck et al. (2018) may not sufficiently fulfill the current research needs especially for studies focusing on change detection in Köppen climates. There exists an urgent need to compile a long-term time series of global maps of Köppen climate classification with high resolution and improved accuracy. Multiple observed global temperature and precipitation datasets collected over the last two centuries can be integrated to achieve the goal. Moreover, global climate model simulations of future climate offer a possibility to address the need of the future climate classification maps. Moreover, the only climate classification map product that applied KTC published by Belda et al. (2014) used CRU TS 3.1 (Harris et al., 2014) datasets with a coarse resolution of 0.5°. As KTC has an advantage of more detailed description and a stronger relationship with climax

vegetation types, quality global KTC maps with higher resolution, various time coverages, and reduced uncertainty are needed to support further applications at both global and regional scales.

2.5 Observed climate zone changes

Many studies apply the Köppen classification for climatology observations or paleoclimate reconstructions to examine the changes in the global geographical distribution of climate patterns (Belda et al., 2014; Chan & Wu, 2015; D. Chen & Chen, 2013; Rohli, Andrew, et al., 2015; Yoo & Rohli, 2016). The observed area changes in climate zones detected in previous studies, including the significant and non-conclusive ones, are summarized in Table 2-S2. This section presents discussions on the observed climate zone changes over the past century, organized by a set of metrics, covering three aspects: area changes, and latitude and elevation shifts.

2.5.1 Changes in the areas of climate zones

The changes in the areas of climate zones indicate the expansion or shrinkage of the spatial extent of the Earth's macro-climatic conditions, potentially implying the retreat or spread of biomes as well as threats of species range contraction or opportunities for range expansion. One of the most pronounced changes in the area of climate zones during the past century is the shrinkage of the polar (E) climate zone with the size equivalent to 0.50–0.98% of the Earth's total land area (C. Beck, Grieser, Kottek, et al., 2005; Belda et al., 2014; Chan & Wu, 2015; D. Chen & Chen, 2013; Fraedrich et al., 2001; Kalvová et al., 2003; Rohli, Andrew, et al., 2015). Another dominating area change since the 1900s is the area expansion of the arid (B) climate zone, which is equivalent to 0.68–1.51% of the Earth's total land area, reported in recent studies

that used KGC criteria to define the arid (B) climate zone (C. Beck, Grieser, Kottek, et al., 2005; Chan & Wu, 2015; D. Chen & Chen, 2013; Rohli, Andrew, et al., 2015).

Nevertheless, substantial discrepancies remain in the observed changes in the area of the tropical (A) climate zone. The expansion of the tropical (A) climate zone is not conclusive because most studies have not discovered observational supporting evidence (C. Beck, Grieser, Kottek, et al., 2005; Chan & Wu, 2015; D. Chen & Chen, 2013; Rohli, Andrew, et al., 2015) and only a few studies have identified this expansion trend (Belda et al., 2014; Fraedrich et al., 2001; Kalvová et al., 2003). Moreover, there is no significant change in the area of the temperate (C) climate zone (C. Beck, Grieser, Kottek, et al., 2005; Belda et al., 2014; Chan & Wu, 2015; D. Chen & Chen, 2013; Fraedrich et al., 2001; Kalvová et al., 2003; Rohli, Andrew, et al., 2015). In addition, the total area of the boreal (D) climate zone that ranges from 33°N to 74°N has demonstrated no significant change (Chan & Wu, 2015; D. Chen & Chen, 2013; Kalvová et al., 2003; Rohli, Andrew, et al., 2015). However, at high northern latitudes (north of 55°N), a statistical expansion of the boreal (D) climate zone up to 0.39–1.19% of the Earth's total land area was detected, while at the mid-latitude regions (south of 55°N), a significant area shrinkage (1.06% of the Earth's total land area) was observed (Chan & Wu, 2015) These contrasting patterns indicate a spatial shift of the boreal (D) climate zone towards higher latitudes; the same pattern was detected in the temperate (C) climate zone (Chan & Wu, 2015; D. Chen & Chen, 2013; Rohli, Andrew, et al., 2015). The major changes in the area of the climate zones in the past century and their estimated magnitudes are shown in Table 2-S2, represented by the changes in the percentage of the total land area.

(a)
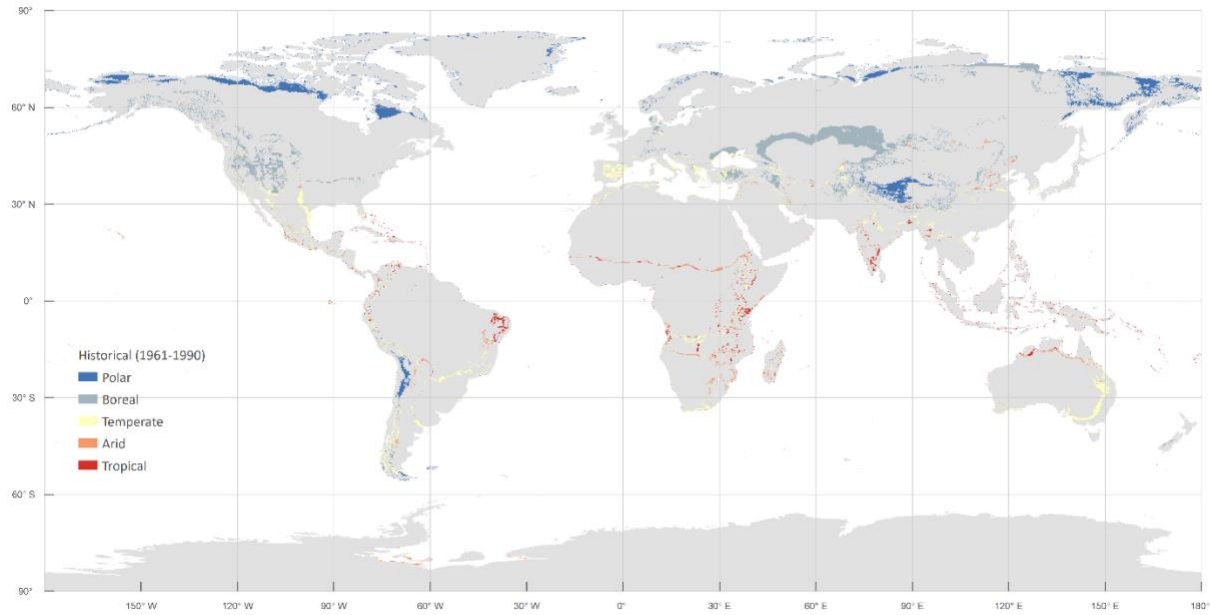
(b)
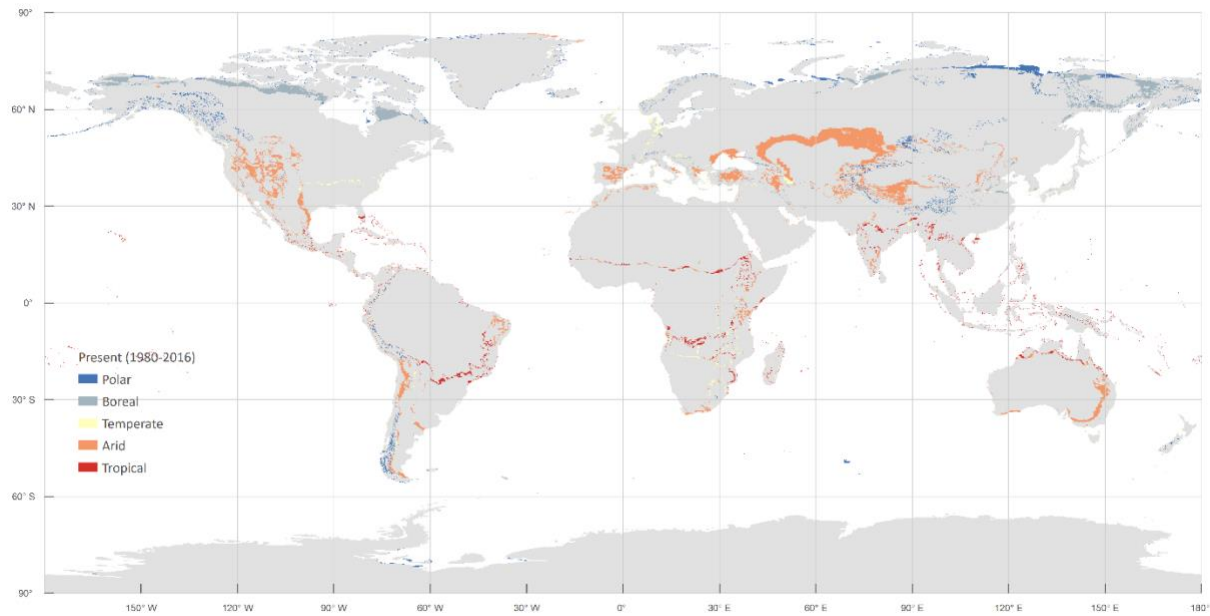
Figure 2-2 Maps of regions observed to undergo climate zone changes since the 1980s. (a) Historical major climates of these regions in 1961–1990 from historical data of Köppen-Geiger climatic zones (Kriticos et al., 2012). (b) Present major climates of these regions in 1980–2016 from the present-day Köppen-Geiger climate classification map (Beck et al., 2018).

Significant changes in the area of the climate zones have been the most detectable since the 1980s, It is indicated that specifically arid (B) and polar (E) climate zones, were highly susceptible to accelerated global warming since the 1980s (Chan & Wu, 2015; D. Chen & Chen, 2013; Zhang & Yan, 2014). This is evidenced in a) more consistent significant changes in the area of climate zones beginning around the 1980s (Chan & Wu, 2015), b) larger area variations in climate zones in 1976–2009 (Zhang & Yan, 2014), c) and distinct changes in the area of the two most susceptible climate zones, arid (B) and polar (E) climate zones, since the 1980s (D. Chen & Chen, 2013). The regions observed to undergo climate zone changes since the 1980s are illustrated in Figure 2-2. The area percentage of these regions with respect to the total land area is estimated to be 5.31% based on the historical (Kriticos et al., 2012) and present KGC maps (H. E. Beck et al., 2018). In comparison, since 1950, around 5.7% of the global total land area underwent climate zone changes, based on an ensemble of observational datasets from the CRU, the University of Delaware (UD), and the Goddard Institute for Space Studies (GISS), using the 15-yr time scale and a recently updated KGC scheme (Chan & Wu, 2015). This suggests that the changes in the area of the climate zones have dramatically accelerated since the 1980s. With the long-term 50-yr period of 1951–2000 as a baseline, 3.3% of the land area is estimated to experience climate zone changes in the latter half of the 20th century (C. Beck, Grieser, Kottek, et al., 2005). KTC results show that 4.4–5.1% of the land area has gone through climate zone changes during the 20th century (Belda et al., 2014; Fraedrich et al., 2001). The average decadal trends based on the three observational datasets, UD, CRU, and GISS, are shown in Figure 2-3.

Different climate subtypes are responsible for temporally varied contributions to the total area changes with large regional differences. The tropical (A) climate zone showed the largest variations in area changes among all climate zones over the past century, indicated by stagnation

or a slight decrease in the first half of the 20th century, followed by an accelerated area reduction in the late 1960s. Since the 1990s, there has been continuous area growth (Belda et al., 2014; Chan & Wu, 2015; Fraedrich et al., 2001). Among the tropical (A) climates, the tropical rainforest (Af) and monsoon (Am) climate zones showed slight variations while the tropical savanna (Aw) climate zone was the most variable subtype (D. Chen & Chen, 2013). The most recent area increase in the tropical (A) climate zone was largely driven by the area increase in the tropical savanna (Aw) climate zone on the expense of temperate (C) climates (C. Beck, Grieser, Kottek, et al., 2005; Belda et al., 2014; Chan & Wu, 2015). The significant shift from temperate (C) climates to tropical savanna (Aw) climates was observed since the 1980s over southern Africa, the southern edge of Brazilian Highlands, and Northern India (Figure 2-2), mainly driven by temperature increase (Chan & Wu, 2015).

The arid (B) climate zone occupies the largest area on Earth and is observed to have undergone the most conspicuous area expansion in the second half of the 20th century, at the expense of primarily temperate (C) and mid-latitude boreal (D) climates. The expansion of the arid (B) climate zone has accelerated since the 1980s at a rate of $4.2 \times 10^5 \text{ km}^2 \text{ dec}^{-1}$, which is equal to approximately 115 $\text{km}^2 \text{d}^{-1}$ (Chan & Wu, 2015). This increase is mainly attributed to a large area increase of the subtype semi-arid (BS) climate zone, also known as the steppe climate (Belda et al., 2014; Chan & Wu, 2015). The other climate subtype, the desert (BW) climate, exhibited relatively large fluctuations throughout the 20th century, with opposite changes to the semi-arid (BS) climate, which can be explained by the mutual replacement of the two in the arid (B) climate zone (Belda et al., 2014). In the 1980s, a significant phase shift of semi-arid (BS) and desert (BW) climates occurred, followed by the increasing expansion of the semi-arid (BS) climate zone and the reduced shrinkage of the desert (BW) climate zone (Belda et al., 2014). The

extension of the semi-arid (BS) climate zone since the 1980s has mainly occurred in the

Mediterranean, south-central United States, southeastern Australia, and southern South Africa,

which previously had a temperate (C) climate, as well as in some mid-latitude areas classified as

boreal (D) climate zone, including Central Asia and western North and South America (Figure 2-

2). In high-altitude mountainous regions, particularly northern Tibetan Plateau and the Central

Andes, part of the area has experienced a climate shift from polar (E) to semi-arid (BS) climate

in the past few decades. In the tropics, especially in small areas of southern India and eastern

Africa, tropical (A) climates were replaced by arid (B) climates.

Although no significant changes were observed in the area of temperate (C) climate zones, a

remarkable spatial poleward shift has been identified. A considerable part of the temperate (C)

climate zone was replaced by the warmer and drier climate subtypes in tropical (A) and arid (B)

climate zones. The area loss was compensated by the climate shift from the boreal (D) and polar

(D) climates to temperate (C) climates. Moreover, concerning a mutual interchange of the area

within the temperate (C) climate zone, subtype dry summer (Cs) climate has replaced the fully

humid (Cf) climate zone since the 1980s. Like the temperate (C) climate zone, the boreal (D)

zone showed no significant change in the total area but a general shift towards high latitudes.

The area of the largest subtype, the boreal fully humid (Df) climate, remained relatively stable in

the past century, while the area of the small subtype, the dry winter (Dw) climate, was more

variable but showed a small change overall. Moreover, the high northern latitude (north of 55°N)

boreal climates, mainly fully humid (Df) and dry summer (Ds) climates, have expanded into the

polar (E) climate zone at a rate of 2.2×10^5 km^2 dec^{-1} (approximately 60 km^2 d^{-1}) in the second

half of the 20th century (D. Chen & Chen, 2013). In comparison, the mid-latitude (south of 55°N)

boreal climates decreased in the area at a larger rate of 2.9×10^5 km^2 dec^{-1} (approximately 79

km^2 d^{-1}) (D. Chen & Chen, 2013). The area increase in high latitudes and decrease in mid-latitudes demonstrated the poleward shift of the boreal (D) climate zone, together with potential shrinkage in the future.

The prominent shrinkage of the polar (E) climate zone had a rate of 2.8×10^5 km^2 dec^{-1} (approximately 77 km^2 d^{-1}) in the second half of the 20th century (Chan & Wu, 2015). The enhanced warming in the Arctic region led to a pronounced area reduction of the frost (EF) climate zone in the Arctic, which was largely replaced by the tundra (ET) climate. Some regions in high northern latitudes have experienced the replacement of the tundra (ET) climate by the boreal (D) climate, especially some low-level regions, which are more likely to be affected by increased warming. The replacement was mainly observed in northern Canada and northern and eastern Siberia. Over some high-altitude mountainous areas in middle and low latitudes, particularly the Tibetan Plateau and the Andes, the tundra (ET) climate was replaced by warmer climate zones at low altitudes. Note that considerable uncertainty remains in the climatology data over high latitudes and high-altitude regions, where station networks tend to be sparsely distributed. As a result, the polar (E) and boreal (D) climate zones are likely to be misclassified due to data limitations.

2.5.2 Latitude and elevation shifts of climate zones

The position shifts of the climate zones provide additional insight into the climate zone changes, with a special focus on the change direction and velocity. The latitude and elevation shift of climates at a regional scale significantly affect the ability of species to track climatic conditions. The species range replacement can be hampered where the climate zone change direction goes across areas of adverse topography or unfavorable habitats. Moreover, if the shift velocity

exceeds the species' dispersal abilities, it poses a serious threat to regional biodiversity (Garcia et al., 2014). By applying the climate classification to incorporate information of annual circles of temperature and precipitation, Chan and Wu (2015) examined the latitude and elevation shifts of major climate zones (Chan & Wu, 2015). Based on the absolute latitude changes in 1953–2003 from the UD observational dataset, significant poleward shifts were detected in temperate (C), boreal (D), and polar (E) climates at average rates of 35.4, 16.2, and 12.6 km dec^{-1} (0.32, 0.15, and 0.11° latitude dec^{-1}), respectively, and significant shifts to high elevation were detected in tropical (A) and polar (E) climate zones at rates of 3.0 and 14.3 m dec^{-1}, respectively (Chan & Wu, 2015). The observed trends in latitude and elevation shifts for the five climate zones from CRU and GISS datasets are shown in Figure 2-3.
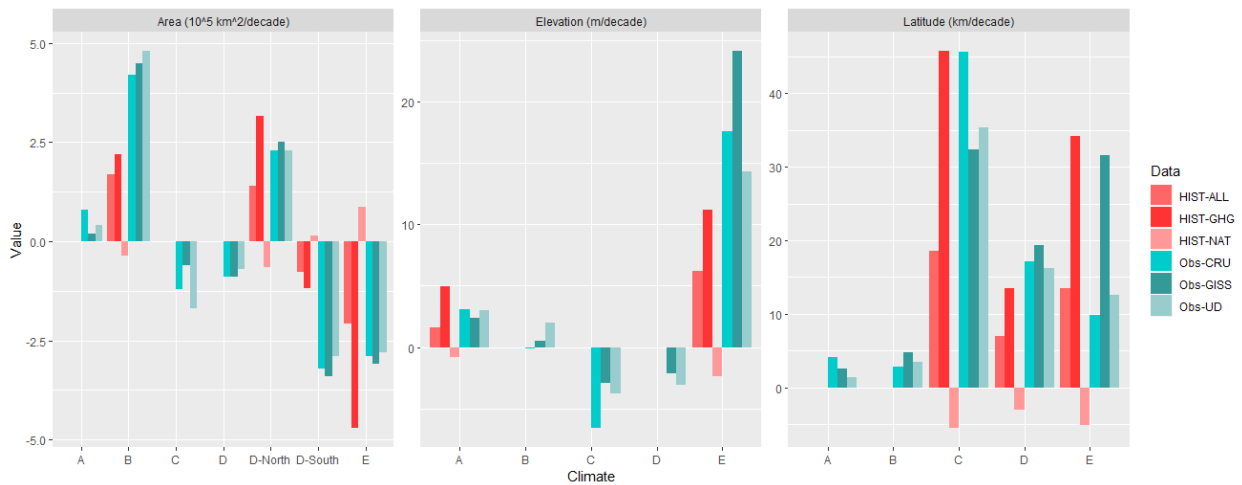
Figure 2-3 Decadal trends in total area, average elevation, and average absolute latitude of climate zones estimated from different observational datasets, UD, GISS, and CRU, as well as HIST-ALL, HIST-GHG, and HIST-NAT CMIP5 runs. Only significant model-simulated trends are shown. HIST-ALL runs are driven by forcing reconstructed from observational data, such as greenhouse gas concentrations and volcanic eruptions. HIST-GHG is forced by greenhouse gas concentrations only, and HIST-NAT is forced by natural factors only. Reprinted with the permission of Chan and Wu (2015).

In the tropical (A) climate zone, the expansion of the savanna (Aw) climate into high-elevation regions in the tropics is the major reason for the significant elevation shift of tropical (A) climates, particularly since the 1990s. The elevation increases in the tropical (A) climate zone

occurred over the southern edge of the Brazilian Highlands in South America and the southern end of the Congo Basin in Africa. Polar (E) climates, previously distributed in relatively low elevations in high northern latitudes and mountainous regions, such as northern and eastern Siberia, western Tibetan Plateau, and the Central Andes, were largely replaced by warmer and drier climates, mainly boreal (D) and arid (B) climates. The area loss of polar (E) climates in low elevations, driven by increased warming, resulted in a significant average elevation increase in the polar (E) climate zone at a high rate of 14.3 m dec^{-1} (Chan & Wu, 2015). The global shifts of warmer and drier climate zones into higher elevations pose a substantial risk to vulnerable species and vegetation around or at the edge of the mountainous regions.

The position shifts of the three mid- and high-latitude climates are characterized by a significant poleward direction. The temperate (C) climate zone exhibited the most prominent poleward shifts at a rate of 0.32° latitude dec^{-1} along with a slightly decreased total area. A similar case was observed in the boreal (D) climate zone but at a relatively slower rate of 0.15° latitude dec^{-1} (Chan & Wu, 2015). The polar (E) climate zone turned out to be the most susceptible climate zone to global warming due to the combined and interacting effects of different factors, including greater warming trends, ice-albedo feedback, and restricted areas for climate displacement. The polar (E) climate zone was forced to shift into higher latitudes and higher elevations at considerably high rates, leading to a dramatic area shrinkage in the second half of the 20th century.

2.6 Projected climate zone changes and assessment

The projected changes in temperature and precipitation in the 21st century can cause significant climate zone changes over the global land area. There is a growing body of literature applying

the Köppen climate classification scheme to model simulations to project future changes in the Köppen climate zones (Belda et al., 2016; Chan & Wu, 2015; Feng et al., 2014; Rohli, Andrew, et al., 2015). The projected climate zone changes identified in previous studies are summarized in Table 2-S3. The Köppen climate classifications of model outputs have been used to assess environmental changes, but systematic analyses of the discrepancies between models and scenarios are scarce. Since the GCMs present different physical parameterizations and varied grid sizes, large uncertainties exist in the model results of global climate classifications. This section first reviews the recent studies examining the future climate zone changes by the middle or the end of the 21st century using different ensembles of climate model projections. The three independent aspects, changes in the area and latitude and elevation shifts, are included to fully capture the spatial change patterns of global climate zones. The last part focuses on the studies of the model performance on climate classification to further evaluate the uncertainties in the changes in model projected climate zones.

2.6.1 Projected changes in climate zones in the 21st century

2.6.1.1 Area changes of climate zones

In the 21st century, the climate zones are projected to shift towards warmer and drier climates, consistent with the observed change pattern in the 20th century. The area of the tropical (A) climate zone exhibited large variations in the second half of the 20th century, characterized by a rapid area decrease in the 1980s and a dramatic area extension since the 1990s. Even though the long-term observed tropical (A) climate expansion is not conclusive, the tropical (A) climate is projected to experience significant expansion in the 21st century, in both high-end and low-end scenarios (H. E. Beck et al., 2018; Belda et al., 2014; Chan & Wu, 2015; Feng et al., 2014; Hanf

et al., 2012; Kalvová et al., 2003; Mahlstein et al., 2013; Rohli, Andrew, et al., 2015; Rubel & Kottek, 2010). The projections indicate that the arid (B) climate zone could continue to expand during the 21st century. The largest changes are projected in the Northern Hemisphere north of 30°N (Feng et al., 2014; Rubel & Kottek, 2010). Driven by the significantly expanding tropical (A) and arid (B) climates in the tropics and subtropics, the mid- and high-latitude climates, including temperate (C) and boreal (D) climates, are forced to shift poleward successively. Although observations show insignificant changes in the area of temperate (C) and boreal (D) climate zones, projections suggest an accelerated decrease in the area of two climate zones by the end of 21st century, especially under RCP8.5 and A1F1 scenarios from the Special Report on Emissions Scenarios (SRES) (H. E. Beck et al., 2018; Chan & Wu, 2015; Hanf et al., 2012; Mahlstein et al., 2013; Rohli, Andrew, et al., 2015; Rubel & Kottek, 2010). The pronounced area shrinkage of the polar (E) climate zone is projected to continue at the same rate in this century. Table 2-S3 summarizes the projected changes in the area of the climate zones and the percentage of the total land area projected to undergo certain changes by the end of the 21st century.

(a)

(b)

(c)

(d)
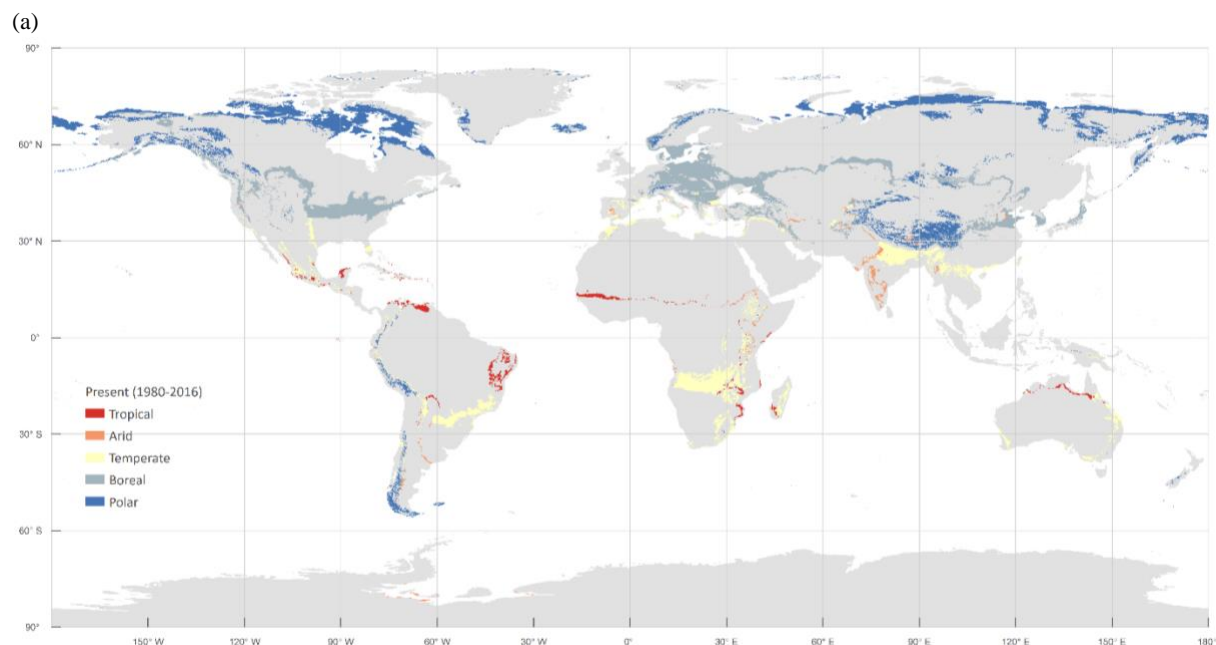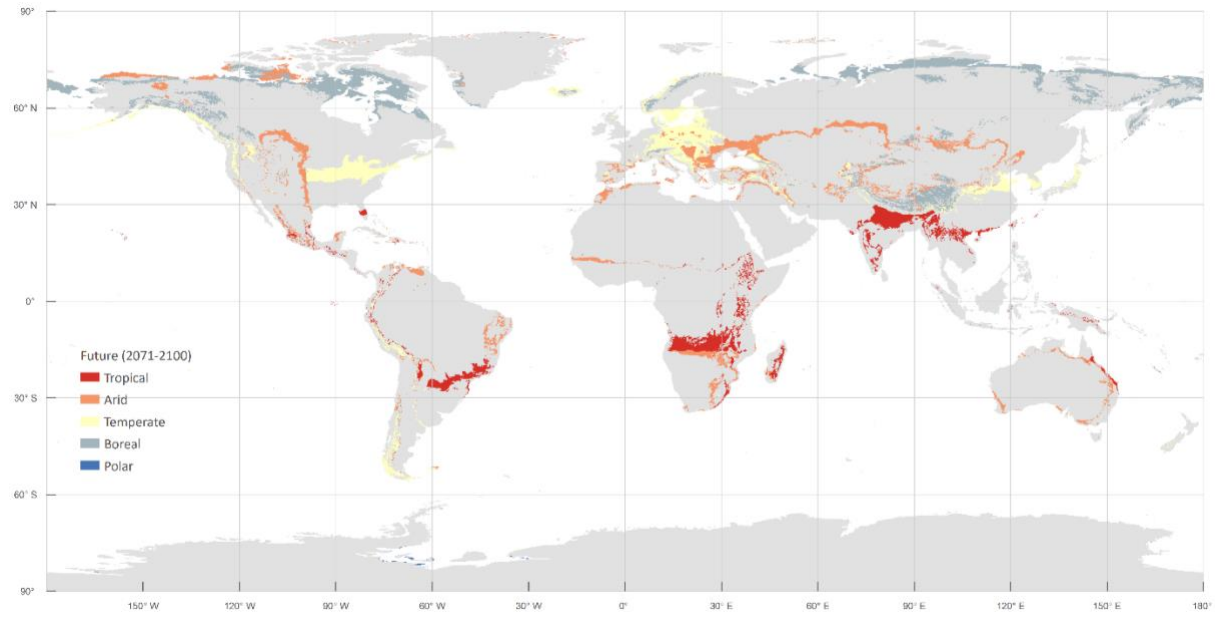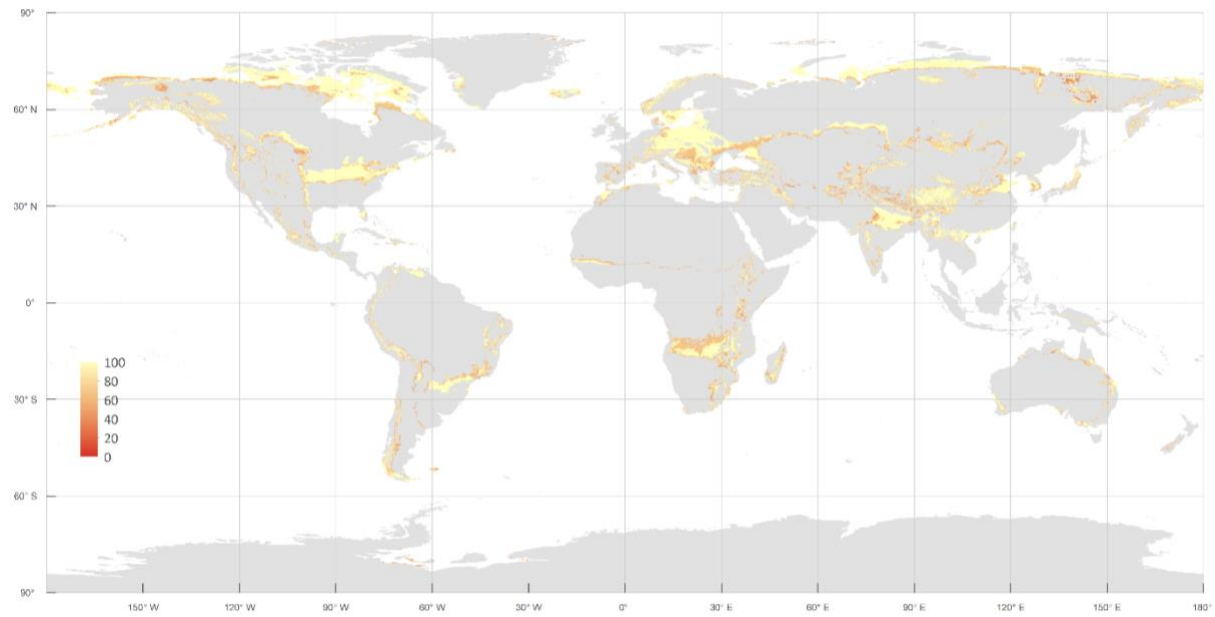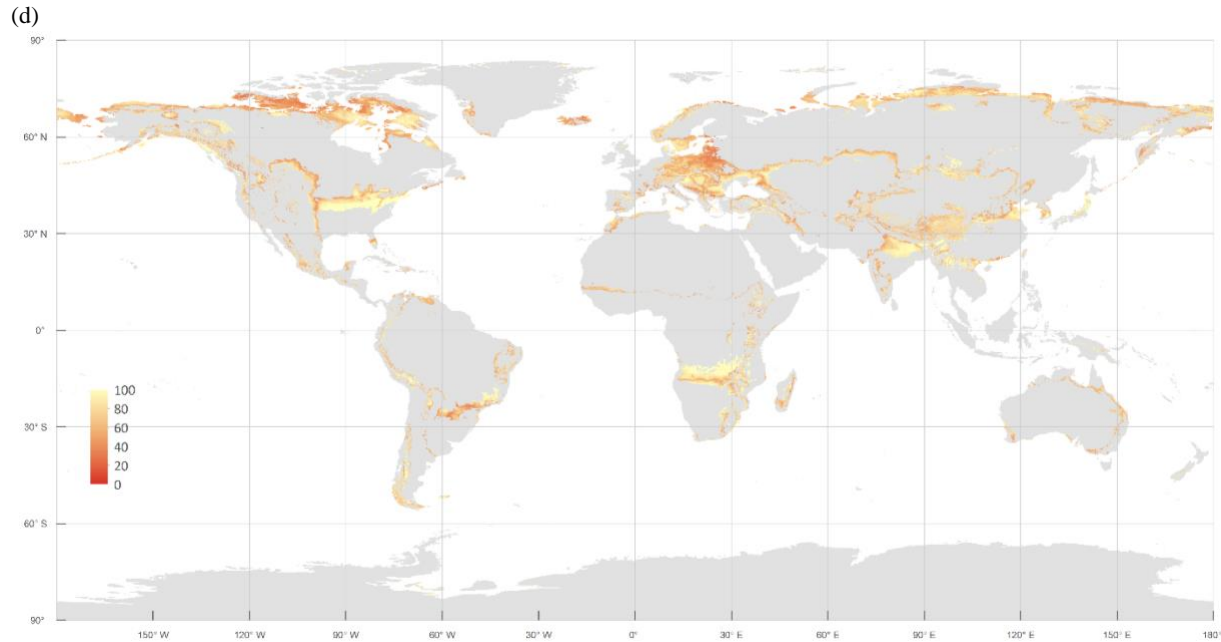
Figure 2-4 Maps of regions that are projected to undergo changes by the end of the 21st century. (a) and (b) show the major climates of these regions for the present-day (1980–2016) and projected conditions (2071–2100), respectively. (c) and (d) show the confidence levels (%) associated with the classification accuracy for the present-day (1980–2016) and projected conditions (2071–2100), respectively. Data from present and future Köppen-Geiger climate classification maps at 1-km resolution (Beck et al., 2018).

The regions projected to undergo climate zone changes in the 21st century together with the confidence levels (%) of the projected changes are shown in Figure 2-4. By the end of the 21st century, under the RCP8.5 scenario, around 13% of the land area is projected to experience changes in macro climatic conditions at the time scale of 30-yr (H. E. Beck et al., 2018) and 20% at a shorter time scale of 5-yr (Mahlstein et al., 2013). Based on the KTC results, the percentage is projected to be as large as 20% using a 30-yr average (Belda et al., 2016) and 39–54% using a 15-yr average (Feng et al., 2014) under RCP8.5. Furthermore, the rate of total climate zone area changes (% $°C^{-1}$) is found to increase linearly with the rising global mean temperature (Mahlstein et al., 2013). Using the RCP8.5 emissions pathway, the rate of the climate zone area changes nearly doubles compared to the early 20th century and reaches 5.4% $°C^{-1}$ by the end of this

century (Mahlstein et al., 2013). This quadratic increase in the total percentage of the land area changes implies that the magnitude of the global-scale climate zone changes will be further amplified with continued warming. However, this finding is not applicable to all climate zones. Only the decrease in the projected area of the boreal (D) climate zone demonstrates a pronounced acceleration under RCP8.5 in the second half of the 21st century while the other climate zones show divergent change patterns (Chan & Wu, 2015).
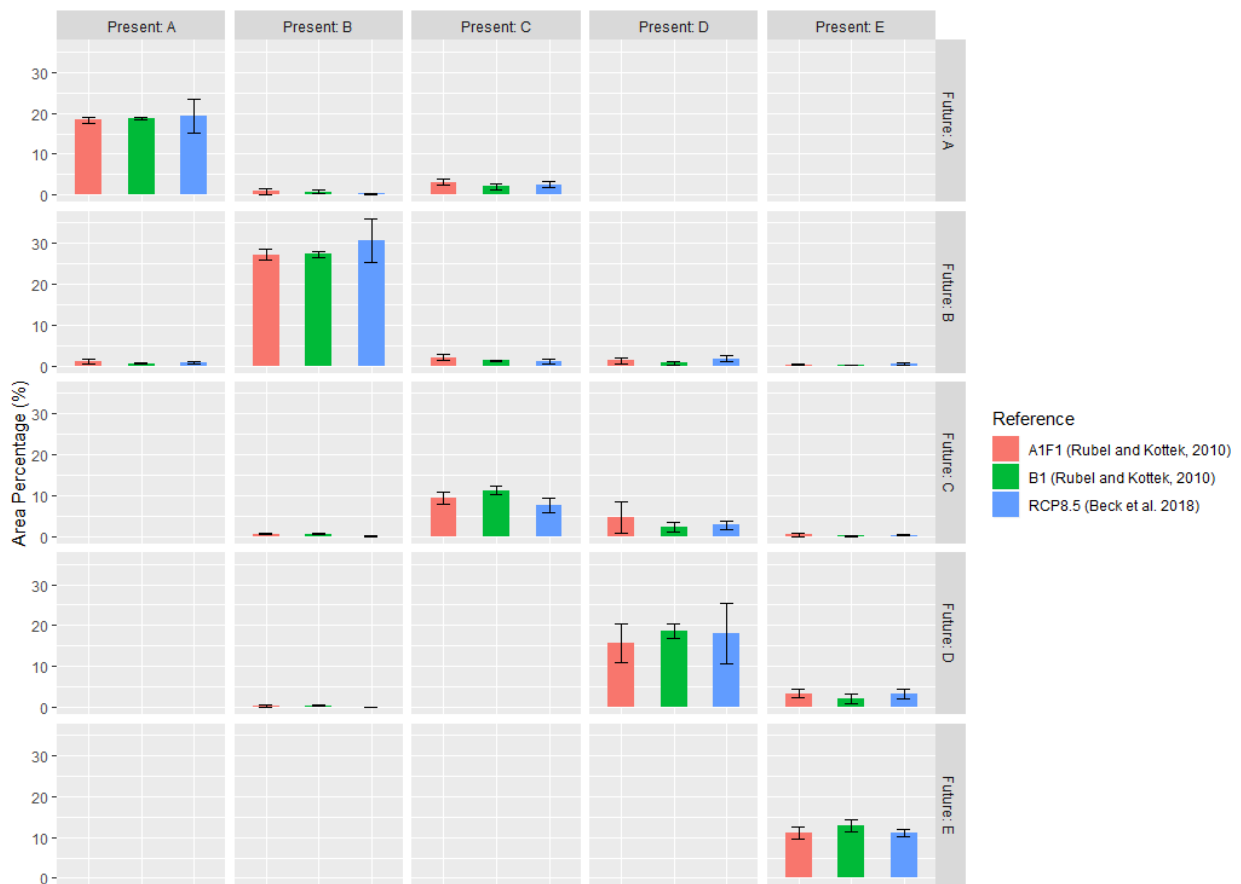
Figure 2-5 Shifts between climate zones in the 21st century under different scenarios

Many regions are projected to change by one or two climate subtypes, which is difficult to detect by the total climate zone area change. The climate subtypes within each climate zone exhibit different projected changes in this century, leading to varied regional influence. The statistical summary of the shifts between the climate zones under different scenarios is presented in Figure

6. All tropical (A) climates expand and reach a significant level by 2020 (Chan & Wu, 2015; Feng et al., 2014). The savannah (Aw) climate zone is expected to undergo the most significant expansion particularly during the first half of the 21st century and reach a stabilized level over the last few decades (Hanf et al., 2012). The temperate monsoon (Cw) climate zones in large areas of southern Africa, northern India, and central North America, which is estimated to account for 2.57% of the global land area under RCP8.5, will be replaced by tropical savanna (Aw) climate zones by the end of the 21st century (Beck et al., 2018).

In the subtropics, arid (B) climates, including both semi-arid (BSh) and desert (BWh) climates, are projected to expand continuously over the entire 21st century (Feng et al., 2014; Hanf et al., 2012; Mahlstein et al., 2013; Rohli, Andrew et al., 2015). The semi-arid (BS) climates are projected to expand into some mid-latitude areas such as western North America, Mediterranean, and Central Eurasia, which currently experience temperate (C) or boreal (D) climates under RCP8.5. Around 1.10% of the land area will change from temperate (C) climates to arid (B) climates and 1.74% from boreal (D) climates in this century (Beck et al., 2018).

For the temperate (C) climate zone, the area gain and loss are balanced out and estimated to be 3.30% and 3.67% of the land area under RCP8.5, respectively (Beck et al., 2018). Projections indicate a substantial loss of the temperate monsoon (Cw) climate, which is replaced largely by the savannah (Aw) climate in northern India, southern Africa, and central South America. The most extensive temperate (C) climate subtype is the temperate humid hot summer (Cfa) climate, which is projected to take the place of a part of boreal humid (Df) climates, occupying 2.83% of the land area under RCP8.5 (Beck et al., 2018). Moreover, a large fraction of the temperate (C) climate zone changes from cool summer climates (i.e., Cwc and Cfc) to hot summer climates (i.e., Cwa and Cfa) (Mahlstein et al., 2013; Rohli, Andrew et al., 2015).

Within the boreal (D) climate zone in the Northern Hemisphere, like the temperate (C) climate zone, climates are projected to shift substantially from cold or very cold summers (Dfc and Dfd) to hot summers (Dfa) (Mahlstein et al., 2013; Rohli, Andrew et al., 2015). A large area in the subarctic region will change from boreal humid (Df) climates to dry summer (Ds) climates. Under RCP8.5, roughly 4.57% of the land area occupied by boreal (D) climates will be replaced by temperate (C) and arid (B) climate zones, accounting for 2.83% and 1.74% of the total land area, respectively; at the same time, the boreal (D) climate zone will shift northward and take up 3.19% of the land area in the polar (E) climate zone (Beck et al., 2018). However, the RCP4.5 scenario shows no significant changes in the area of the boreal (D) climate zone over the 21st century (Chan & Wu, 2015).

The significant area loss of tundra (ET) and frost (EF) climate zones are the most significant climate zone changes in the 21st century to date, identified across all models (Mahlstein et al., 2013). The shrinkage of tundra (ET) and frost (EF) climate zones are projected to occur not only in the high latitudes but also in high elevations of the Himalayas and the Andes (Belda et al., 2016). The area reduction of the polar (E) climate zones is estimated to be 4% of the total land area by the end of this century under RCP8.5 (H. E. Beck et al., 2018). During the second half of this century, the decreasing trend of the polar (E) climate zones is expected to weaken under both RCP8.5 and RCP4.5 scenarios (Chan & Wu, 2015; Hanf et al., 2012).

2.6.1.2 Latitude and elevation shifts of climate zones

The change in the relative land areas of the climate zones is not the only measure of the climate zone variations. The potential geographical shifts of the climate zones are also important. Associated with the projected expansion of the tropical (A) climate zone, a slightly increasing

trend is projected in the average absolute latitude of the tropical (A) climate zones; it is expected to reach statistical significance by 2020 (Chan & Wu, 2015). There exist large discrepancies among models in the projected latitudinal shift of the arid (B) climate zone (Belda et al., 2016). As arid (B) climates are distributed near the equator and cover a wide range of latitudes, the latitudinal shift of the arid (B) climate zone is not evident in the 20th century (Belda et al., 2016; Chan & Wu, 2015). By contrast, the projected poleward shifts of mid- and high-latitude climates are important, particularly in the Northern Hemisphere north of 30°N (Belda et al., 2016; Chan & Wu, 2015; Feng et al., 2014). The poleward shifts in temperate (C) and polar (E) climate zones are projected to accelerate in the first few decades of the 21st century (Chan & Wu, 2015).

Due to the warming effect, climate zones are driven to shift not only poleward but also towards high elevations. The mean elevation increase in the tropical (A) and polar (E) climate zones is projected to continue in the 21st century (Chan & Wu, 2015). Many low-latitude mountainous regions and their lee sides are expected to experience climate zone shifts due to increasing temperatures and changing precipitation patterns (Mahlstein et al., 2013). In the high-latitude mountainous regions of Greenland and Antarctica, low-level regions are projected to be affected first (Mahlstein et al., 2013). This projection suggests that in high-latitude regions, higher elevations can maintain the existing cold climate zone, whereas higher elevations in low-latitude regions are more susceptible to climate change. Consequently, as climate zones are driven to shift poleward and towards high elevations, risk of extinctions will increase, especially for high-elevation and high-latitude species.

2.6.2 Assessment of model simulations for climate zone distribution

Large areas of climate zones have been found to be misclassified by the GCMs compared to the reference climate zones established by the observational data. Some early results showed that the Atmosphere-Ocean General Circulation Models (AOGCMs) fail to simulate the observed Köppen climate zones in 20–30% of the land area (Gnanadesikan & Stouffer, 2006), and the range is estimated to be 24–39% in Hanf et al. (2012). Phillips and Bonfils (2015) found that the CMIP5 simulations agree with the observational reference in at most 70% of the land area. The results of Zhang and Yan (2016) showed that approximately 30–50% of the total land area was allocated incorrectly by most GCMs. However, in terms of the simulations of climate zone shifts, previous assessments reached different conclusions. Zhang and Yuan (2014) concluded that both the locations and areas of the climate zone shifts were poorly simulated by the GCMs. Tapiador et al. (2019) showed the consensus between CMIP5 models regarding the extent and intensity of changes for present climate zones. Further systematic methods are required to evaluate the model performance on the detection of the changes in climate zones.

The performance of GCMs in some climate zones and continents has been shown to be relatively poor. The obvious deficiencies remain in simulating tropical (A), arid (B), and temperate (C) climate zones (Belda et al., 2015; Phillips & Bonfils, 2015). According to Belda et al. (2015), the highest variance between models is associated with failure to reproduce the extent of temperate monsoon (Cw) and desert (BW) climates. Moreover, the desert (BW) and semi-arid (BS) climates are underestimated by half of the 43 models based on the results of Belda et al. (2015), and the central desert region in Australia is an example. Many models have problems capturing the rainforest (Af) climate, mainly in Amazonia (Belda et al., 2015). Meanwhile, Europe and Africa show the highest reliability in the multi-model ensemble mean simulation (Hanf et al., 2012).

Different quantitative methods show different agreement levels between simulated and observed Köppen climate types. A few studies employed the kappa value, which can provide a general quantification of the similarity of spatial patterns, to evaluate the performance of GCMs in simulating the distribution of global climate zones (Elguindi et al., 2014; Zhang et al., 2017; Zhang & Yan, 2014). Belda et al. (2015) used normalized error to statistically assess the total relative difference between the area classified by GCMs and the area from the observational data, as well as the overlap percentage to quantify the relative matching area in model results and observational data.

Sources of the uncertainties in the simulated climate distribution from GCMs include but are not limited to 1) the choice of reference data, 2) model resolution, and 3) deficiencies in model physics. Phillips and Bonfils (2015) addressed the first two limitations and showed that the Köppen-based performance metrics are quite insensitive to alternative choices of observational reference data or to differences in model resolution. The synthetic analysis by Tapiador et al. (2019) also revealed that uncertainties are not attributable to the model grid size or limitations in the reference datasets but more likely to the deficiencies in model physics. For the resolution problem, Belda et al. (2015) also indicated that there is no clear tendency for GCMs to improve the climate classification at higher resolution. Finer resolution might improve the results when the level of climate subtype is added into the classification or when regional models rather than GCMs are applied, which require a more accurate representation of surface characteristics (Belda et al., 2015). Concerning the model deficiencies, the inaccuracy of the precipitation estimation is the major contributor to the uncertainties (Tapiador et al., 2019). The deficiencies in the model physics are known to greatly affect the model precipitation outputs because the ability of GCMs to recreate the spatial distribution of precipitation is largely related to their reflection of the

large-scale atmospheric circulation, land surface modeling, and other physical aspects of model design (Zhang et al., 2017).

To ensure better simulation results of climate classification, the multi-model ensemble mean or other preprocessing methods, such as the delta-change method (Hanf et al., 2012), have been utilized to account for the bias effects on the threshold-based classification scheme. However, the multi-model ensemble mean has shown poorer performance than some individual models (Belda et al., 2015; Zhang et al., 2017). This finding is contrasted to the cases involving single-variable simulations, where multi-model ensembles achieve better results than any single model (Weigel et al., 2008; Zhang et al., 2016). A possible explanation is that unlike variables, the climate classification schemes integrate multiple aspects of air temperature and precipitation fields and therefore no simple cancellation of errors can be expected (Belda et al., 2015). As suggested by Zhang et al. (2017), applying models with comparatively better performance than others in an ensemble is the best approach to obtain optimal results.

2.7 Conclusion

This article has reviewed the literature on the application of the Köppen climate classification scheme to detect the spatial shifts of large-scale climatic conditions. First, the article discussed the definitions of Köppen climate zones, summarized the current Köppen map products, and then reviewed the results of the previous studies on the detection and assessment of the past and projected changes in the global Köppen climate zones.

A growing body of literature applied Köppen classification schemes to estimate how large the observed and projected shifts between different climate classes are, to detect the first-order

bioclimatic influence of the past, or of future climate change projected via climate model simulations. Köppen climate zones demonstrate a strong correlation with major biome distribution and can incorporate the amplitude and seasonal phase of temperature and precipitation annual cycles, thus providing a highly effective means to simplify spatial variability and aggregate climate gradients into simple but ecologically meaningful classes. Future studies should focus on the application and improvement of the Köppen classification scheme to indicate the potential changes in biomes and ecosystems, which can provide valuable insights into the bioclimatic changes under global warming.

The increased availability of globally gridded datasets of climatic variables allowed for the generation of maps for the global distribution of Köppen climate types. Most existing Köppen climate classification world maps have a relatively low resolution of 0.5°. Current single or non-comparable period coverage cannot sufficiently fulfill the needs of change detection research. Further applications of Köppen climate maps in the detection of interannual or interdecadal changes in climate zones require continuous long-term temporal coverage and more accurate depiction of fine-grained climatic conditions. There exists a great need to compile a long-term time series of global maps of the Köppen climate classification with high resolution and improved accuracy.

The recent accelerated global warming since the 1980s has led to large-scale shifts in macro climatic conditions over approximately 5.3–5.7% (7.9–8.5 million km^2) of the total land area. During the 21st century, 13–20% (19.6–29.8 million km^2) of the total land area is projected to undergo climate zone changes under the high-emission RCP8.5 scenario. The arid and hot climates in the tropics and subtropics are expected to expand worldwide into the large areas of

the middle and high latitudes while the high-latitude climates are projected to shift poleward and upward, leading to a significant area shrinkage.

The area changes and latitude and elevation shifts, together with their decadal trends for each climate zone from observations and projections have been examined previously using both observations and projections. The tropical (A) climate zone experienced large area variations in the second half of the 20th century. The increase in the area of the tropical (A) climate zone is largely caused by the expansion of the savanna (Aw) climate zone into the low-latitude mountainous regions in the tropics. The largest climate zone, the arid (B) climate zone, experienced the most conspicuous area expansion in the second half of the 20th century, primarily at the expense of temperate (C) and boreal (D) climates. This trend is mainly attributed to the large increase in the area of the subtype semi-arid (BS) climate. In the temperate (C), boreal (D), and polar (E) climate zones, significant poleward shifts have been detected in the observations since the 1950s. Although observations show insignificant changes in the area of the temperate (C) and boreal (D) climate zones, the projections suggest a small decrease in the area of the two climate zones by the end of the 21st century under RCP8.5. Within the two climate zones, a large fraction changes from cold summer climates (Cwc and Dfc) to hot summer climates (Cwa and Cfa). The prominent shrinkage of the polar (E) climate zone is projected to occur not only in high latitudes but also in high elevations of the Himalayas and the Andes in middle and low latitudes.

One of the existing problems is that, according to the assessment results of model simulations for climate zone distribution, large areas of climate zones were misclassified by the GCMs compared to the reference climate zones established by observational data, ranging from 20% to 50% of the total land area. The uncertainties are not attributable to the model grid size or

limitations in the reference datasets but more likely to be attributed to the deficiencies in the model physics. Further systematic methods to evaluate and optimize the model performance for the detection of future changes in global climate zones are needed.

In addition to these climate zone changes, changes in biomes and their constituent ecosystems are also expected to occur. As a primary driver of the biological processes ranging from individuals to ecosystems, climate constrains ecosystem functions and species distribution. The changes in the climate distribution can impose a significant threat to ecosystems and biodiversity. The global shifts of the warmer and drier climate zones into higher latitudes and elevations indicate a substantial risk to the vulnerable species and vegetation in the transition zones or at the edges of mountainous regions. Although there are some mechanisms allowing species to cope with warming, such as shifting biogeographic ranges and altering phenology to accommodate changes in ambient temperature, shifts in species distribution and abundance can substantially increase the risk of extinction by altering the community structure and disrupting ecological interactions and ecosystem functioning. The magnitude of disruptions in ecosystems will be strongly determined by the time frame, pace, and direction of the climate zone changes. There is an urgent need to address the large-scale bioclimatic impacts of global climate zone change and the resulting concerns related to the vulnerability, adaptability, and resilience of species living in mountainous regions and climate transition zones.

2.8 Supplementary materials

Table 2-S1 Summary of existing global maps of Köppen climate classification

Product	Reference	Data	Stations	Accuracy[*]	Time Period	Spatial Resolution	Format	URL
Historical and Present Climate Classification Maps								

Title	Reference	Var	Data	Stations	Agreement	Period	Resolution	Format	URL
World Map of the Köppen-Geiger Climate Classification Updated	Kottek et al., 2006	T	CRU TS 2.1	7,000-17,000	66.1%	1951-2000	0.5º	Image ASCII	http://koeppen-geiger.vu-wien.ac.at/present.htm
		P	GPCC VASClimO v1.1	9,343					
New gridded maps of Köppen climate classification	Grieser, Gommes, Cofield, & Bernardi, 2006	T	CRU TS 2.1	7,000-17,000		1951-2000 1951-1975 1961-1990 1976-2000	0.5º	Csv IDA GeoTiff	http://www.fao.org/nr/climpag/globgrids/kc_classification_en.asp
		P	CRU TS 2.1 GPCC VASClimO v1.1 GPCC Full Data	10,000 9,343 40,000					
Updated world map of the Köppen-Geiger climate classification	Peel et al., 2007	T	GHCN 2.0	4,844	70.9%	1951-2000	0.1º	KML ASCII	https://people.eng.unimelb.edu.au/mpeel/koppen.html
		P	GHCN 2.0	12,396					
Observed world maps of the Köppen-Geiger climate classification	Rubel & Kottek, 2010	T	CRU TS 2.1	7,000-17,000		1901-1925 1926-1950 1951-1975 1976-2000	0.5º	ASCII Shapefile KMZ	http://koeppen-geiger.vu-wien.ac.at/shifts.htm
		P	GPCC Full Data	40,000					
Historical data of Köppen-Geiger climatic zones	Kriticos et al., 2012	T	Worldclim V1	24,542	73.4%	1961-1990	0.167 º 0.5º	ESRI grid shapefile	https://www.climond.org/Koppen.aspx
		P	Worldclim V1	47,554					
Observed climate according to the Köppen-Trewartha climate classification	Belda et al., 2014	T	CRU TS 3.1	7,000-17,000		1901-2005 (30-yr internal)	0.5º	Image	http://kfa.mff.cuni.cz/projects/trewartha/obs.php
		P	CRU TS 3.1	7,000-17,000					
High Resolution World Map of the Köppen-Geiger Climate Classification Updated	Kottek et al., 2006; Rubel, Brugger, Haslinger, & Auer, 2017	T	CRU TS 2.1	7,000-17,000		1986-2010	0.083º 0.167º 0.5º	R Raster KMZ	http://koeppen-geiger.vu-wien.ac.at/present.htm
		P	GPCC VASClimO v1.1	9,343					
Present Köppen-Geiger climate classification maps	Beck et al., 2018	T	CRU TS 4.01, CHELSA V1.2, WorldClim V1 & V2	34,542	80.0%	1980-2016	0.0083º 0.083º 0.5º	GeoTiff	http://www.gloh2o.org/koppen/
		P	GPCC FDR V7, CHELSA V1.2, CHPclim V1, WorldClim V1 & V2	20,268					

Future Climate Classification Maps

Projected world maps of the Köppen-Geiger climate classification	Rubel & Kottek, 2010	Model	TYN SC 2.0 (CGCM2, CSIRO-MK 2.0, DOE PCM, HadCM3, ECHam4)			2001-2025 2026-2050 2051-2075 2076-2100	0.5º	ASCII Shapefile KMZ	http://koeppen-geiger.vu-wien.ac.at/shifts.htm
		Scenario	IPCC IV SRES (A1F1, A2, B1, B2)						
		Model	CSIRO-MK 3.0, MIROC-H			2001-2030	0.167 º		

				2021-2050	0.5º		
Future scenario data of Köppen-Geiger climatic zones	Kriticos et al., 2012	Scenario	IPCC IV SRES (A1B, A2)	2041-2070 2051-2080 2061-2090 2071-2100		ESRI grid shapefile	https://www.climond.org/Koppen.aspx
Future Köppen-Geiger climate classification maps	Beck et al., 2018	Model Scenario	32 CMIP5 GCMs RCP8.5	2071-2100	0.0083º 0.083º 0.5º	GeoTiff	http://www.gloh2o.org/koppen/

* The percentage of correct classes calculated using stations observations as reference (22,078 stations from GHCN-D and GSOD) from Beck et al., 2018

Table 2-S2 Summary of observed area changes in climate zones in the past century

Reference	Method	Data	Time Period	Scale	Significant Shrinkage	Significant Expansion	No Significant Area Changes	Total Area Change
Observed climate zone changes based on KGC since the 1900s								
Rohli, Andrew et al., 2015	Updated KGC	NCAR Reanalysis	1901-1925 1976-2000	25-yr 25-yr	E (-0.69%)	B (0.68%)	C (-0.03%) D (-0.24%) A (0.27%)	-
Chen & Chen, 2013	Original KGC	UD	1901-2010 1981-2010	long-term 30-yr	E (-0.53%)	B (0.87%)	A (0.05%) C (-0.07%) D (-0.31%)	-
Kalvová, Halenka, Bezpalcová, & Nemešová, 2003	Original KGC	CRU	1901−1921 1961−1990	20-yr 30-yr	E (-0.50%)	A (0.44%) D (0.35%)	B (-0.13%) C (-0.16%)	-
Observed climate zone changes based on KTC since the 1900s								
Belda et al., 2014	KTC w/ Patton threshold	CRU	1901-1930 1976-2005	30-yr 30-yr	F (-0.66%) E (-0.41%)	D (0.82%) A (0.38%)	B (0.04%) C (-0.17%)	5.08%
Fraedrich, Gerstengarbe, & Wnerner, 2001	KTC w/ Patton threshold	CRU	1901-1915 1981-1995	15-yr 15-yr	F (-1.07%)	A (0.46%)	B, C, D, E	4.4%
Observed climate zone changes based on KGC since the 1950s								
Chan & Wu, 2015	Updated KGC	UD, CRU, GISS	1950-1964 1989-2003	15-yr 15-yr	D-SH (-1.06±0.08%) E (-0.98±0.05%)	B (1.51±0.10%) D-NH (0.79±0.4%)	A (-0.15±0.10%) D (-0.28±0.04%) C (-0.39±0.18%)	5.7%
Beck, Grieser, Kottek, Rubel, & Rudolf, 2005	Original KGC	CRU, VASClimO	1951-2000 1986-2000	long-term 15-yr	E (-0.53%) D (-0.46%)	B (0.78%)	A (0.09%) C (0.12%)	3.3%

Estimated percentage of total land area that have experienced climate zone changes in the past century. All the area changes are represented by the changes in the percentage of total land area (approximately 148.94 million km^2).

Table 2-S3 Summary of future projected future area changes of climate zones by the end of the 21st century

Reference	Method	Data	Time Period	Scale	Significant Shrinkage	Significant Expansion	Not Conclusive	Total Area Change
Projected climate zone changes based on KGC by the end of the 21st century								
Beck et al., 2018	Updated KGC	CRU, GPCC, CHELSA, CHPclim, WorldClim; 32 CMIP5 GCMs	1980-2016 2071-2100	30-yr	E (-3.98±1.54%) D (-1.33±2.98%)	B (3.80±1.91%) A (2.16±1.28%)	C (-0.37±2.43%)	13.36% (RCP8.5)
Chan & Wu, 2015	Updated KGC	32 CMIP5 GCMs	2010-2100	15-yr	E (-3.29±0.81%) D (-2.42±2.62%) E (-1.77±0.67%) D (-0.13±1.21%)	B (3.09±3.01%) A (1.75±1.61%) B (1.34±1.21%) A (1.01±1.07%)	C (-0.07±1.68%) C (-0.47±0.94%)	- (RCP8.5) - (RCP4.5)
Rohli, Andrew et al., 2015	Updated KGC	NCAR Reanalysis	1981-2010 2076-2100	25-yr	E (-3.32%)	A (2.53%) B (0.94%)	D (0.18%) C (-0.24%)	28% (A1FI)
Mahlstein et al., 2013	Original KGC	13 CMIP5 GCMs	1900–2098	5-yr	E	B	A, C, D	20% (RCP8.5)
Hanf et al., 2012	Original KGC	7 GCMs	1980–2099	20-yr	D, E	A, B	C	-
Rubel & Kottek, 2010	Original KGC	CRU, GPCC; 5 GCMs	1976-2000 2076-2100	25-yr	E (-4.11±1.14%) D (-2.14±4.66%) E (-2.94±1.33%)	A (3.04±1.44%) B (2.68±2.54%) A (2.27±1.01%) B (0.93±1.27%)	C (0.53±3.37%) D (0.13±1.25%) C (-0.38±0.97%)	18.32% (A1FI) 11.15% (B1)
Projected climate zone changes based on KTC by the end of the 21st century								
Belda et al., 2016	KTC w/ Patton's threshold	CRU; 30 CMIP5 GCMs	1961-1990 2071-2100	30-yr	E (-5.82±3.30%) F (-4.29±1.93%) C (-1.31±1.24%)	B (5.07±2.04%) D (3.93±1.39%) A (3.05±2.06%)	-	20% (RCP8.5)
Feng et al., 2014	KTC w/ aridity threshold	CPC, UD; 20 CMIP5 GCMs	1961-1990 2071-2100	15-yr	E (-10.4±3.5%) F (-5.6±1.0%) C (-1.9±1.1%) E (-5.4±2.7%) F (-3.8±1.1%) C (-1.9±0.7%)	D (8.0±2.7%) B (6.6±2.2%) A (3.3±1.1%) D (4.9±2.6%) B (3.5±1.2%) A (2.7±0.9%)	- -	46.3±7.5% (RCP8.5) 31.4±7.6% (RCP4.5)
Projected climate zone changes based on KGC by the middle of the 21st century								
Kalvová et al., 2003	Original KGC	4 GCMs	1961-1990 2036-2065	30-yr	D (-2.28±1.54%) E (-1.80±0.98%)	B (2.41±0.66%) A (2.06±1.21%)	C (-0.47±0.98%)	-
Projected climate zone changes based on KTC by the middle of the 21st century								
Feng et al., 2014	KTC w/ aridity threshold	CPC, UD; 20 CMIP5 GCMs	1961-1990 2036-2065	15-yr	E (-5.2±2.3%) F (-3.8±1.0%) C (-1.9±0.6%) E (-3.8±1.9%) F (-3.2±1.0%) C (-1.6±0.6%)	D (4.7±2.2%) B (3.6±1.4%) A (2.7±0.8%) D (3.7±2.0%) B (2.7±1.2%) A (2.2±0.7%)	- -	31.2±6.9% (RCP8.5) 25.5±6.4% (RCP4.5)

Chapter 3: A 1 km global dataset of historical and future Köppen–Geiger climate classification and bioclimatic variables

3.1 Abstract

The Köppen–Geiger classification scheme provides an effective and ecologically meaningful way to characterize climatic conditions and has been widely applied in climate change studies. Significant changes in the Köppen climates have been observed and projected in the last 2 centuries. Current accuracy, temporal coverage and spatial and temporal resolution of historical and future climate classification maps cannot sufficiently fulfill the current needs of climate change research. Comprehensive assessment of climate change impacts requires a more accurate depiction of fine-grained climatic conditions and continuous long-term time coverage. Here, we present a series of improved 1 km Köppen–Geiger climate classification maps for six historical periods in 1979–2013 and four future periods in 2020–2099 under RCP2.6, 4.5, 6.0, and 8.5. The historical maps are derived from multiple downscaled observational datasets, and the future maps are derived from an ensemble of bias-corrected downscaled CMIP5 projections. In addition to climate classification maps, we calculate 12 bioclimatic variables at 1 km resolution, providing detailed descriptions of annual averages, seasonality, and stressful conditions of climates. The new maps offer higher classification accuracy than existing climate map products and demonstrate the ability to capture recent and future projected changes in spatial distribution of climate zones. On regional and continental scales, the new maps show accurate depictions of

topographic features and correspond closely with vegetation distribution. We also provide a heuristic application example to detect long-term global-scale area changes of climate zones. This high-resolution dataset of the Köppen–Geiger climate classification and bioclimatic variables can be used in conjunction with species distribution models to promote biodiversity conservation and to analyze and identify recent and future interannual or interdecadal changes in climate zones on a global or regional scale. The dataset referred to as KGClim is publicly available via http://glass.umd.edu/KGClim.

3.2 Introduction

Climate has direct impacts on the processes and functioning of the ecosystem as well as on the distribution of species. (I.-C. Chen et al., 2011; Ordonez & Williams, 2013; Pinsky et al., 2013; Thuiller et al., 2005). The spatial patterns of climates have been often identified using the Köppen climate classification system. The Köppen classification system was designed to map the distribution of the world's biomes based on the amplitude and seasonal phase of annual cycles of surface air temperature and precipitation (Köppen, 1936). Compared with other human expertise based climate mapping methods (Holdridge, 1947; Thornthwaite, 1931; Walter & Elwood, 1975) and clustering approaches (Netzel & Stepinski, 2016), which suffer from a lack in meteorological basis, the Köppen classification demonstrates stronger correlation with distribution of biomes and soil types (Bockheim et al., 2005; Rohli, Joyner, et al., 2015). It provides an ecologically relevant and effective method to classify climate conditions by combining seasonal cycles of surface air temperature and precipitation (Cui, Liang, & Wang, 2021).

The Köppen classification has been widely applied in biological science, earth and planetary sciences, and environmental science (Rubel & Kottek, 2011). It is a convenient and integrated tool to identify spatial patterns of climate distribution and to examine relationships between climates and biological systems. It has been found useful for a variety of issues on climate change, such as hydrological cycle studies (Manabe & Holloway, 1975; Peel et al., 2001), Arctic climate change (Feng et al., 2012; Wang & Overland, 2004), assessment of climate change impacts on ecosystem (Roderfeld et al., 2008), biome distribution (Leemans et al., 1996; Rohli, Joyner, et al., 2015) and biodiversity (Garcia et al., 2014).

There has been a resurgence in the application of the Köppen climate classification in climate change research over the recent decades. The Köppen climate classification has been used to set up dynamic global vegetation models (Poulter et al., 2011), to characterize species composition (Brugger & Rubel, 2013), to model the species range distribution (Tererai & Wood, 2014; Webber et al., 2011), and to analyze the species growth behavior (Tarkan & Vilizzi, 2015). The Köppen classification has also been applied to detect the shifts in geographical distribution of climate zones (Belda et al., 2016; Chan & Wu, 2015; Feng et al., 2014; Mahlstein et al., 2013). It also has the potential to aggregate climate information on warmth and precipitation seasonality into ecologically important climate classes thereby simplifying spatial variability. This climate classification system adds a new direction to develop climate change metrics and can provide support for the growth of species distribution modeling (SDM).

The recent Köppen climate classification maps have a resolution ranging between 0.5° and 1-km. Early published Köppen climate classification maps have a relatively low resolution of 0.5° (Belda et al., 2014; Grieser et al., 2006; Kottek et al., 2006; Kriticos et al., 2012; Rubel & Kottek, 2010). Several map products used interpolation methods to obtain a higher resolution of

~0.1° (Kriticos et al., 2012; Peel et al., 2007; Rubel et al., 2017). Fine resolutions of at least 1-km are required to detect microrefugia and promote effective conservation. As the only 1-km global climate classification map product, Beck et al. (2018) provided global climate classification maps for two periods 1980-2016 and 2071-2100 under RCP8.5. The maps were derived using climate data from WorldClim V1 and V2 (Fick & Hijmans, 2017), CHELSA V1.2 (Karger et al., 2017), and CHPclim V1 (Funk et al., 2015). To represent historical climates, they adjusted the inconsistent temporal spans of climatology datasets to the period 1980-2016, by adding interpolated temperature change offsets or multiplying precipitation factors, which may lead to biased coverage of the historical period. Current classification accuracy, temporal coverage, spatial and temporal resolution of historical and future climate classification maps cannot sufficiently fulfill the current needs of climate change research. Significant changes in the Köppen climates have been observed and projected in the recent two centuries (Belda et al., 2014; Chan & Wu, 2015; D. Chen & Chen, 2013; Rohli, Andrew, et al., 2015; Yoo & Rohli, 2016). Previous studies found that large-scale shifts in climate zones have been observed over more than 5% of the total land area since the 1980s, and approximately 20% of the total land area is projected to experience climate zone changes under RCP8.5 by 2100 (Cui, Liang, & Wang, 2021). Detection of recent and future changes in climate zones with the application of the Köppen climate maps needs more accurate depiction of fine-grained climatic conditions, continuous and longer temporal coverage.

This creates the urgent need for global maps of the Köppen climate classification with increased accuracy, finer spatial and temporal resolutions. Currently available global observational datasets of temperature and precipitation collected during the recent centuries, and the global climate simulations under alternative future climate scenarios have offered the possibility to create a

comprehensive dataset for past and future climates. In this study, we presented an improved

long-term Köppen-Geiger climate classification map series for 1) six historical 30-yr periods of

the observational record (1979-2008,1980-2009, 1981-2010, 1982-2011, 1983-2012, 1984-2013)

and four future 30-yr periods (2020-2049, 2040-2069, 2060-2089, 2070-2099) under four RCPs

(RCP2.6, 4.5, 6.0 and 8.5). To improve the classification accuracy and achieve a resolution as

fine as 1-km (30 arc-second), we combined multiple datasets, including WorldClim V2 (Fick &

Hijmans, 2017), CHELSA V1.2 (Karger et al., 2017), CRU TS v4.03 (New et al., 2000), UDEL

(Willmott & Matsuura, 2001), GPCC datasets (C. Beck, Grieser, Rudolf, et al., 2005) and bias-

corrected downscaled Coupled Model Intercomparison Project Phase 5 (CMIP5) model

simulations (Navarro-Racines et al., 2020) (Table 3-1). We used the WorldClim Historical

Climate Data V2 (Fick & Hijmans, 2017) to downscale the 0.5° climatology datasets including

CRU, UDEL and GPCC, and derive high resolution climate data for the historical periods. To

determine the final climate class, we used the climate class with the highest agreement level from

an ensemble of climate maps derived from different combinations of surface air temperature and

precipitation products, as implemented in Beck et al. (2018). In addition to the Köppen-Geiger

climate maps, we also calculated 12 bioclimatic variables at the same 1-km resolution using

these climate datasets for the same historical and future periods. This dataset can be used in

conjunction with SDMs to promote biodiversity conservation, or to map plant functional type

distribution for earth system model simulations, or to analyze and identify recent and future

changes in climate zones on a global or regional scale.

To validate the Köppen-Geiger climate classification maps, we used the station observations

from Global Historical Climatology Network-Daily (GHCN-D) (Menne et al., 2012), and Global

Summary Of the Day (GSOD) (National Climatic Data Center et al., 2015) database. At the

regional and continental scale, we compared our Köppen-Geiger climate classification maps with previous map products, associated maps of forest cover, and elevation distribution, for 1) regions with large spatial gradients in climates, including central and eastern Africa, Europe, North America, and 2) regions with sharp elevation gradients, including Tibetan Plateau, central Rocky Mountains, central Andes. Further, we conducted sensitivity analysis with respect to temporal scale, dataset input, and data integration methods. We also provided a heuristic example which used climate classification map series to detect the long-term area changes of climate zones, showing how the Köppen-Geiger climate classification map series can be applied in climate change studies.

3.3 Climatology datasets

Table 3-1 Climatology datasets to generate global maps of the Köppen climate classification

Dataset	Usage	Spatial Res.	Temporal Span	Variable	Source and Description
Present Köppen classification map series with resolution of 30 arc-second (1km)					
CRU	Map Input	0.5°	1979-2017	T	Climatic Research Unit (CRU) TS v4.03
UDEL	Map Input	0.5°	1979-2017	T, P	U. of Delaware Precipitation and Air Temperature
WorldClim	Downscaling	0.0083°	1970-2000	T, P	WorldClim Historical Climate Data V2
CHELSA	Map Input	0.0083°	1979-2013	T, P	Climatologies at high resolution for the earth's land surface areas (CHELSA)
GPCC	Map Input	0.5°	1979-2016	P	Global Precipitation Climatology Centre (GPCC)
PREC/L	Data Selection	0.5°	1979-2012	P	NOAA's PRECipitation REConstruction over Land (PREC/L)
GHCN_CAMS	Data Selection	0.5°	1979-2017	T	GHCN_CAMS Gridded 2m Temperature (Land)
Future Köppen classification map series with resolution of 30 arc-second (1km)					
CMIP5	Map Input	0.0083°	2020-2100	T, P	CCAFS-Climate Statistically Downscaled Delta Method CMIP5 data

WorldClim	Downscaling	0.0083°	1970-2000	T, P	WorldClim Historical Climate Data V2

Table 3-1 lists the climatology datasets with global coverage and on a monthly time step, used to generate historical and future Köppen-Geiger climate map series. The present 1-km Köppen-Geiger classification map series for 1979-2013 was derived from the Climatologies at High-resolution for the Earth's Land Surface Areas (CHELSA) V1.2 (Karger et al., 2017), WorldClim Historical Climate Data V2 (Fick & Hijmans, 2017) and the statistically downscaled Climatic Research Unit (CRU) TS v4.03 (New et al., 2000), University of Delaware Precipitation and Air Temperature (UDEL) (Willmott & Matsuura, 2001) and Global Precipitation Climatology Centre (GPCC) (C. Beck, Grieser, Rudolf, et al., 2005) datasets. To decide the datasets to use, we conducted a sensitivity analysis on the input climatology datasets and utilized monthly air temperature datasets from CRU, UDEL, GHCN_CAMS Gridded 2m Temperature (Fan & Dool, 2008) and monthly precipitation datasets from GPCC, UDEL, NOAA's PRECipitation REConstruction over Land (PREC/L) (M. Chen et al., 2002). Evaluation results indicated that incorporating only CRU, UDEL temperature datasets and UDEL, GPCC precipitation datasets and excluding GHCN_CAMS and PREC/L datasets led to higher accuracy in the classification results. Therefore, we chose CRU, UDEL, and GPCC datasets as the classification system input to boost the final accuracy.

To explicitly correct the topographic effect, we used 1-km CHELSA V1.2 and WorldClim V2 datasets in addition to the 0.5° resolution datasets. The CHELSEA dataset statistically downscaled temperature data from the ERA-Interim climatic reanalysis. For precipitation data, it incorporated multiple orographic predictors and performed bias correction (Karger et al., 2017).

With major topo-climatic drivers considered, the CHELSA dataset demonstrated good performance in ecological science studies. CHELSA data exhibited comparable accuracy for temperatures and better predicted precipitation patterns based on the validation results.

We produced the future Köppen classification map series using the CCAFS climate statistically bias-corrected and downscaled CMIP5 projections (Navarro-Racines et al., 2020). The CCAFS presented a global database of future climates developed by a climate model bias correction method based on the CMIP5 GCM simulations (Taylor et al., 2012) archive, coordinated by the World Climate Research Programme in support of the IPCC Fifth Assessment Report (AR5) (Hartmann et al., 2013). The total is 35 GCMs, and all RCPs, RCP 2.6, 4.5, 6.0 and 8.5 (Table 3-S1). Projections are available at varied coarse scales (70–400km). To achieve high-resolution (1km) climate representations, downscaling method has been applied with the use of the WorldClim data. Technical evaluation showed that the bias-correction method that CCAFS data applied reduced climate model bias by 50–70%, which could potentially address the bias issue in model simulations for the threshold-based Köppen classification scheme (Navarro-Racines et al., 2020).

3.4 Methodology

3.4.1 Köppen-Geiger climate classification

Table 3-2 Criteria of the Köppen-Geiger climate classification

1st	2nd	3rd	Description	Criterion
A			Tropical	Not (B) & $T_{cold} \geq 18$
	f		- Rainforest	$P_{dry} \geq 60$
	m		- Monsoon	Not (Af) & $P_{dry} \geq 100 - MAP/25$
	w		- Savannah	Not (Af) & $P_{dry} < 100 - MAP/25$
B			Arid	$MAP < 10 \times P_{threshold}$

	W			- Desert	$MAP<5\times P_{threshold}$
	S			- Steppe	$MAP\geq5\times P_{threshold}$
		h		-- Hot	$MAT\geq18$
		k		-- Cold	$MAT<18$
C				Temperate	Not (B) & $T_{hot}>10$ & $-3<T_{cold}<18$
	w			- Dry winter	$P_{wdry}<P_{swet}/10$
	s			- Dry summer	Not (w) & $P_{sdry}<40$ & $P_{sdry}<P_{wwet}/3$
	f			- Without dry season	Not (s) or (w)
		a		-- Hot summer	$T_{hot}\geq22$
		b		-- Warm summer	Not (a) & $T_{mon10}\geq4$
		c		-- Cold summer	Not (a or b) & $1\leq T_{mon10}<4$
D				Boreal	Not (B) & $T_{hot}>10$ & $T_{cold}\leq-3$
	w			- Dry winter	$P_{wdry}<P_{swet}/10$
	s			- Dry summer	Not (w) & $P_{sdry}<40$ & $P_{sdry}<P_{wwet}/3$
	f			- Without dry season	Not (s) or (w)
		a		- Hot summer	$T_{hot}\geq22$
		b		- Warm summer	Not (a) & $T_{mon10}\geq4$
		c		- Cold summer	Not (a), (b) or (d)
		d		- Very cold winter	Not (a) or (b) & $T_{cold}<-38$
E				Polar	Not (B) & $T_{hot}\leq10$
	T			- Tundra	$T_{hot}>0$
	F			- Frost	$T_{hot}\leq0$

Temperature in oC and precipitation in mm. MAT = mean annual air temperature (°C); T_{cold} = the air temperature of the coldest month (°C); T_{hot} = the air temperature of the warmest month (°C); T_{mon10} = the number of months with air temperature >10 °C; MAP = mean annual precipitation (mm y^{-1}); P_{dry} = precipitation in the driest month (mm month^{-1}); P_{sdry} = precipitation in the driest month in summer (mm month^{-1}); P_{wdry} = precipitation in the driest month in winter (mm month^{-1}); P_{swet} = precipitation in the wettest month in summer (mm month^{-1}); P_{wwet} = precipitation in the wettest month in winter (mm month^{-1}); $P_{threshold}=2\times MAT$ if >70% of precipitation falls in winter, $P_{threshold}=2\times MAT+28$ if >70% of precipitation falls in summer, otherwise $P_{threshold}=2\times MAT+14$.

The Köppen climate classification scheme was first introduced by Wladimir Köppen (Köppen, 1936). It is one of the earliest quantitative classification systems of Earth's climates. Its modification, the Köppen-Geiger classification (KGC) was first published in 1936, developed by Wladimir Köppen and Rudolf Geiger. KGC identifies climates based on their effects on plant growth from the aspects of warmth and aridity and classifies climate into five main climate classes and 30 subtypes (Rubel & Kottek, 2011). The five main climate zones distinguish between plants of the tropical climate zone (A), the arid climate zone (B), the temperate climate zone (C), the boreal climate zone (D) and the polar climate zone (E), referring to the five major

climate zones (Sanderson, 1999). All these main climate zones are thermal zones except the arid (B) climate zone, which is defined based on precipitation threshold.

This research followed the Köppen-Geiger climate classification as described in Kottek et al. (2006), and Rubel and Kottek (2010). This latest version of the KGC scheme was first presented by Geiger (1961) (Table 2). Several existing Köppen-Geiger climate map products, including Peel et al. (2007), Kriticos et al. (2012), and Beck et al. (2018) applied the KGC scheme modified following Russell (1931). Russell (1931) adjusted the definition of the boundary of temperate (C) and boreal (D) climate zones using the coldest monthly temperature > 0 °C instead of >-3 °C. This threshold was proposed because the 0°C line fits the distribution of the topographical features and vegetation in western United States, where at that time meteorological stations were sparsely distributed (Jones, 1932). However, the application of the 0°C boundary to the global climates has not been validated. Therefore, this research didn't utilize Russell's modification (1931) and followed the latest version KGC proposed by Geiger (1961).

3.4.2 Statistical downscaling
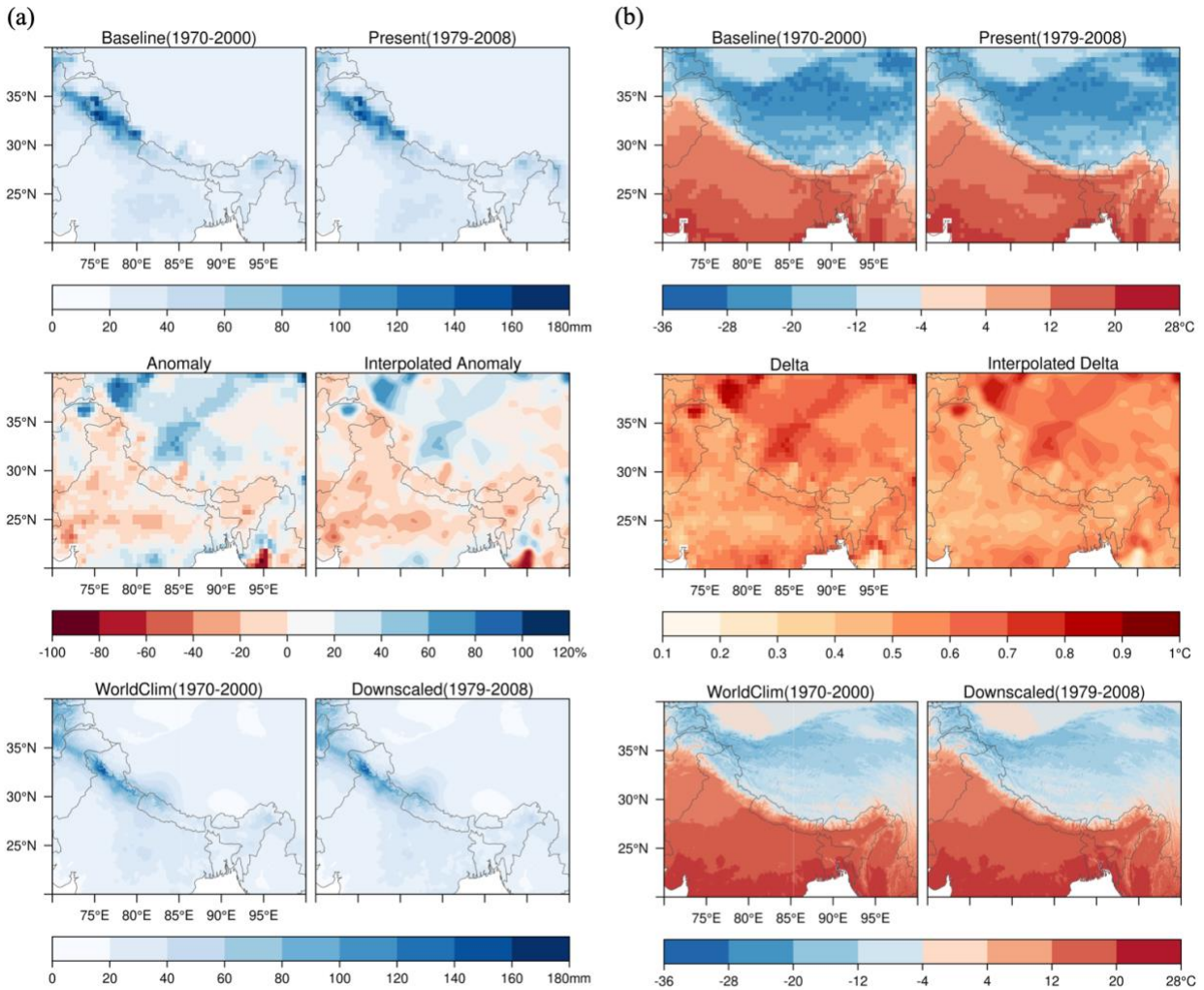
Figure 3-1. Illustration of downscaling process. (a) Anomaly downscaling method with January total precipitation from GPCC dataset and (b) delta downscaling method with January temperature from CRU dataset. Baseline (1970-2000) and present-day climate data (e.g., 1979-2008) are from CRU, UDEL, or GPCC datasets, which have a coarse spatial resolution of 0.5°. Precipitation anomaly is the change factor of monthly precipitation from baseline to present-day climates. Temperature delta is change in monthly air temperature from baseline to present-day climates. WorldClim (1970-2000) climate data is adjusted by multiplying 30 arc-second interpolated anomaly (for precipitation) or adding 30 arc-second interpolated delta (for temperature) to generate the downscaled climate surfaces with 30 arc-second resolutions. Precipitation values in mm/month and temperature values in °C.

Due to limited number of available observational datasets with high resolution and long-term continuous temporal coverage, the research implemented the delta method by applying a delta change or change factor (Hay et al., 2000) onto the WorldClim historical observations (Fick &

Hijmans, 2017) to achieve 30-yr average climatology data with a 1-km resolution based on the CRU, UDEL and GPCC datasets. The delta method is a statistical downscaling method that assumes that the relationship between climatic variables remains relatively constant at local scale (Wilby and Wigley, 1997). We applied the delta method to downscale the long-term (30-yr) mean climates using coarse-resolution monthly climatology datasets. The delta changes or change factors are calculated as the differences between the 30-yr long-term means of temperature or precipitation of baseline (1970-2000) and present-day climates. The delta method comprises the following four steps: 1) calculate 30-yr averages for baseline (1970-2000) and present day of monthly temperature and precipitation; 2) calculate anomaly for precipitation and delta for temperature; 3) apply thin-plate splines interpolation (TPS) to create 1km surface of precipitation anomaly and temperature delta; 4) multiply anomaly or add delta to historical climates based on WorldClim dataset (Figure 3-1).

First, using monthly time series from CRU, UDEL and GPCC datasets, we calculated 30-yr means as a baseline (1970-2000), for each climatology dataset and each variable. We used 1970-2000 as the baseline period, for consistency with WorldClim Historical Climate Data V2. Next, we calculated 30-yr means for each month and each 30-yr present-day period in 1979-2013 We then calculated anomalies as proportional differences between present-day and baseline in total precipitation and delta as difference in temperature. To derive 30 arc-second (1-km) anomaly or delta surfaces, we applied thin-plate splines (TPS) interpolation (Franke, 1982; Schempp et al., 1977; Craven and Wahba, 1978) on precipitation anomaly and temperature delta. TPS has been widely used in climate science (Hijmans et al., 2005; Navarro-Racines et al., 2020) as it produced a smooth and continuous surface, which is infinitely differentiable. Last, we multiplied

the change factor or added the delta to the WorldClim (1970-2000) data to get downscaled present-day monthly climate data.

Our future Köppen-Geiger map series are based on an ensemble of maps derived from the CCAFS bias-corrected and downscaled climate projections, which include 35 CMIP5 GCMs, and 4 RCPs (Navarro-Racines et al., 2020). Large misclassifications exist within the GCMs as detected in previous assessment of large areas ranging between 20-50% of the total land area (Cui, Liang, & Wang, 2021). Deficiencies in model physics are also more likely to contribute to uncertainties in the maps than grid size or reference dataset limitations (Tapiador et al., 2019). Multi-model mean and delta-change methods can mitigate the bias effects from the threshold-based classification scheme and have been utilized to simulate better results of climate classification (Hanf et al., 2012). Therefore, we chose the CCAFS bias-corrected and downscaled CMIP5 projections (Navarro-Racines et al., 2020) to reduce the amplified errors due to uncertainty of climate projections. Navarro-Racines et al. (2020) interpolated anomalies of original GCM outputs using thin plate spline spatial interpolation to achieve a baseline climate with a 1km surface. Then they applied the delta method to the interpolated baseline climates to correct the model biases (Hay et al., 2000; Ho et al., 2012).

3.4.3 Data integration
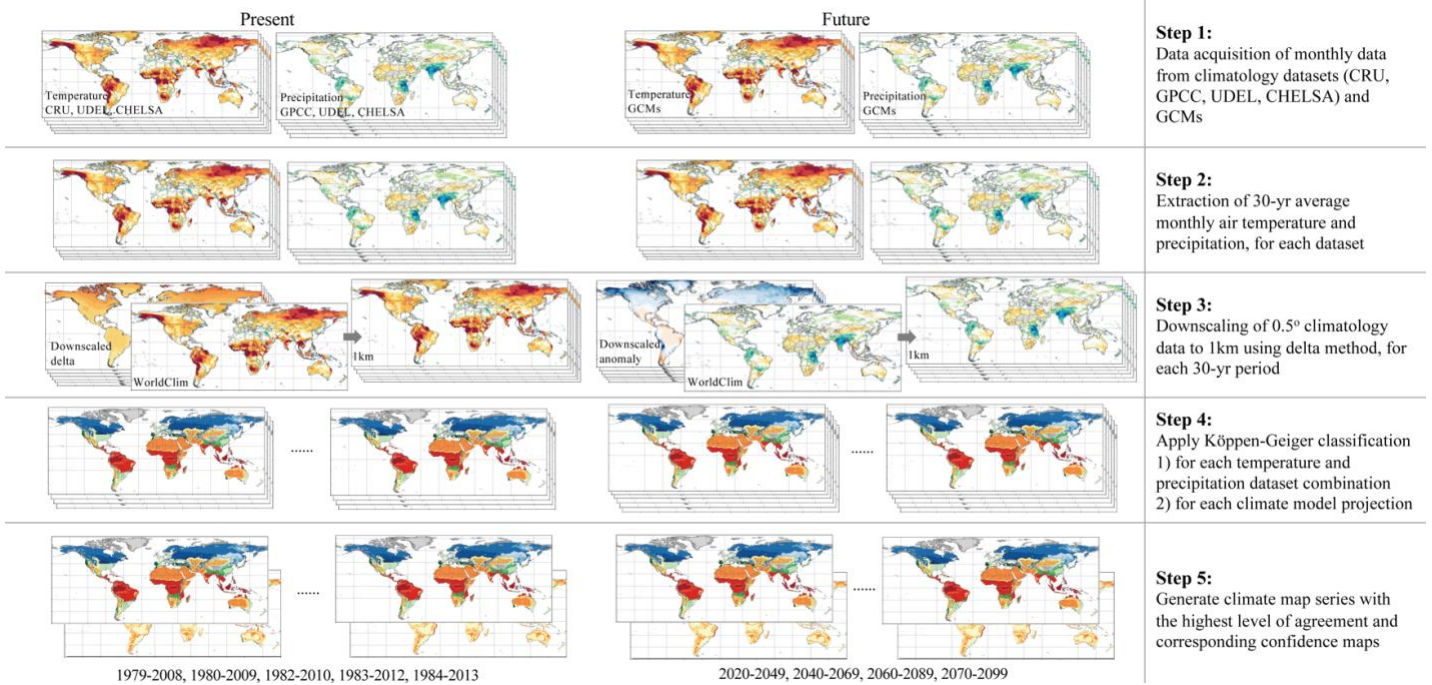
Figure 3-2 Step by step process to generate Köppen-Geiger climate map series

The historical Köppen-Geiger climate classification map series was generated using the highest

confidence class from an ensemble of maps using all combinations of surface air temperature and

precipitation products (Figure 3-2), as described in Beck et al. (2018). The highest confidence

was given to the most common climate class for each grid cell. The final historical climate map

series were derived using the climate class with the highest level of confidence in an ensemble of

$3 \times 3 = 9$ classification maps based on combinations of the 3 precipitation datasets (CRU,

UDEL, and CHELSA) and 3 surface air temperature datasets (GPCC, UDEL, and CHELSA). To

further test the sensitivity of the method using the climate with the highest level of agreement,

we incorporated another data integration method using the mean of multiple datasets. We

quantified the degree of confidence placed in the Köppen-Geiger climate map series using the

degree of confidence at the grid cell level calculated by dividing the occurrence frequency of the

climate class with the highest level of agreement by the ensemble size. The calculated

confidence level can be viewed as the agreement degree in classification results derived from different climatology datasets.

The future Köppen-Geiger climate classification map series under 4 RCPs, were derived based on the most common climate class from an ensemble of future climate maps. We generated a future Köppen-Geiger climate classification map for each climate model projection, using the CCAFS bias-corrected and downscaled CMIP5 GCM dataset. For example, the future Köppen-Geiger climate classification map series under RCP8.5 was derived from an ensemble of 30 maps based on 30 CMIP5 models. The level of confidence was estimated using the ratio between the frequency of the climate class with the highest level of agreement in the future map results, and the ensemble size.

3.4.4 Validation

We validated the historical climate maps using the station observations from Global Historical Climatology Network-Daily (GHCN-D) (Menne et al., 2012) and Global Summary Of the Day (GSOD) database (National Climatic Data Center et al., 2015) as reference data. GHCN-D dataset provides daily climate data over global land areas and contains records from over 80,000 weather stations worldwide, about one third of which have both temperature and precipitation data available (Menne et al., 2012). GSOD dataset includes global daily summary data over 9,000 stations, of which the historical data from 1973 being the most complete (National Climatic Data Center et al., 2015). For each station, time series of monthly temperature and precipitation were calculated from the daily observations with months with <15 daily values discarded. Then if ≥6 months are present, monthly climatology were generated subsequently by averaging the monthly means for the given 30-yr period. We removed duplicate stations in the

two datasets and discarded stations with gap years or missing data in the given 30 years. For each

station and each 30-yr period, we applied the Köppen-Geiger climate classification, and then

evaluated overall classification performance for each climate map using total accuracy, which is

defined as the percentage of correct classes, and average precision, which is the averaged

fraction of correct classification for all climate classes.

Using the same validation datasets and station selection process, we also evaluated the previous

climate maps from Beck et al., (2018) Kriticos et al., (2012), Peel et al., (2007), and Kottek et al.,

(2006). We applied the same Köppen-Geiger climate classification criteria described in the

previous studies to assess the overall accuracy of the map products. To further validate the

climate classification results, we performed sensitivity analysis on the data integration method,

the climate classification time scale, and climatology dataset input, using the same validation

datasets from GHCN-D and GSOD. In addition, we compared the climate classification results

with forest cover and elevation maps, and with the two high-resolution comparable climate map

products, Beck et al., (2018) (1-km) and Kriticos et al., (2012) (0.167 º), at regional and

continental scale. The forest cover map we used is the 2000 30m Landsat-based forest cover map

(Hansen et al., 2013). The elevation data is from the NASA SRTM Digital Elevation 30m data

(Farr et al., 2007).

3.5 Results and Discussion

3.5.1 Historical Köppen-Geiger climate maps

Figure 3-3 Historical global maps of the Köppen-Geiger climate classification and associated confidence levels. (a) Historical maps of the Köppen-Geiger climate classification and (b) confidence levels associated with the Köppen-Geiger climate classification for the historical periods (1979-2008, 1980-2009, 1981-2010, 1982-1011, 1983-2012, 1984-2013)

Global map series of the Köppen-Geiger climate classification for historical periods and

associated corresponding confidence levels are shown in Figure 3-3. Based on the distribution of

confidence level, over 90% of the land area exhibit high levels of confidence as classification results based on different climate data show excellent agreement. Relatively lower confidence level and large discrepancy in classification results are found especially in mountainous regions such as Andes Mountains, Rocky Mountains, Tibetan Plateau, and major climate transitional zones located in mid and high latitudes of Northern Hemisphere, Central Africa, and Central Asia.

Regional distribution of climatic conditions is largely created by local variation in topography in rugged terrain (Dobrowski et al., 2013; Franklin et al., 2013). The climate classification and confidence level maps of mountainous areas of Central Rocky Mountains and Tibetan Plateau are shown in Figure 3-S1 and 3-S2 respectively. For each combination of precipitation and surface air temperature datasets, we generated a Köppen-Geiger climate classification map (see Fig. 3-S1a and 3-S2a for 1979-2008 maps for the central Rocky Mountains and Tibetan Plateau). The final Köppen-Geiger classification map is derived based on the most common climate type among all the climate maps (Figure 3-S1b and 3-S2b). We then calculated corresponding confidence levels to quantify the uncertainty in the classification maps (Figure 3-S1c and 3-S2c). The uncertainty in climate classification in mountainous areas is attributed to the uncertainty existing in climate data, especially precipitation data. In rugged terrain, CHELSA precipitation data shows more detailed precipitation patterns, causing disagreement in classification results of the 3rd level climate classes which depict precipitation seasonality.

3.5.2 Validation
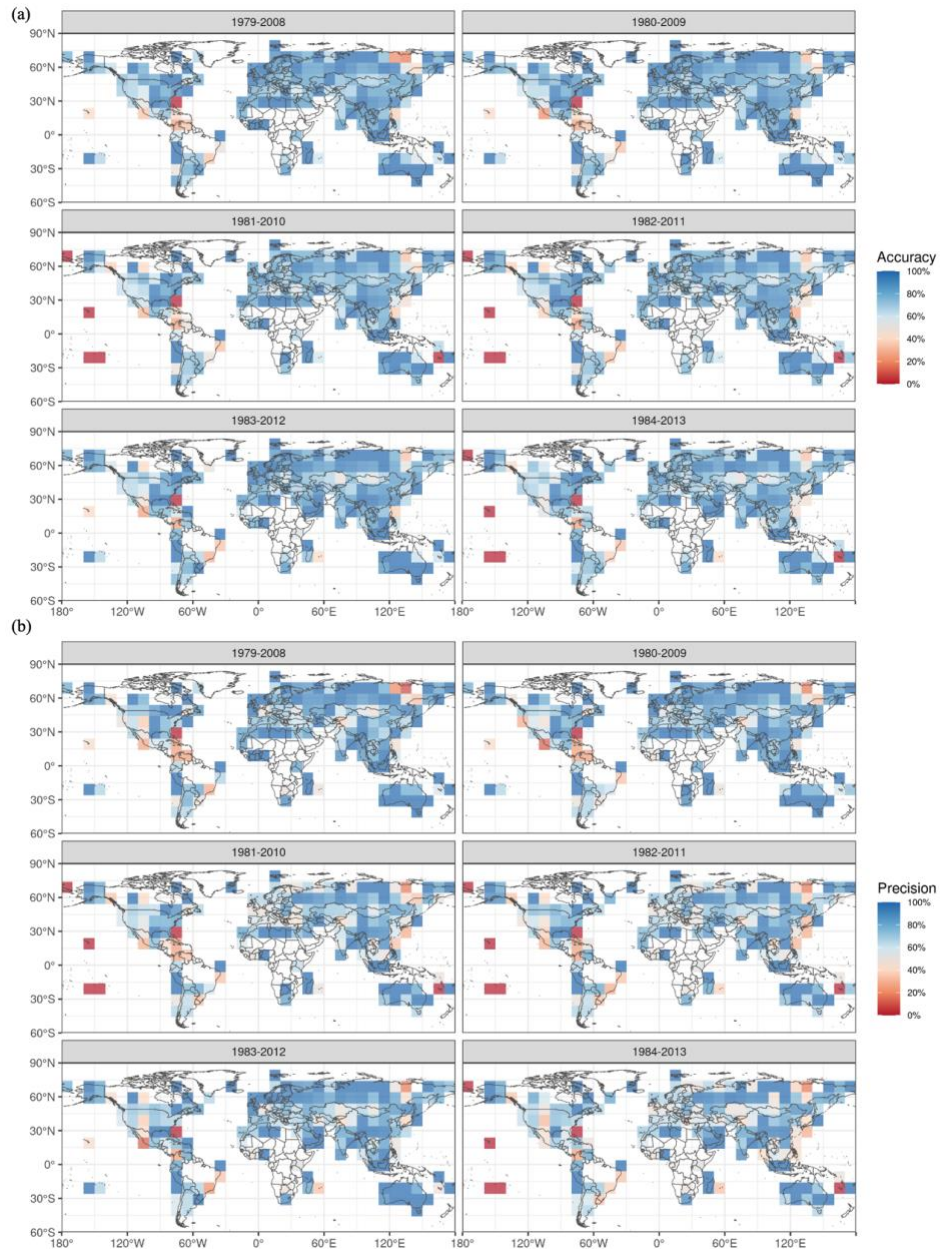
Figure 3-4. Validation of the historical Köppen-Geiger climate map series (1979-2008, 1980-2009, 1981-2010, 1982-2011, 1983-2012, 1984-2013). (a) Small-scale accuracy of historical Köppen-Geiger climate maps. (b) Small-scale precision of historical Köppen-Geiger climate maps. Climate classification has been applied for each station. The small-scale accuracy and precision are calculated based on the classification results of all the stations within the given region, with a minimum of 3 stations in the 5° search radius.

We validated the historical climate maps using the station observations from Global Historical

Climatology Network-Daily (GHCN-D) (Menne et al., 2012) and Global Summary Of the Day

(GSOD) database (National Climatic Data Center et al., 2015). Figure 3-4 shows the small-scale distribution of total accuracy and average precision for historical Köppen-Geiger climate map series with 10° grid cells. Due to uneven distribution of weather stations, remote areas in the Pacific islands, Central Africa, and Amazon Forest suffer from a lack of station observations or an underrepresented validation result.

We summarized the overall accuracy, average precision, and confidence levels for each continent and the whole globe (Table 3-S2). The global overall classification accuracy of the historical Köppen-Geiger climate maps is estimated to be 82.39% with the lowest in South America (68.58%) and highest in Oceania (92.01%). The global average precision, which is calculated as an averaged fraction of correct classification for all climate classes, is 73.33%. Like overall accuracy, South America has the lowest precision level, equal to 66.35% and Oceania the highest, 92.23%. Having a good correspondence with accuracy and precision values, the continental average confidence levels range from 91.55% to 94.93%, and the global level is 92.90% (Table 3-S2). Overall, the spatial patterns of total accuracy and average precision show good correspondence with classification confidence levels (Figure 3-3), indicating a potential of confidence level to represent classification uncertainty.

Table 3-3 Accuracy of the 1km Köppen-Geiger climate map series derived from different combinations of temperature and precipitation dataset input, and by different means of integration of multiple datasets. The values represent overall accuracy based on the technical validation using ground observation as reference.

Temperature Precipitation	CHELSA, Downscaled CRU and UDEL CHELSA, Downscaled GPCC and UDEL		Downscaled CRU and UDEL Downscaled GPCC and UDEL		CHELSA CHELSA
Integration of multiple datasets	Highest agreement level	Mean of multiple datasets	Highest agreement level	Mean of multiple datasets	-
1979-2008	83.25%	83.66%	83.13%	83.33%	79.72%
1980-2009	82.96%	83.44%	82.74%	82.78%	79.14%
1981-2010	82.63%	82.86%	81.95%	82.38%	78.03%
1982-2011	82.42%	82.73%	81.93%	82.11%	78.47%
1983-2012	81.48%	82.34%	81.14%	81.49%	78.32%

1984-2013	81.62%	82.05%	80.84%	81.27%	78.26%
1985-2014	-	-	80.23%	80.86%	-
1986-2015	-	-	79.79%	80.58%	-
1987-2016	-	-	78.76%	79.62%	-
1988-2017	-	-	-	78.65%	-
Average	82.39%	82.85%	81.17%	81.31%	78.66%
1980-2017 (Beck et al. 2018)	77.65%				
1961-1990 (Kriticos et al., (2012)	64.70%				

Using the same validation datasets from GHCN-D and GSOD, we tested sensitivity of the
climate map series using different combinations of temperature and precipitation dataset, and
different methods of data integration (Table 3-3). Results indicated an average total accuracy of
the 1km Köppen-Geiger classification maps generated with all the CHELSA, downscaled CRU,
GPCC and UDEL datasets and with only downscaled CRU, GPCC, UDEL datasets as 82.39%
and 81.17% respectively. Using the mean of multiple datasets which can potentially reduce the
data bias, led to better classification results. We estimated the total accuracy of the previous high
resolution Köppen-Geiger climate map products using the same validation datasets. We applied
the same classification system described in the previous studies and the same time period of the
previous climate map product to process the station observation data and estimate their overall
accuracy. Compared with the previous high resolution Köppen-Geiger climate map products,
Beck et al. (2018) and Kriticos et al., (2012), the newly generated Köppen-Geiger climate map
series showed greater accuracy in total.

We conducted sensitivity analysis of the Köppen classification scheme and tested multiple time
scales, 10-yr, 20-yr, and 30-yr. The selection criteria of station observations were adjusted
accordingly based on the time scale utilized. Accuracy results exhibited decreasing accuracy for
a shorter time scale (Figure 3-S3). Further, we estimated the total accuracy for the Köppen-

Geiger climate classification maps from previous studies, Beck et al., (2018) Kriticos et al., (2012), Peel et al., (2007), and Kottek et al., (2006), using the same validation dataset and consistent Köppen-Geiger climate classification scheme the corresponding study applied. The validation results demonstrate that the new Köppen-Geiger maps have comparatively higher overall accuracy than all the previous studies.

3.5.3 Regional and continental scale comparison
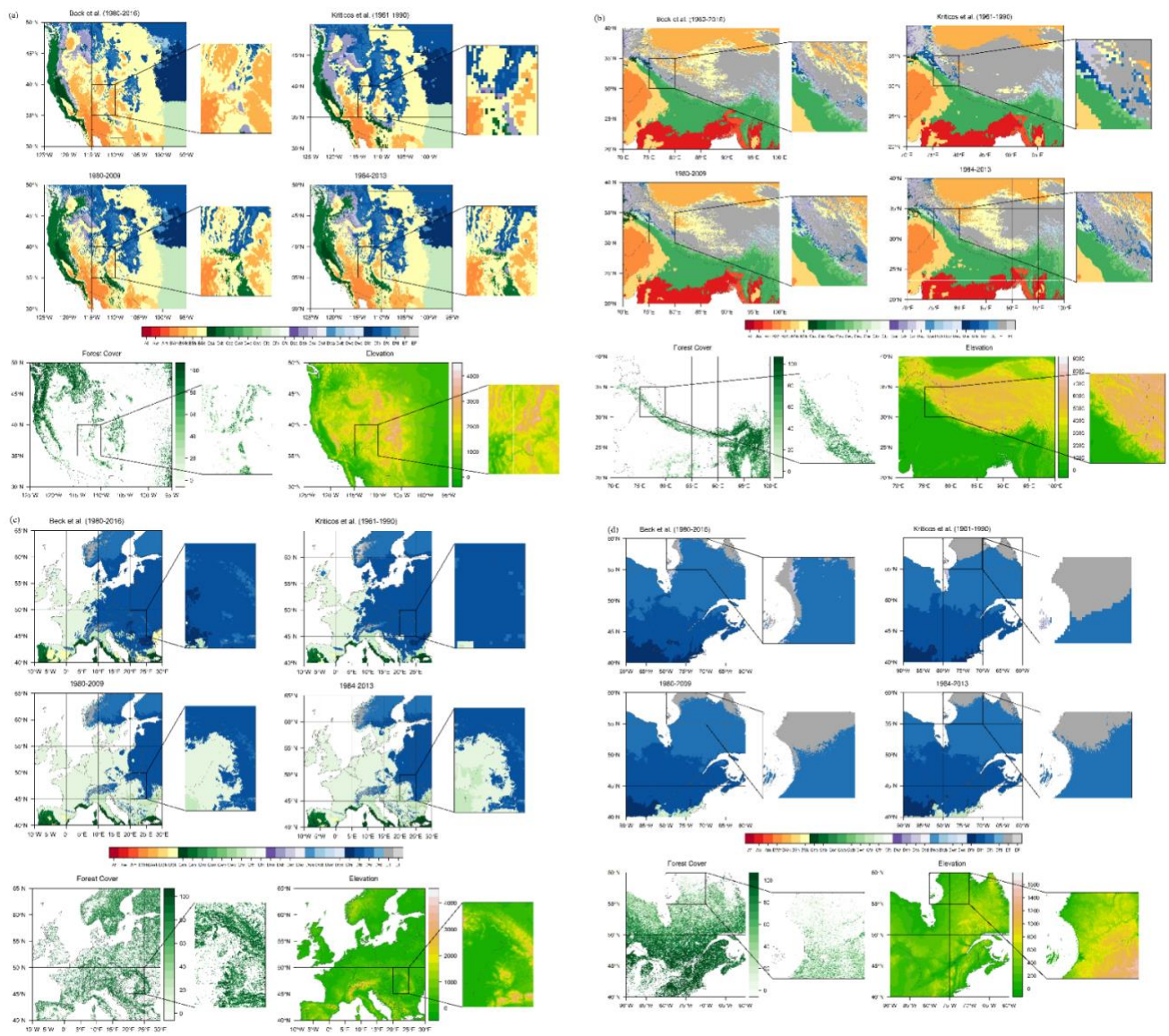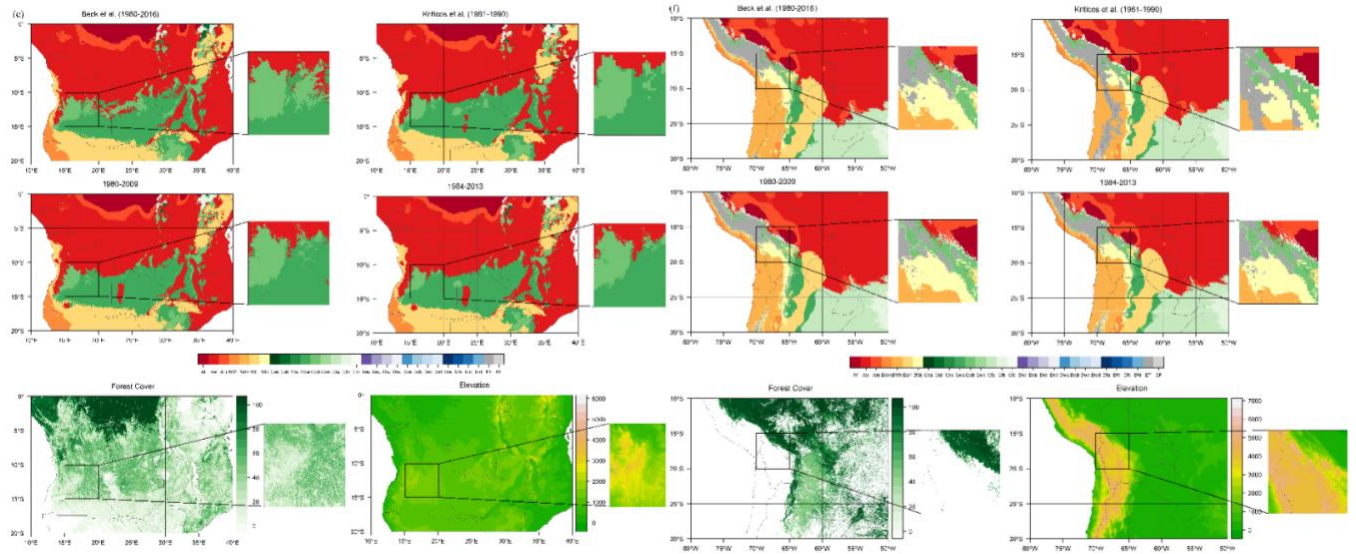
Figure 3-5. Köppen-Geiger climate classification maps from previous studies, Beck et al., 2018 (1-km, 1980-2016), and Kriticos et al., 2012 (0.167°, 1961-1990), our study (1-km, 1979-2009 to 1984-2013), associated forest cover and elevation maps, for regions with large spatial gradients in climates or sharp elevation gradients. (a) central Rocky Mountains, (b) Tibetan Plateau, (c) Europe, (d) high latitudes in North America, (e) Central and eastern Africa, and (f) central Andes. The forest cover map is the 30m Landsat-based forest cover map for 2000 (Hansen et al., 2013). The elevation data is the NASA SRTM Digital Elevation 30m data (Farr et al., 2007). The representative period of each map is listed in parentheses.

At the regional and continental scale, we compared our Köppen-Geiger climate classification maps with previous map products for regions with large spatial gradients in climates, including central and eastern Africa, Europe, North America, and regions with sharp elevation gradients, including Tibetan Plateau, central Rocky Mountains, central Andes (Figure 3-5). We compared the new 1-km Köppen-Geiger climate classification maps from our study for time periods of 1980-2009, and 1984-2013 with the high-resolution Köppen-Geiger maps from two previous studies, Beck et al., (2018), which has a resolution of 1-km and temporal coverage of 1980-2016, and Kriticos et al., (2012), which has a resolution of 0.0167° and covers 1961-1990. The Köppen classifications demonstrate good correlation with natural landscape distribution (Belda et al., 2014; Köppen, 1936; Trewartha, 1954). To show the agreement between the improved Köppen-Geiger climate classification maps and regional landscape distribution, we also showed maps of

forest cover, and elevation distribution for these regions. Figure 8 illustrates the enhanced regional details of the maps.

Compared with the Köppen-Geiger climate maps from previous studies with only one time period, the series of the Köppen-Geiger climate maps from our study demonstrate the ability to capture recent changes in spatial distribution of climate zones. For example, our maps can detect the significant changes in the climate zones specifically driven by the accelerated global warming since the 1980s, for example, the poleward movements of boreal (D) and polar (E) climates in high latitudes in North America shown in the comparison between the 1980-2009 and 1984-2013 Köppen-Geiger climate maps (Figure 3-5d). Another example is the expansion of savanna (Aw) climate into temperature (Cw) climate zone, witnessed in Central Africa (Figure 3-5e).

Another improvement of the new series of the Köppen-Geiger climate maps is the application of threshold of -3 °C as the boundary of temperate (C) and boreal (D) climate zones, which show better agreement with global boreal forest distribution at regional scale compared with Russell's modification of 0 °C (1931), which Beck et al., (2018), and Kriticos et al., (2012) utilized. Based on the comparison results of the Köppen climate zones and the biome classifications from the World Wildlife Federation (WWF), the boreal (D) climate zone largely corresponds to the distribution of boreal forest (Rohli, Joyner, et al., 2015). For example, evidenced in Figure 3-5c, the new Köppen-Geiger climate classification maps from our study show better agreement with the boreal forest in Carpathian Mountains across Central and Eastern Europe than Beck et al., (2018), and Kriticos et al., (2012). Figure 8d also shows good agreement of the northern boundary of the boreal (D) climate zone in northern part of Quebec in Canada with the boundary of Canada's boreal forest.

73

Moreover, the new Köppen-Geiger maps can show accurate depiction of important topographic features over the regions with complex topography. For example, the topo-climate of the Himalayas southern front determined by the mountain ranges are represented with more details in the new Köppen-Geiger maps compared with Beck et al., (2018), and Kriticos et al., (2012) (Figure 3-5b). The abrupt changes in climate along the edges of the Andes mountains are also well described in the new maps (Figure 3-5f).

In addition, the distribution of tropical (A), temperate (C) and boreal(D) climate zones in the new Köppen-Geiger maps correspond closely with tree lines in the forest cover maps. The temperate (C) and boreal (D) climate distribution based on the Köppen-Geiger maps show a better agreement with the forest distribution of the Middle and Southern Rocky Mountains than Beck et al., (2018), and Kriticos et al., (2012) (Figure 3-5a). For another example, the boundaries of the tropical rainforest in Central Africa and South America are clearly delineated in the new Köppen-Geiger maps (Figure 3-5e and 3-5f).

3.5.4 Bioclimatic variables

Beyond the Köppen-Geiger climate classification maps, we calculated a set of bioclimatic variables from the monthly climate data (see full list in Table 3-S3). The bioclimatic variables at 1-km spatial resolution can capture regional environmental variations especially in mountainous areas and areas with strong climate variations. These bioclimatic variables can be used in studies of environmental, agricultural and biological sciences, for example, development of species distribution modeling and assessment of biological impacts induced by climate change. The variables provide descriptions of annual averages, and seasonality of climates. The warmest half

year or the coldest half year is defined as the period of the warmest six months or the coldest six months.
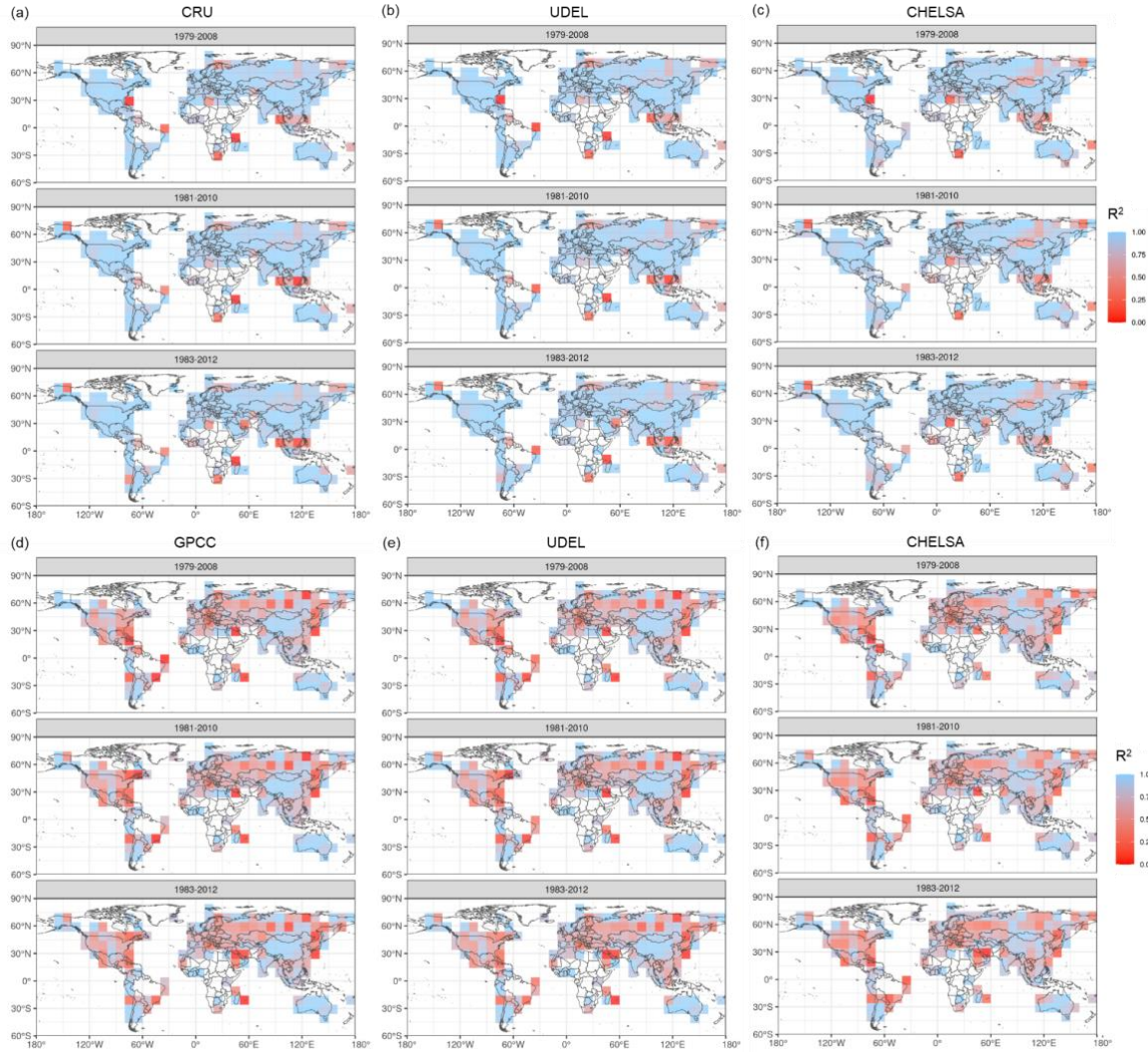
Figure 3-6. Small-scale comparison of annual temperature (MAT) and mean annual precipitation (MAP) variables derived from different datasets with station data. Small-scale correlation between the 30-yr average mean annual temperature (MAT) and mean annual precipitation (MAP) data and ground observations for three historical periods (1979-2008, 1981-2010, 1983-2012). The station data is from GHCN-D and GSOD databases. The figure shows the R^2 value for 10° grid cells. (a), (b), and (c) are MAT results. (d), (e), and (f) are MAP results. (a) MAT is calculated from downscaled monthly temperature data from CRU dataset, (b) from UDEL dataset and (c) from CHELSA dataset. (d) MAP is calculated from downscaled monthly precipitation data from GPCC dataset, (e) from UDEL dataset and (f) from CHELSA dataset.

We validated the bioclimatic variables from different datasets with station data from GHCN-D

(Menne et al., 2012) and GSOD database (National Climatic Data Center et al., 2015) (Figure 3-

S4). We calculated a linear regression model for the 12 bioclimatic variables for each 10° grid

cell (Figure 3-6). The 30-yr average mean annual temperature (MAT) from CHELSA dataset

shows overall highest fit with station data, with CRU, and UDEL datasets showing smaller, but

still strong correlation with station data. The 30-yr average mean annual precipitation (MAP)

estimates from GPCC, UDEL, and CHELSA datasets have considerable uncertainties, indicated

by relatively low correlation with station observations. In current precipitation datasets, there

exists a varied degree of discrepancy in annual estimates over multiple time scales (Sun et al.,

2018).

3.5.5 Future Köppen-Geiger climate maps
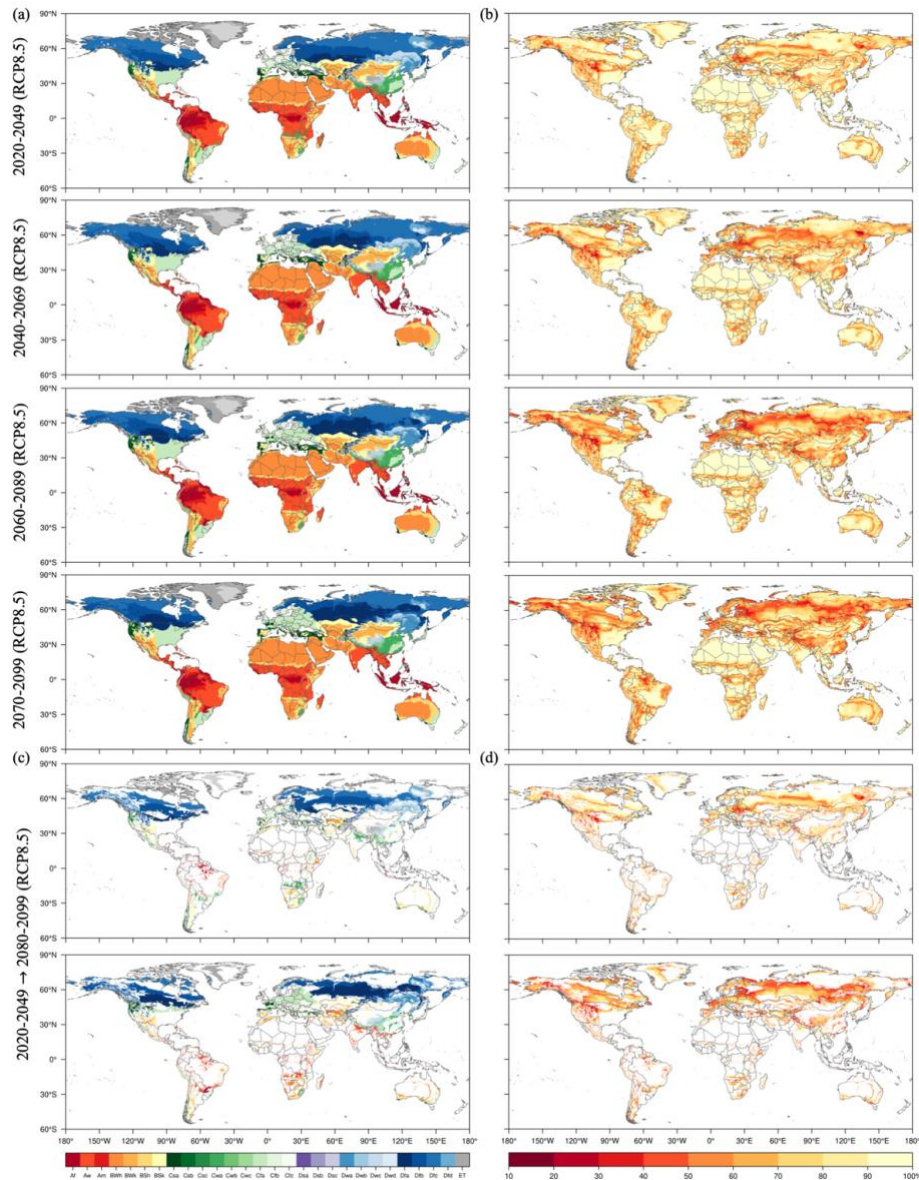
Figure 3-8 Global maps of the Köppen-Geiger climate classification for the future periods (2020-2049, 2040-2069, 2060-2089, 2070-2099) under RCP8.5 and associated classification confidence levels. (a) Future maps of the Köppen-Geiger climate classification and (b) confidence levels associated with the Köppen-Geiger climate classification. (c) Future changes in Köppen-Geiger climates from 2020-2049 to 2080-2099 and (d) the associated confidence levels.

Future Köppen-Geiger climate classification maps under RCP8.5 and associated confidence levels are shown in Figure 3-7. Indicated by confidence levels, there exist larger uncertainties in the final future climate maps than historical maps, particularly at mid and high latitudes. Climate

map for the future period of 2070-2099 shows the largest uncertainty compared with the other future periods.

Future climate classifications derived from the diverse GCM projections for four RCPs, which are inherently uncertain (Winsberg, 2012; Gleckler et al., 2008), provide a proxy of global distribution of climatic conditions and can represent potential spatial changes in climate zones under global warming. The large uncertainty and strong disagreement in projected climate classification maps at high latitudes and in regions with rugged terrain can be indicated by relatively low confidence levels. Figure 3-S5 and 3-S6 show the future Köppen-Geiger climate classification maps based on GCM projections under RCP8.5 and associated confidence levels for the central Rocky Mountains and Tibetan Plateau. We generated a future Köppen-Geiger climate classification map for each bias-corrected and downscaled CMIP5 GCM projection (see Figure 3-S5a and 3-S6a for 2070-2099 maps for the central Rocky Mountains and Tibetan Plateau). Noticeable regional changes in climate zones have been projected by comparing the 2070-2099 and 1979-2008 climate classification maps (see Figure 3-S5b and 3-S5c for the central Rocky Mountains, and Figure 3-S6b and 3-S6c for Tibetan Plateau).

3.5.6 Application example: detection of area changes in climate zones
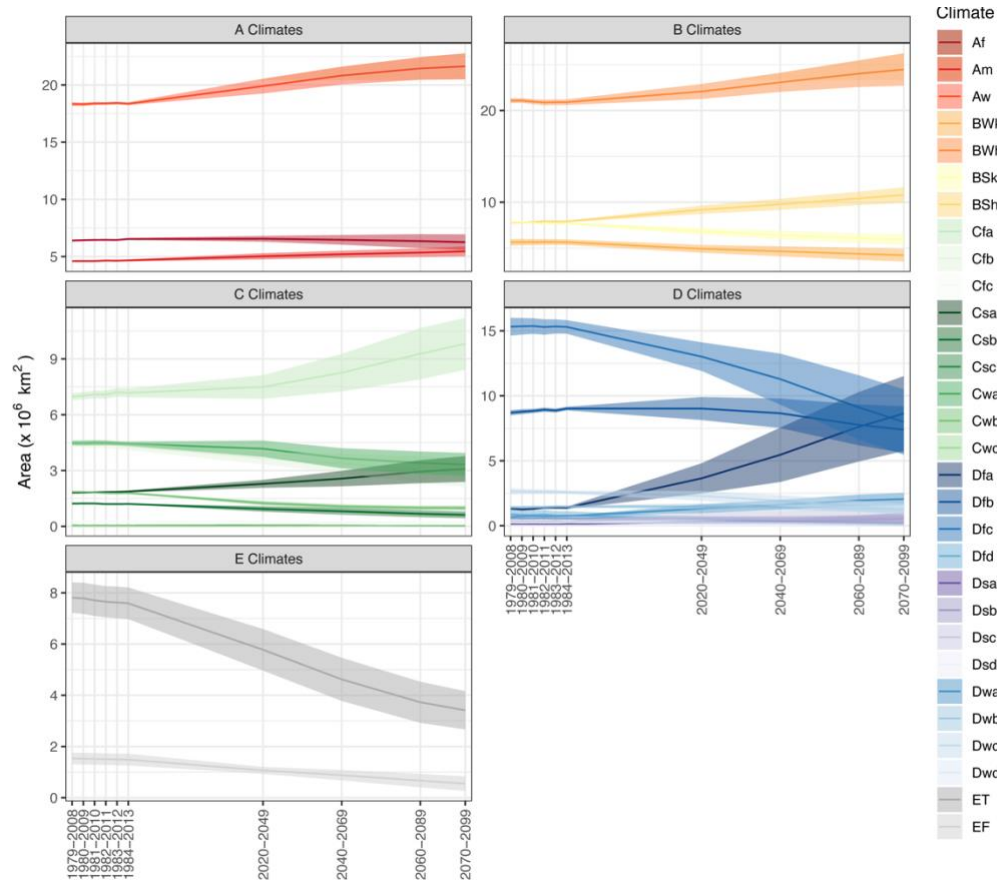
Figure 3-9. Area changes in climate zones since the 1980s on a global scale under RCP8.5. The error bars for historical periods (1979-2014) indicate standard error in the Köppen-Geiger classification results based on the 9 combinations of observational air temperature and precipitation datasets and for future periods (2020-2099), the error bars indicate standard error in the Köppen-Geiger classification results based on the 30 GCMs.

Changes in climatic conditions under global warming have significant impacts on biodiversity and ecological systems. Area changes of climate zones can indicate spatial shrinkage or expansion of analogous climatic conditions, potentially implying threats for species range contraction or opportunities for range expansion (Cui, Liang, & Wang, 2021). To examine the area changes of climate zones, we calculated the total area covered by each climate type for each historical and future period under high-emission RCP8.5 scenario (Figure 3-9). Our results of changes in areas occupied by different climate zones demonstrate good agreement with results

from previous studies (Chan & Wu, 2015). Results show that accelerated anthropogenic global warming since the 1980s has caused large-scale changes in climate zones and the shifts into warmer and drier climates are projected in this century. The tropical and arid climates are expanding into large areas in mid latitudes whereas the high-latitude climates will experience significant area shrinkage.

3.6 Conclusion

Changes in broad-scale climatic conditions, driven by anthropogenic global warming, lead to the redistribution of species diversity and the reorganization of ecosystems. Distribution of the Earth's climatic conditions has been widely characterized based on the Köppen climate classification system. The Köppen climate classification maps require fine resolutions of at least 1-km to detect relevant microrefugia and promote effective conservation. Studies examining recent and future interannual or interdecadal changes in climate zones at regional scale need more accurate depiction of fine-grained climatic conditions, continuous and longer temporal coverage.

We presented an improved long-term Köppen-Geiger climate classification map series for six historical 30-yr periods in 1979-2013 and four future 30-yr periods in 2020-2099 under RCP2.6, 4.5, 6.0 and 8.5. To improve the classification accuracy and achieve a resolution as fine as 1-km, we combined multiple datasets, including WorldClim V2, CHELSA V1.2, CRU TS v4.03, UDEL, GPCC datasets and bias-corrected downscaled CMIP5 model simulations from CCAFS. The historical climate maps are based on the most common climate type from an ensemble of climate maps derived from combinations of observational climatology datasets. The future climate maps are based on an ensemble of climate maps derived from 35 GCMs. We estimated

the corresponding confidence levels to quantify the uncertainty in climate maps. We also calculated 12 bioclimatic variables at the same 1-km resolution using these climate datasets for the same historical and future periods to provide data of annual averages, seasonality, and stressful conditions of climates.

To validate the Köppen-Geiger climate classification maps, we used the station observations from GHCN-D and GSOD databases. Our validation results show that the new Köppen-Geiger maps have comparatively higher overall accuracy than all the previous studies. Although the new maps exhibit improved overall accuracy, relatively lower confidence level and larger discrepancy in classification results are found especially in mountainous regions and major climate transitional zones located in mid and high latitudes. The confidence levels can provide a useful quantification of classification uncertainty.

Compared with climate maps from previous studies with a single present-day period, the series of the Köppen-Geiger climate maps from our study demonstrate the ability to capture recent and future projected changes in spatial distribution of climate zones. On regional and continental scale, the new maps show accurate depictions of topographic features and correspond closely with vegetation distribution. Our Köppen-Geiger climate classification maps can offer a descriptive and ecological relevant way to provide insights into changes in spatial distribution of climate zones.

One of the limitations is that the future Köppen-Geiger climate maps built on downscaled climate model projections exist unavoidable uncertainties. The classification agreement levels of GCMs are relatively low at high latitudes and in regions with rugged terrain. The main sources of model discrepancies and uncertainties are deficiencies in model physics and varied model

resolution. The climate model outputs have coarse spatial resolution varying from 70-400 km and cannot well represent future climate change at the same scale of 1-km as our baseline climatology. Through bias-correction and downscaling methods, we made assumptions that local relationships between climatic variables remain constant across different scales, leading to a compromise between spatial scale and climate model physics.

We also tested the sensitivity of classification results to different time scales, dataset input, and data integration methods. Results show that the 30-yr time scale exhibited the highest accuracy results. Moreover, using the mean of multiple datasets from CHELSA, CRU, UDEL, and GPCC could lead to better classification results. Last, we provided a heuristic example which used climate classification map series to detect the long-term area changes of climate zones, showing how the new Köppen-Geiger climate classification map series can be applied in climate change studies. With improved accuracy, high spatial resolution, long-term continuous time coverage, this global dataset of the Köppen-Geiger climate classification and bioclimatic variables can be used to in conjunction with species distribution models to promote biodiversity conservation, and to analyze and identify recent and future interannual or interdecadal changes in climate zones on a global or regional scale.

3.7 Supplementary materials
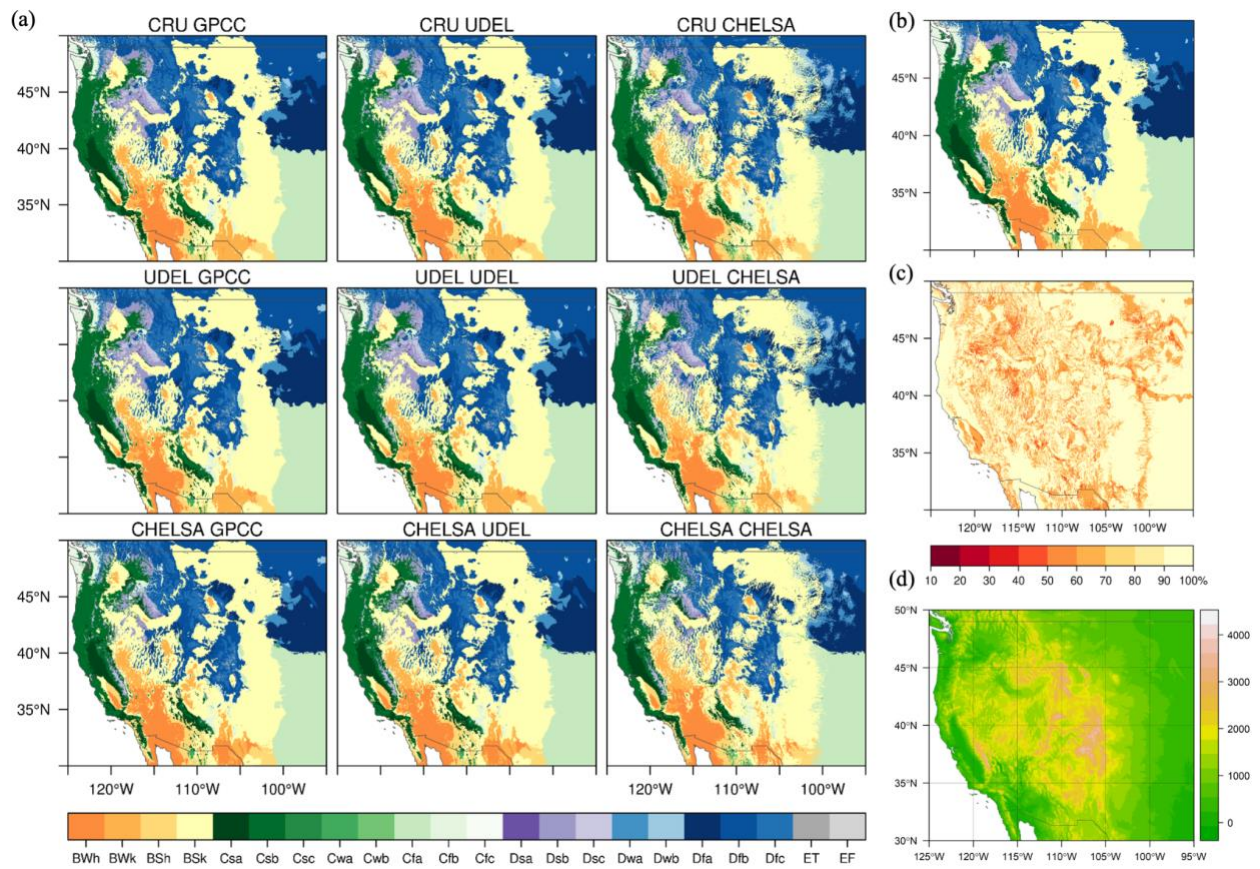
Figure 3-S1. Present Köppen-Geiger classification and confidence map for 1979-2008 with resolution of 1km for the central Rocky Mountains in North America. (a) Climate maps based on the 9 combinations of the 3 precipitation datasets × 3 surface air temperature datasets, (b) the final climate map derived from the most common climate class among the 9 climate maps, (c) confidence level distribution of the final climate map, and (d) elevation map for the the central Rocky Mountains in North America.
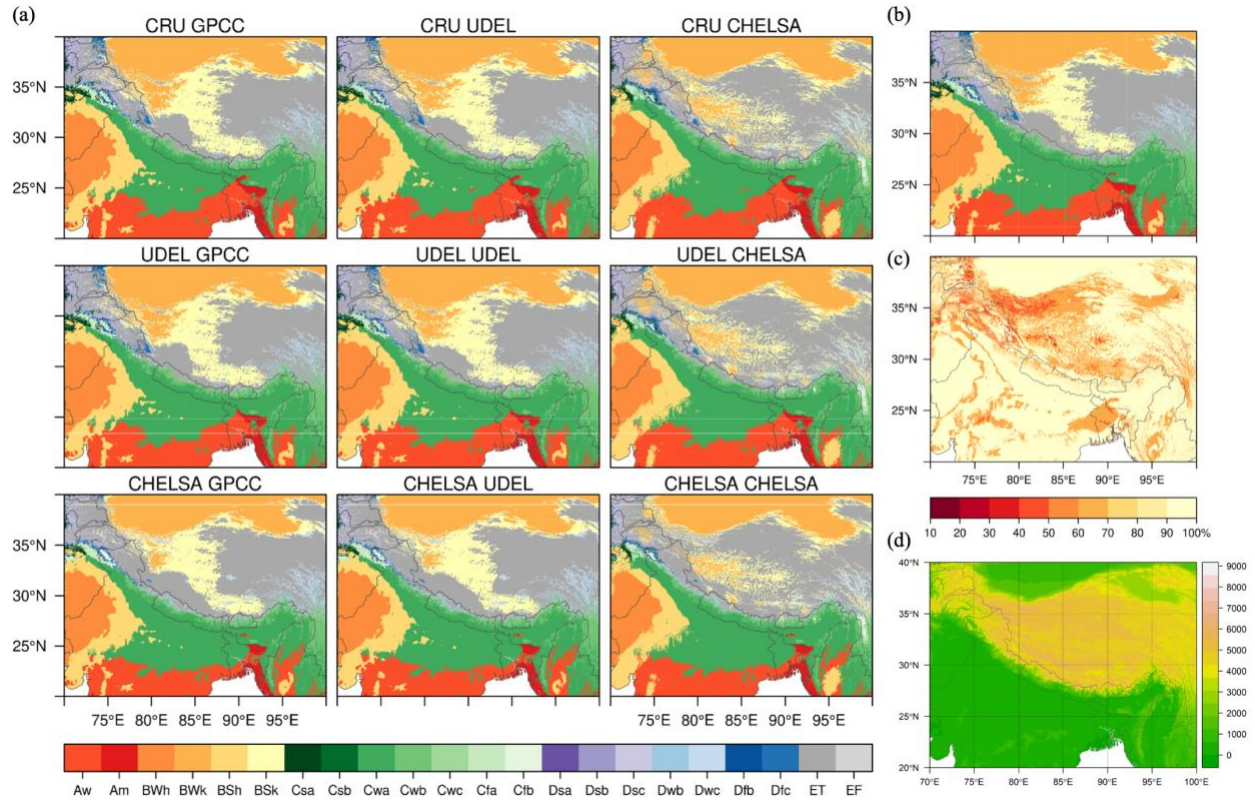
Figure 3-S2. Present Köppen-Geiger classification and confidence map for 1979-2008 with resolution of 1km for the Tibetan Plateau. (a) Climate maps based on the 9 combinations of the 3 precipitation datasets × 3 surface air temperature datasets, (b) the final climate map derived from the most common climate class among the 9 climate maps, (c) confidence level distribution of the final climate map, and (d) elevation map for the Tibetan Plateau
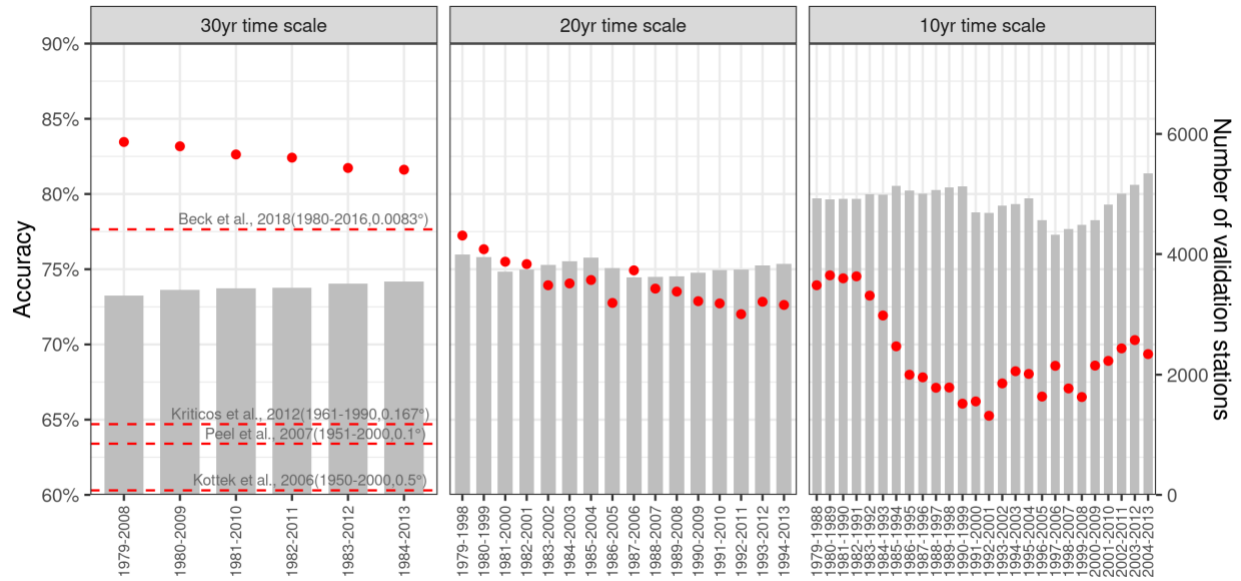
Figure 3-S3. Validation of downscaled data of bioclimatic variables and the generated Köppen-Geiger climate map.
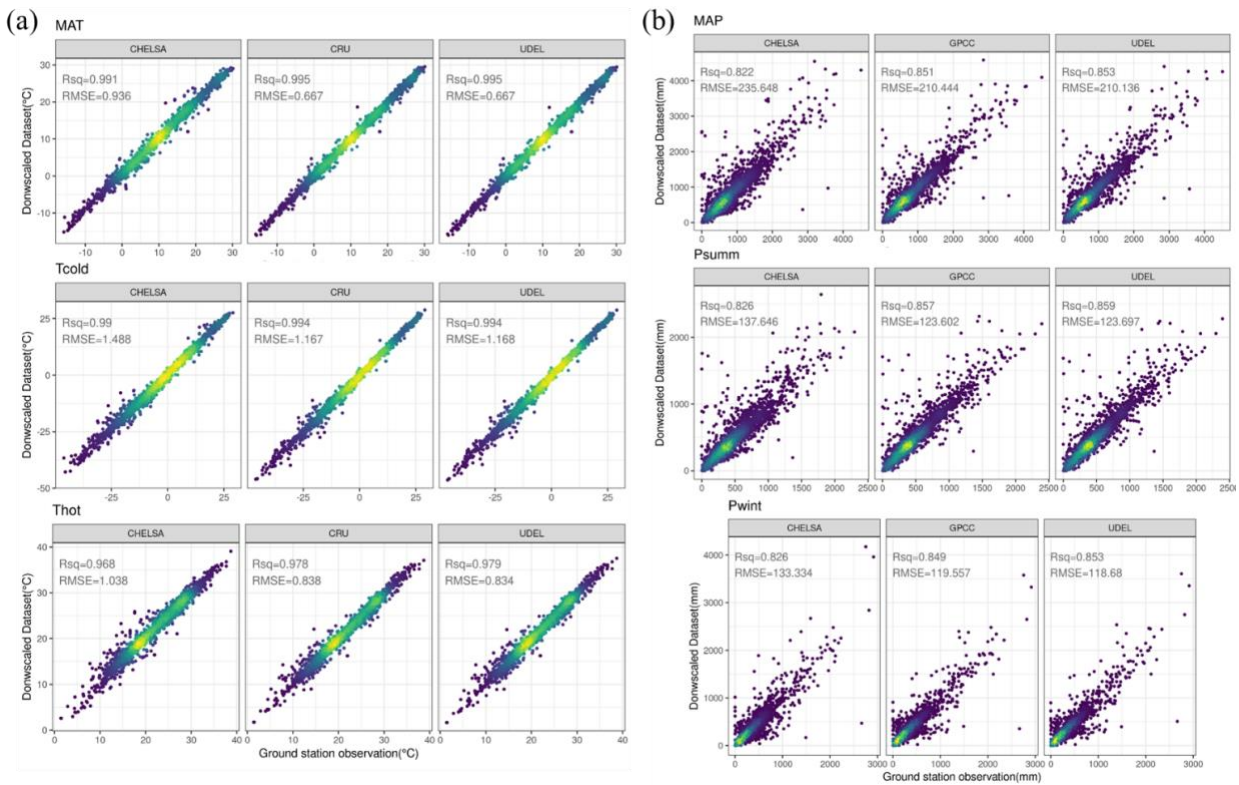
Figure 3-S4. Scatter plots of the station observations and estimates of bioclimatic variables from downscaled climatology data. The bioclimatic variables include the 30-yr means of annual temperature (MAT), the air temperature of the coldest month (Tcold), the air temperature of the warmest month (Thot), total annual precipitation (MAP), precipitation of the summer half year (Psumm), and precipitation of the winter half year (Pwint). (a) Scatter plots of the station observations and downscaled temperature data from CHELSA, CRU, UDEL datasets, and (b) and downscaled precipitation data from CHELSA, GPCC, UDEL datasets.

85
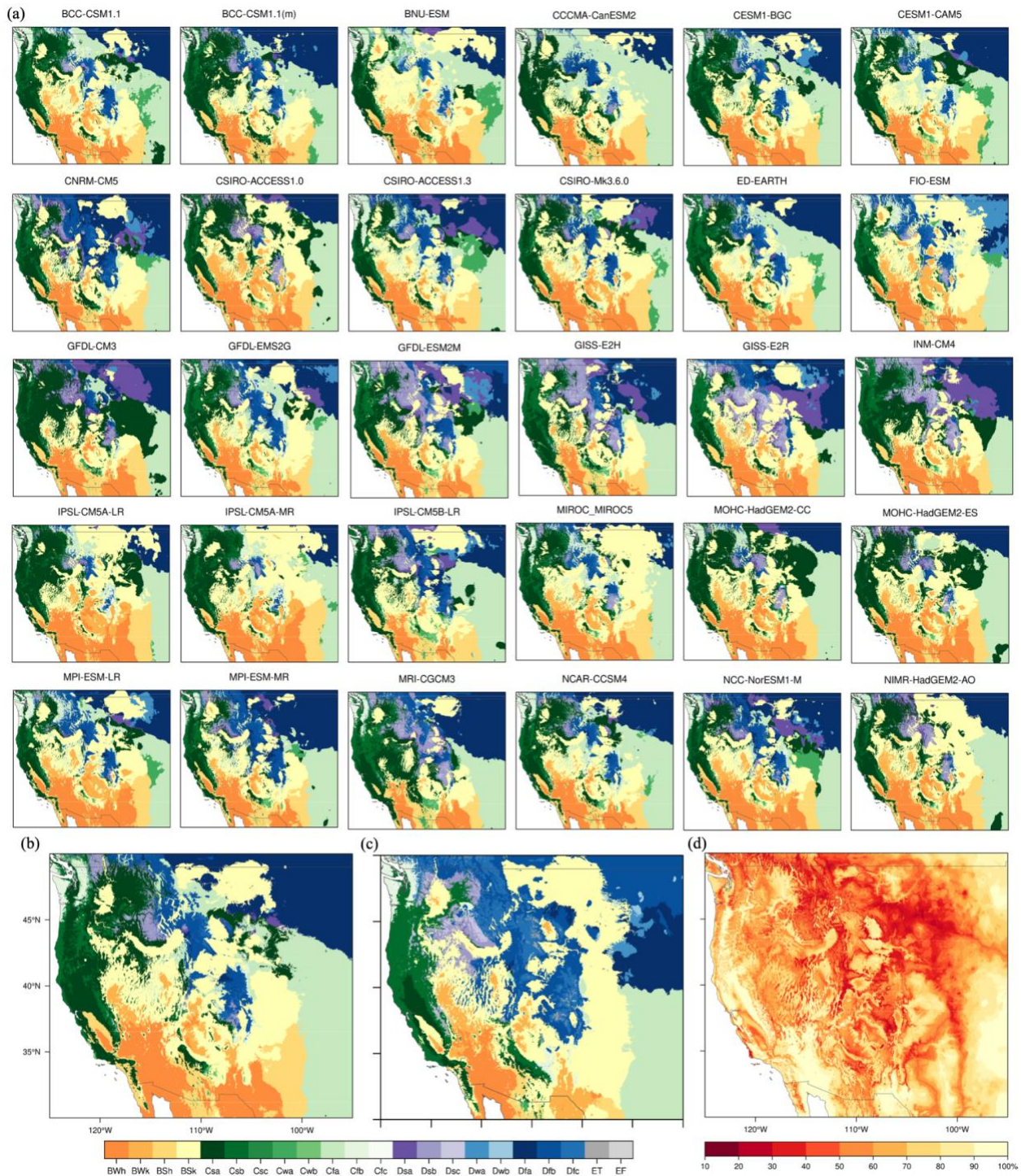
Figure 3-S5. Future Köppen-Geiger classification and confidence map for 2060-2089 under RCP8.5 with resolution of 1km for the central Rocky Mountains in North America. (a) Climate maps based on 30 GCMs, (b) the final climate map derived from the most common climate class among all the 30 climate maps, (c) present climate map of 1979-2008, and (d) confidence level distribution of the final climate map.
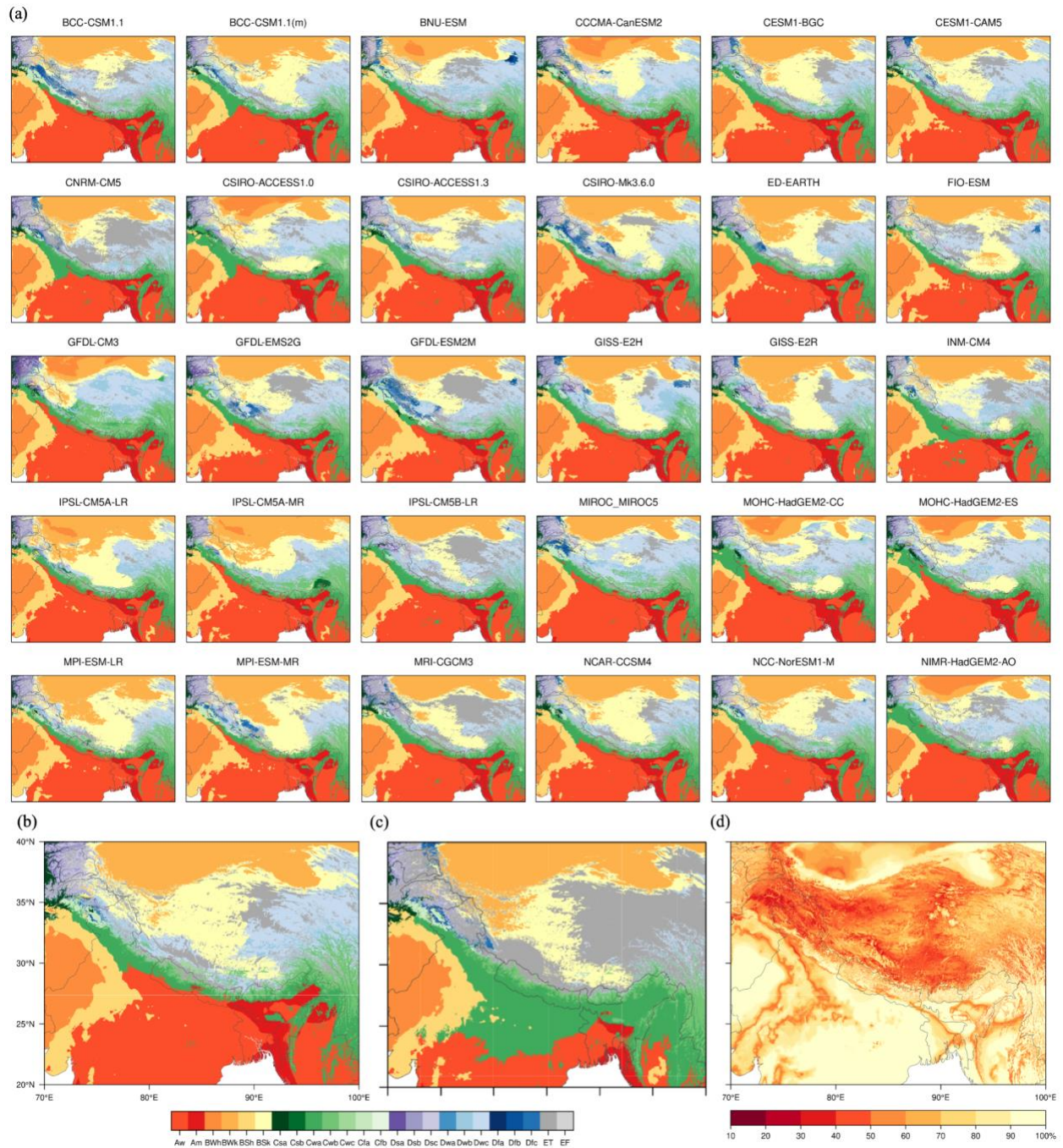
Figure 3-S6. Future Köppen-Geiger classification and confidence map for 2060-2089 under RCP8.5 with resolution of 1km for the Tibetan Plateau. (a) Climate maps based on 30 GCMs, (b) the final climate map derived from the most common climate class among all the 30 climate maps, (c) present climate map of 1979-2008, and (d) confidence level distribution of the final climate map.

87

Table 3-S1 CMIP5 GCMs for four RCPs used to generate future Köppen climate map series.

Model	Institute	RCP2.6	RCP4.5	RCP6.0	RCP8.5
BCC-CSM1.1	Beijing Climate Center, China Meteorological Administration	√	√	√	√
BCC-CSM1.1(m)	Beijing Climate Center, China Meteorological Administration	√	√	√	√
BNU-ESM	Beijing Normal University	√	√		√
CCCMA-CanESM2	Canadian Centre for Climate Modeling and Analysis	√	√		√
CESM1-BGC	National Science Foundation, Department of Energy, National Center for Atmospheric Research		√		√
CESM1-CAM5	National Science Foundation, Department of Energy, National Center for Atmospheric Research	√	√	√	√
CNRM-CM5	Centre National de Recherches Meteorologiques and Centre Europeen de Recherche et Formation Avancees en Calcul Scientifique	√	√		√
CSIRO-ACCESS1.0	Commonwealth Scientific and Industrial Research Organization (CSIRO) and Bureau of Meteorology (BOM), Australia		√		√
CSIRO-ACCESS1.3	Commonwealth Scientific and Industrial Research Organization (CSIRO) and Bureau of Meteorology (BOM), Australia		√		√
CSIRO-Mk3.6.0	Queensland Climate Change Centre of Excellence and Commonwealth Scientific and Industrial Research Organization	√	√	√	√
EC-EARTH	European Centre for Medium-Range Weather Forecasts (ECMWF)				√
FIO-ESM	The First Institute of Oceanography, State Oceanic Administration, China	√	√	√	√
GFDL-CM3	NOAA Geophysical Fluid Dynamics Laboratory	√	√	√	√
GFDL-ESM2G	NOAA Geophysical Fluid Dynamics Laboratory	√	√	√	√
GFDL-ESM2M	NOAA Geophysical Fluid Dynamics Laboratory	√	√	√	√
GISS-E2H	NASA Goddard Institute for Space Studies USA	√		√	√
GISS-E2HCC	NASA Goddard Institute for Space Studies USA		√		
GISS-E2R	NASA Goddard Institute for Space Studies USA	√	√	√	√
GISS-E2RCC	NASA Goddard Institute for Space Studies USA		√		
INM-CM4	Institute of Numerical Mathematics of the Russian Academy of Sciences		√		√
IPSL-CM5A-LR	Institut Pierre Simon Laplace	√	√	√	√
IPSL-CM5A-MR	Institut Pierre Simon Laplace	√	√		√
IPSL-CM5B-LR	Institut Pierre Simon Laplace				√
LASG-FGOALS-G2	Institute of Atmospheric Physics (LASG) and Tsinghua University (CESS)	√	√		
MIROC-ESM	University of Tokyo, National Institute for Environmental Studies and Japan Agency for Marine-Earth Science and Technology	√	√	√	
MIROC-ESM-CHEM	University of Tokyo, National Institute for Environmental Studies and Japan Agency for Marine-Earth Science and Technology	√	√	√	

MIROC-MIROC5	University of Tokyo, National Institute for Environmental Studies and Japan Agency for Marine-Earth Science and Technology	√	√	√	√
MOHC-HadGEM2-CC	UK Met Office Hadley Centre		√		√
MOHC-HadGEM2-ES	UK Met Office Hadley Centre	√	√	√	√
MPI-ESM-LR	Max Planck Institute for Meteorology	√	√		√
MPI-ESM-MR	Max Planck Institute for Meteorology	√			√
MRI-CGCM3	Meteorological Research Institute	√	√	√	√
NCAR-CCSM4	US National Centre for Atmospheric Research	√	√	√	√
NCC-NorESM1-M	Norwegian Climate Centre	√	√	√	√
NIMR-HadGEM2-AO	National Institute of Meteorological Research and Korea Meteorological Administration	√	√	√	√

Table 3-S2 Continental and global overall accuracy, average precision, and confidence level of the historical Köppen-Geiger climate map series.

	Region	Africa	Asia	Oceania	Europe	North America	South America	Global
A **c** **c** **u** **r** **a** **c** **y**	1979-2008	88.24%	84.05%	92.39%	85.11%	79.37%	69.18%	83.25%
	1980-2009	87.67%	85.00%	90.11%	84.24%	76.94%	70.00%	82.96%
	1981-2010	85.71%	84.29%	93.48%	84.23%	75.61%	68.75%	82.63%
	1982-2011	83.78%	85.06%	91.30%	84.10%	74.79%	68.90%	82.42%
	1983-2012	85.43%	83.64%	92.39%	83.51%	71.99%	66.67%	81.48%
	1984-2013	85.81%	81.32%	92.39%	84.38%	71.84%	68.00%	81.62%
	Average	86.11%	83.89%	92.01%	84.26%	75.09%	68.58%	82.39%
P **r** **e** **c** **i** **s** **i** **o** **n**	1979-2008	80.24%	72.77%	92.77%	75.71%	64.41%	66.20%	71.27%
	1980-2009	88.33%	73.40%	89.83%	75.58%	65.15%	68.11%	73.39%
	1981-2010	79.54%	71.19%	94.21%	74.77%	67.75%	67.63%	74.10%
	1982-2011	70.42%	71.34%	91.37%	75.61%	70.62%	66.65%	74.24%
	1983-2012	71.54%	68.99%	92.67%	69.82%	66.73%	64.33%	72.41%
	1984-2013	71.66%	68.08%	92.55%	76.30%	67.95%	65.17%	74.59%
	Average	76.96%	70.96%	92.23%	74.63%	67.10%	66.35%	73.33%
C **o** **n** **fi** **d** **e** **n** **c** **e**	1979-2008	94.93±0.002%	92.08±0.002%	91.82±0.002%	92.29±0.002%	94.55±0.004%	92.31±0.003%	92.94±0.002%
	1980-2009	94.91±0.002%	92.14±0.002%	91.73±0.002%	92.39±0.002%	94.65±0.004%	92.24±0.003%	92.95±0.002%
	1981-2010	94.89±0.002%	92.17±0.002%	91.63±0.002%	92.43±0.002%	94.51±0.004%	92.18±0.003%	92.92±0.002%
	1982-2011	94.92±0.002%	92.16±0.002%	91.48±0.002%	92.41±0.002%	94.35±0.004%	92.13±0.003%	92.87±0.002%
	1983-2012	94.96±0.002%	92.16±0.002%	91.31±0.002%	92.54±0.002%	94.37±0.004%	92.05±0.003%	92.87±0.002%
	1984-2013	94.97±0.002%	91.22±0.002%	91.32±0.002%	92.52±0.002%	94.45±0.004%	92.00±0.003%	92.87±0.002%

| Average | 94.93±0.002% | 91.99±0.002% | 91.55±0.002% | 92.43±0.002% | 94.48±0.004% | 92.15±0.003% | 92.90±0.002% |

Table 3-S3 List of bioclimatic variables derived from downscaled monthly climate data.

Bioclimatic Variables	Description
BIO1	Annual mean temperature (ºC)
BIO2	Temperature of the warmest month (ºC)
BIO3	Temperature of the coldest month (ºC)
BIO4	Annual precipitation (mm)
BIO5	Precipitation of the warmest half year (mm)
BIO6	Precipitation of the coldest half year (mm)
BIO7	Precipitation of the driest month (mm)
BIO8	Precipitation of the driest month in the warmest half year (mm)
BIO9	Precipitation of the driest month in the coldest half year (mm)
BIO10	Precipitation of the wettest month (mm)
BIO11	Precipitation of the wettest month in the warmest half year (mm)
BIO12	Precipitation of the wettest month in the coldest half year (mm)

Chapter 4: Using velocity of climate zone shifts to inform biodiversity conservation in global terrestrial protected areas

4.1 Abstract

Climate change is driving broad-scale redistribution of species on the Earth, greatly undermining the effectiveness of protected areas (PAs) in conserving and restoring global biodiversity. Strategic and adaptive conservation planning that explicitly considers climate shifts is critical to addressing the ongoing biodiversity crisis and achieving future conservation goals. To assess exposure risks of global PAs and understand spatial patterns of near, mid, and long-term climate shifts projected based on different future emission pathways, we develop a new velocity measure

with fine spatial scale (1-km) based on Köppen-Geiger climate classes, which incorporate multiple climatic indicators and integrate biological information. The "climate zone velocity" represents potential minimum movement of species required to track climate zone changes over time and is derived from topographic paths to capture topographic effects on habitat conditions. We find that ~38% of global protected land in more than three fourths of global terrestrial PAs could undergo pronounced climate zone shifts at accelerating rates during the remainder of this century under RCP8.5. Moreover, protected lands are experiencing heightened climate change exposure from novel (8.3% of global protected land) and disappearing (6.6%) climates, shifts of climates outside PA networks (7.6%), and transition to human dominated land use (5.7%). PAs located across arid (B) and boreal (D) climate zones, in mid latitudes of North America, Europe, Russia, and Africa, and those with strict management categories (IUCN category I-II), are facing more rapid and substantial changes. Relationships with PA attributes suggest increased vulnerability over small, high elevation PAs with complex topography and high species richness. Taken together, our findings of climate zone shifts, and exposure assessment of PAs can inform climate adaptation planning and biodiversity conservation prioritization.

4.2 Introduction

As key drivers of the ecological interactions and biological processes, climatic conditions determine global patterns of biomes and biodiversity (Kreft & Jetz, 2007; Woodward et al., 2004). In response to current climate change, species are undergoing evolutionary adaptation (Merilä & Hendry, 2014; Parmesan, 2006), changing phenologies and abundance (Parmesan & Yohe, 2003; Scheffers et al., 2016), and shifting their distribution to track changing climates(I.-C. Chen et al., 2011). Regional changes in availability and positions of climatically suitable areas

have resulted in many observed latitudinal and elevational shifts in species distribution and rearrangement of species assemblages (Garcia et al., 2014; Scheffers et al., 2016). Consequently, ongoing changes in climatic conditions are driving a significant redistribution of life on the Earth, leading to restructured biotic community compositions (Williams & Jackson, 2007), losses of ecosystem services, and increased threats to human welfare across the globe (Kreft & Jetz, 2007; Pecl et al., 2017).

Protected areas (PAs) are widely recognized as a core of present-day biodiversity conservation strategies (Arafeh-Dalmau et al., 2021; Dobrowski et al., 2021) and have demonstrated their importance in protecting the earth's biodiversity by reducing rates of habitat loss (Geldmann et al., 2013) and enhancing species diversity within their boundaries (Gray et al., 2016). PAs also provide various social and economic benefits by preserving natural resources, delivering ecosystem services, and supporting human livelihoods (J. E. M. Watson et al., 2014). Expanding global PA coverage while maintaining the effectiveness of the PA networks are key conservation targets agreed in the post-2020 framework of the Convention on Biological Diversity (CBD) (OECD, 2019; Visconti et al., 2019). However, changes in climate and land use caused by human activities greatly undermine the effectiveness of current PA networks (Arafeh-Dalmau et al., 2021; Batllori et al., 2017; Elsen et al., 2020; Hoffmann et al., 2019). As climate shifts, suitable climates for species may become less accessible and species may track their preferred climatic conditions and move into unprotected and human-dominated areas, increasing risks of extinction (Batllori et al., 2017; Hoffmann et al., 2019; Wessely et al., 2017). Current static boundaries, low connectivity of PAs (Asamoah et al., 2021; Batllori et al., 2017; Lawler et al., 2015), biased PA locations towards areas of low human influence (Joppa & Pfaff, 2009; Venter et al., 2018), and close alignment with existing biodiversity patterns with inadequate

consideration of future changes (Lawler et al., 2015; Loucks et al., 2008; Myers et al., 2000), could further diminish the capacity of PA networks in protecting future biodiversity, thereby impeding the achievement of global conservation goals.

To enhance the effectiveness of global PAs and develop more strategic and adaptive PA conservation approaches, conservation planners need to incorporate potential climate shifts and biodiversity redistribution into PA conservation planning (Dobrowski et al., 2021; Pecl et al., 2017; J. E. M. Watson et al., 2013). Given the limited availability of species data for bioclimatic modeling (Brito-Morales et al., 2018; Garcia et al., 2014), recent studies assessing exposure risks of biodiversity increasingly use metrics of climate change (Garcia et al., 2014), such as climate velocity (Brito-Morales et al., 2018; Loarie et al., 2009), climate analogs (Ordonez & Williams, 2013; Williams & Jackson, 2007), climate stability (J. E. M. Watson et al., 2013), novel and disappearing climates (Garcia et al., 2014; Hoffmann et al., 2019; Williams et al., 2007). These metrics are based on either one climate variable or climate space identified using statistically combined multivariate indices, thus may not necessarily relate to properties and functions of biomes or ecosystems and lack potential to conduct risk evaluation for biodiversity (Brito-Morales et al., 2018; Cui, Liang, & Wang, 2021).

To highlight the linkages in climate and biomes, researchers apply Köppen-Geiger climate classification scheme to examine shifts in climate zones and possible changes in biomes (Chan & Wu, 2015; Mahlstein et al., 2013; Rubel & Kottek, 2010). As a widely used bioclimatic classification scheme, Köppen-Geiger classification (KGC) was first introduced by Wladimir Köppen to map the world's biomes (Köppen, 1936). KGC classifies five major climate classes and 30 subtypes globally by incorporating annual means and seasonal phases of temperature and precipitation (detailed criteria in Table 4-S1), and shows strong correlations with biome

distribution (Cui, Liang, & Wang, 2021; Rohli, Joyner, et al., 2015). Under climate change ,

studies have shown the Köppen-Geiger climate zones shifting poleward and upward into warmer

and drier climates, with significant area expansion in tropical (A) and arid (B) climate zones and

area shrinkage of polar (E) climates (Chan & Wu, 2015; Cui, Liang, & Wang, 2021; Mahlstein et

al., 2013; Rohli, Andrew, et al., 2015).
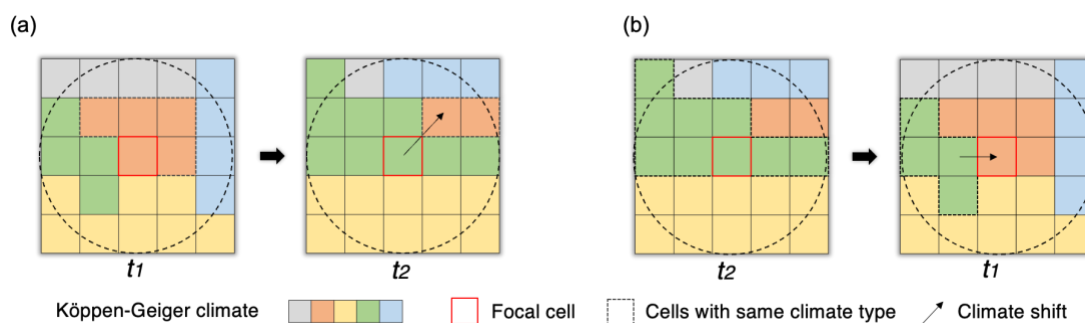
Figure 4-1 Climate zone velocity based on spatial and temporal changes in climate zones. (a) Forward velocity
(present-to-future velocity) indicates distance and direction from present climate locations to the nearest future
destinations with the same Köppen-Geiger climate class. (b) Backward velocity (future-to-present velocity)
measures distance and direction from projected future climate cells back to current climate origins. We derive
climate zone velocity based on 1-km historical (1970-2000) and future (2020-2049, 2040-2069, 2060-2089, and
2070-2099) Köppen-Geiger climate classification maps and use topographic paths to approximate realistic
biological movements. The velocities are identified within a fixed search radius (=1,000 km).

Existing exposure assessments of PAs using climate velocity with coarse resolutions (> 1km)

may overlook topo climatic patterns (Burrows et al., 2014; Carroll et al., 2018; Dobrowski et al.,

2013, 2021; Ordonez et al., 2014), leading to biased estimates especially in rugged terrain

(Dobrowski & Parks, 2016; Heikkinen et al., 2020) and limited ability to detect microrefugia

(Dobrowski, 2011; Lenoir et al., 2017). Moreover, the time frame over which climates become

less favorable for local species and population is critical for understanding temporal patterns of

biological responses, which cannot be captured using a long time frame. Assessment of multiple

future time steps for the near future on an ecologically relevant spatial scale is urgently important

for the achievement of global conservation targets of CBD's 2030 biodiversity strategic plan

(OECD, 2019; Visconti et al., 2019; J. Watson et al., 2022) and 2050 vision of 'living in

harmony with nature'(Convention on Biological Diversity, n.d.). Given the lack in risk assessment of changing conditions for PAs with fine temporal and spatial scales and global extent (Ackerly et al., 2010; Batllori et al., 2017; Carroll et al., 2017), we examine the spatiotemporal patterns of climate zone shifts in global PAs with 1-km spatial scale and multi-decadal temporal scale, and assess the exposure risks of current global PA networks under climate change for near-term, mid-term and long-term futures, projected by different emission scenarios.

We first develop a velocity measure of spatial changes in climate zones (hereafter, "climate zone velocity") using topographic paths to capture topographical effects (Figure 4-S1). The climate zone velocity conforms to climate analog velocity(Batllori et al., 2017; Carroll et al., 2018; Dobrowski et al., 2021; Heikkinen et al., 2020), an approach that identifies distance and direction between present and future climate locations with analogous climates (Figure 4-1). Using a global dataset of Köppen-Geiger climate classification (KGClim) (Cui, Liang, Wang, et al., 2021), which is derived from bias-corrected downscaled Coupled Model Intercomparison Project Phase 5 (CMIP5) model simulations (Navarro-Racines et al., 2020), and WorldClim Historical Climate Data (WorldClim V2) (Fick & Hijmans, 2017), we then calculate climate zone velocity for four future periods (2020-2049, 2040-2069, 2060-2089, 2070-2099) based on four Representative Concentration Pathways (RCP2.6, RCP4.5, RCP6.0 and RCP8.5) with a baseline period of 1971-2000.

To assess effects on conservation capacity of current PA networks and identify additional threats from human-induced land modifications, we categorize the spatial patterns of climate zone shifts based on whether climates are relocated within, among, outside, inside the PA networks (Batllori et al., 2017), or end in unprotected areas with human-dominated land-use, and emergence of

novel or disappearing climate zones for the global terrestrial PAs, using data from the World

Database on Protected Area (WDPA) (UNEP-WCMC and IUCN, 2021) and land use states from

Land-Use Harmonization2 (LUH2) project (Hurtt et al., 2020). We also identify the PAs

projected to undergo shifts of climate zones of great magnitude and investigate the relationships

between climate zone shifts and PA attributes, such as species richness, terrain ruggedness, and

human footprint level. Lastly, we present a case study to integrate climate shifts in PA

prioritization scheme to inform future climate adaptation planning and biodiversity conservation.

4.3 Results

4.3.1 Potential shifts of climate zones in PAs

(a)

(b)

Shifts of climate zones (% of PA area)
- 100%
- 80–100%
- 50–80%
- 20–50%
- 5–20%
- 0–5%
- No change

Canada   Brazil   Europe   United States   Russia   Australia

(c)

1971–2000 to 2020–2049   2020–2049 to 2040–2069   2040–2069 to 2060–2089   2060–2089 to 2070–2099

Forward

Backward

Velocity (km yr^{-1})

(d)

1971–2000 to 2020–2049   2020–2049 to 2040–2069   2040–2069 to 2060–2089   2060–2089 to 2070–2099

Backward

Forward

Climate zone shifts (% protected area)

- Within
- Outside
- Inside
- Disappearing
- Novel

Figure 4-2 Potential shifts of climate zones within global terrestrial PAs. Global and country maps of PAs show PA-level (a) average values of climate zone velocities, and (b) percent area within each PA that is projected to experience climate zone shifts by the end of the 21st century under RCP8.5 scenario, with smoothed latitudinal distribution of pixel-level (c) climate zone velocities, and (d) percent of global PA coverage projected to undergo climate zone shifts by latitudinal bands (1km to 5°) in four future periods. (a) Forward and backward climate zone velocity values are grouped into categories based on equal-area quartiles along each axis (n=22,805). (a,b) Canada, Brazil, Europe, United States, Russia and Australia shown in the maps have large PA coverage. Dark gray represents no changes in climate zones within the PA and light gray areas are unprotected land. (c) black dots mark median velocity values and error bars show first and third quartiles in the latitudinal bands.

Based on the RCP8.5 scenario, over 17,000 terrestrial PAs (75% of the total), a total of 38% of global protected land area could experience changes in climatic conditions that correspond to different climate zones during this century and 20% by mid-century. Under RCP2.6, 18% of global protected land area is projected to undergo climate zone shifts by 2050 and 20% by 2100. More than half of the global terrestrial PAs are projected to have a mean velocity larger than 100 m yr^{-1} and around 9,000 PAs (38%) will face completely different climate zone distribution under RCP8.5 (Figure 4-3a). The median velocity of climate zone shifts within the global PAs is projected to increase from 0.21 km yr^{-1} (Interquartile Range (IQR)=0.57 km yr^{-1}) to 0.25 km yr^{-1} (IQR=0.88 km yr^{-1}) by the century end under RCP8.5. Similar increasing trend in velocity is found in the RCP6.0 scenario but with a smaller magnitude of velocity (Table 4-S3). On the contrary, the projected median velocity reaches its peak by mid-century and slightly decreases to 0.15 km yr^{-1} (IQR=0.39 km yr^{-1}) as the century progresses under RCP2.6. Under RCP4.5, it shows a similar decreasing trend with later peak timing (Table 4-S3). The varying trends in pace of climate zone shifts within global PAs under different emission scenarios are closely associated with projected dynamics of radiative forcing levels (van Vuuren et al., 2011). Under the high emission scenario (RCP8.5) that current global warming trajectory closely aligns (Schwalm et al., 2020), global protected land will undergo pronounced changes in climatic conditions with constantly accelerating rates during the century.

We assess both forward and backward velocities to represent outgoing and incoming changes in climate zones of a region for each time frame. Forward velocity (present-to-future velocity) indicates distance from present climate locations to the nearest future destinations for a given climate class, reflecting the minimum path that species need to migrate to maintain their suitable climatic conditions for the given time window (Batllori et al., 2017; Hamann et al., 2015). Backward velocity (future-to-present velocity) measures distance from projected future climate cells back to current climate origins, indicating the minimum path that species need to migrate to adapt to or colonize the new site. Forward velocity can be interpreted as species exposure to climate change and backward velocity estimates risks for ecosystem functioning and services (Batllori et al., 2017; Carroll et al., 2015; Hamann et al., 2015), providing complementary information to support conservation. Within the global terrestrial PAs, climate zone shifts are intensifying, at an estimated global average forward velocity of 0.64 km yr^{-1} (median=0.22 km yr^{-1}) during the century, lower than backward velocity with a global mean level of 0.79 km yr^{-1} (median=0.25 km yr^{-1}) under RCP8.5 (Table 4-S4).

PAs exposed to both high forward and backward velocities of climate zone shifts are largely located in northern mid latitudes of North America and North Asia, Amazonian, South America, and central Australia (Figure 4-2a). Species and population in these PAs are facing more serious threats from climate change and may fail to track changing climatic conditions or colonize new habitats. Many PAs will have their whole area projected to undergo large magnitude of climate zone shifts during this century. The locations of these PAs are concentrated in southern Canada, northern United States, central Europe, southern Russia, Brazil, Africa, and Australia (Figure 4-2b). The forward and back climate zone velocities exhibit latitudinal variations with peaks in northern high latitudes (north of 60ºN) and southern low latitudes (10ºS to 30ºS; Figure 4-2c),

which approximately correspond with latitudinal PA coverage. The prevalence of area percent with projected climate zone shifts also varies by latitude, with the largest percentage in northern mid-latitude (40°N to 60°N) and southern mid-latitude (30°S to 50°S; Figure 4-2d).

Compared to elsewhere, we find that PAs in northern and southern mid latitudes in United States, Canada, Europe, Russia, Brazil, Africa, and Australia are exposed to more rapid rates of climate zone shifts and larger proportions projected to face shifting climatic conditions, inducing higher threats on biodiversity within these PAs. PAs in Russia, Europe, Canada and Brazil are exposed to higher rates of climate zone shifts, with median velocities during the second half of the century equal to 0.53 km yr^{-1} (IQR=2.1 km yr^{-1}) , 0.35 km yr^{-1} (IQR=0.55 km yr^{-1}), 0.4 km yr^{-1} (IQR=1.11 km yr^{-1}), and 0.39 km yr^{-1} (IQR=0.93 km yr^{-1}), respectively (Figure 4-S5). Moreover, 38% of the terrestrial PAs (n=8,667) could face completely different climate zone distribution under RCP8.5, with half of them in Europe and one third in North America (Figure 4-2b).

We examine the climate zone shifts within global PAs with respect to different International Union for Conservation of Nature (IUCN) management categories, major climate zones, and species groups. We find that the PAs managed as strict nature reserve (IUCN category Ia) and for sustainable use of natural resources (IUCN category VI) have higher velocity, reaching 0.53 km yr^{-1} (IQR=1.67 km yr^{-1}) and 0.62 km yr^{-1} (IQR=2.07 km yr^{-1}; Table S6). Additionally, 22% of the PA area with high levels of restrictions (IUCN category I-II) are undergoing climate zone shifts by the mid-century under RCP8.5 (Figure 4-3c). Forward and backward velocities of climate zone shifts can also be closely related to changing rates of climate zone expansion and shrinkage respectively, indicating different regional patterns. Within the global PAs, arid (B) climate zone is projected to have the highest rates of climate zone shifts and the median forward

velocities will increase from 0.25 km yr^{-1} (IQR=0.55 km yr^{-1}) to 0.34 km yr^{-1} (IQR=0.9 km yr^{-1}) during this century under RCP8.5 (Table 4-S7).

Species in arid (B) climate zones would likely face higher forward velocities and experience more rapid expansions in climatically suitable areas. Boreal (D) climate zone shows the highest median backward velocities (rates of area shrinkage), with significant increase in the mid-century, from 0.28 km yr^{-1} (IQR=1.07 km yr^{-1}) to 0.42 km yr^{-1} (IQR=1.69 km yr^{-1}; Table 4-S7). We also find that within the range of bird species in global PAs, the projected velocity is relatively high, with a median larger than 0.2 km yr^{-1} (IQR=0.59 km yr^{-1}) in the second half of the century under RCP8.5 (Table 4-S7), much below the velocity of observed range shifts (0.6-1.56 km yr^{-1}) of 55 birds in North America (Hitch & Leberg, 2007). But bird migration is highly constrained by shifts in abundance of tree species, of which the post-glacial migration rates are estimated to be much lower (0.06–0.26 km yr^{-1}). Over the protected land where mammal species are distributed, the median climate zone velocity is 0.19 km yr^{-1} (IQR=0.52 km yr^{-1}; Table 4-S7), potentially smaller than the estimated dispersal rates for 493 mammals (0.76-2.79 km yr^{-1}) in the Western Hemisphere (Schloss et al., 2012). But the regional biotic effects on species will be dependent ont only on regional exposure risk and but also on species sensitivity, which can be reflected by their climatic niche width and dispersal capability (Batllori et al., 2017; Carroll et al., 2015).
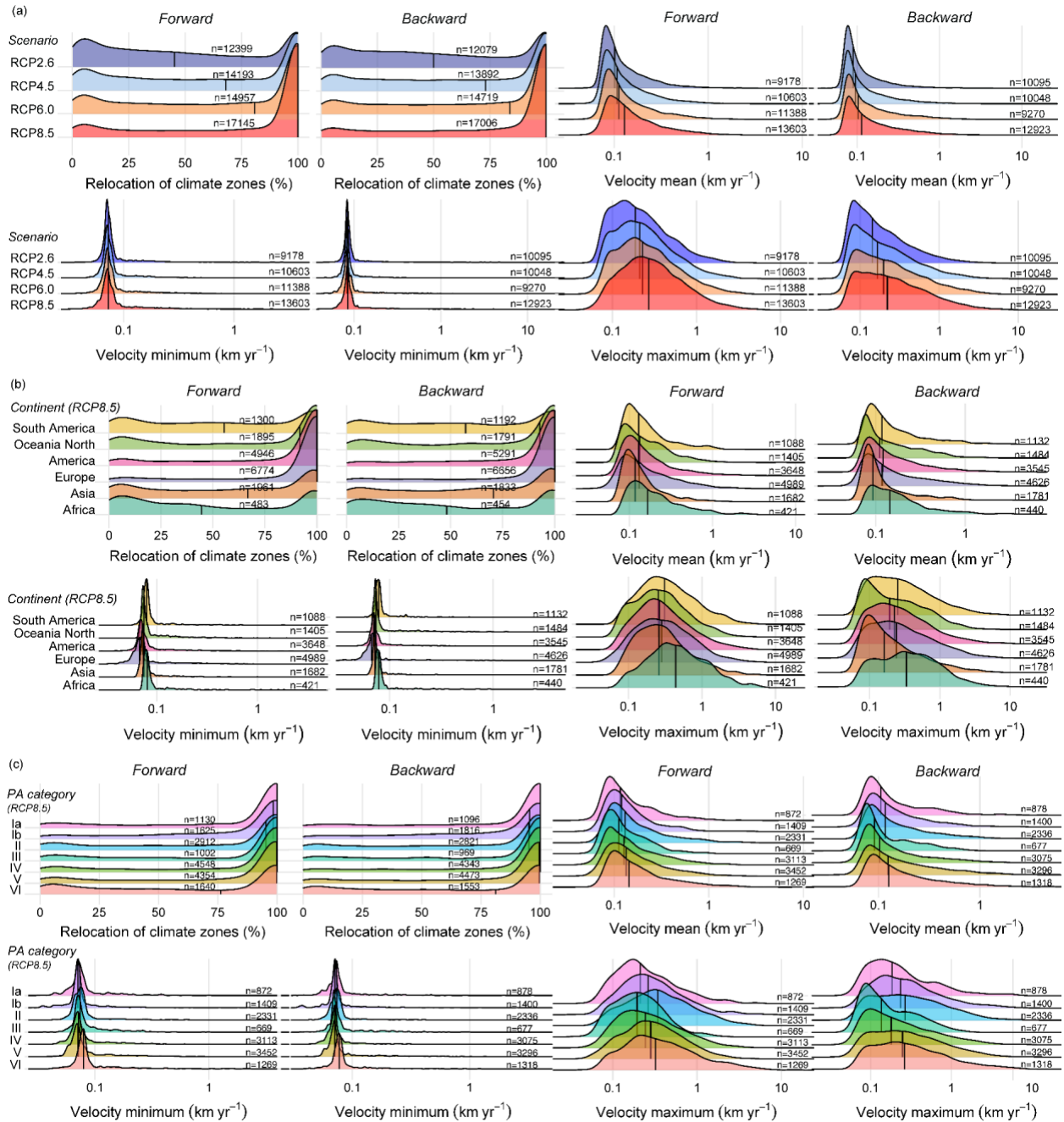
Figure 4-3 Summary of climate zone shifts for global terrestrial PA. Density plots of percent area undergoing climate zone shifts, and climate zone velocity lower, mean, and upper values for the global terrestrial PAs in this century (a) under different RCP scenarios, (b) in different continents, and (c) with different IUCN PA categories. The n numbers indicate the total number of PAs which could experience shifts of climate zones by the end of this century.

Additionally, habitat loss and fragmentation in PAs resulting from land use changes are creating

formidable barriers to species movement and disconnection across PA networks (Jones et al.,

2018; McGuire et al., 2016; Parks et al., 2020; Ward et al., 2020). We identify threats from human-induced land modifications which have negative consequences for biodiversity in the current PA networks. The percent area that could undergo transition from primary or secondary land to human modified land within global PAs is projected to be ~6% under RCP8.5 and is mainly distributed in Africa (Table 4-S4 and 4-S5). Protected areas with strict restrictions (IUCN category I-II) are projected to have ~5% area undergoing human-dominated land use change in this century, with more transition occurring in mid-century (Table 4-S4 and 4-S6). The landscapes within the PAs are normally less influenced by human activities and less fragmented, where keeping pace with changing climatic conditions is more feasible for species (Loarie et al., 2009). Minimizing human-dominated land use changes is critical for enhancing effectiveness of PAs to safeguard primary or secondary vegetation, facilitate species connectivity, and conserve landscapes and biodiversity (Fuller et al., 2010).

4.3.2 Exposure risk assessment
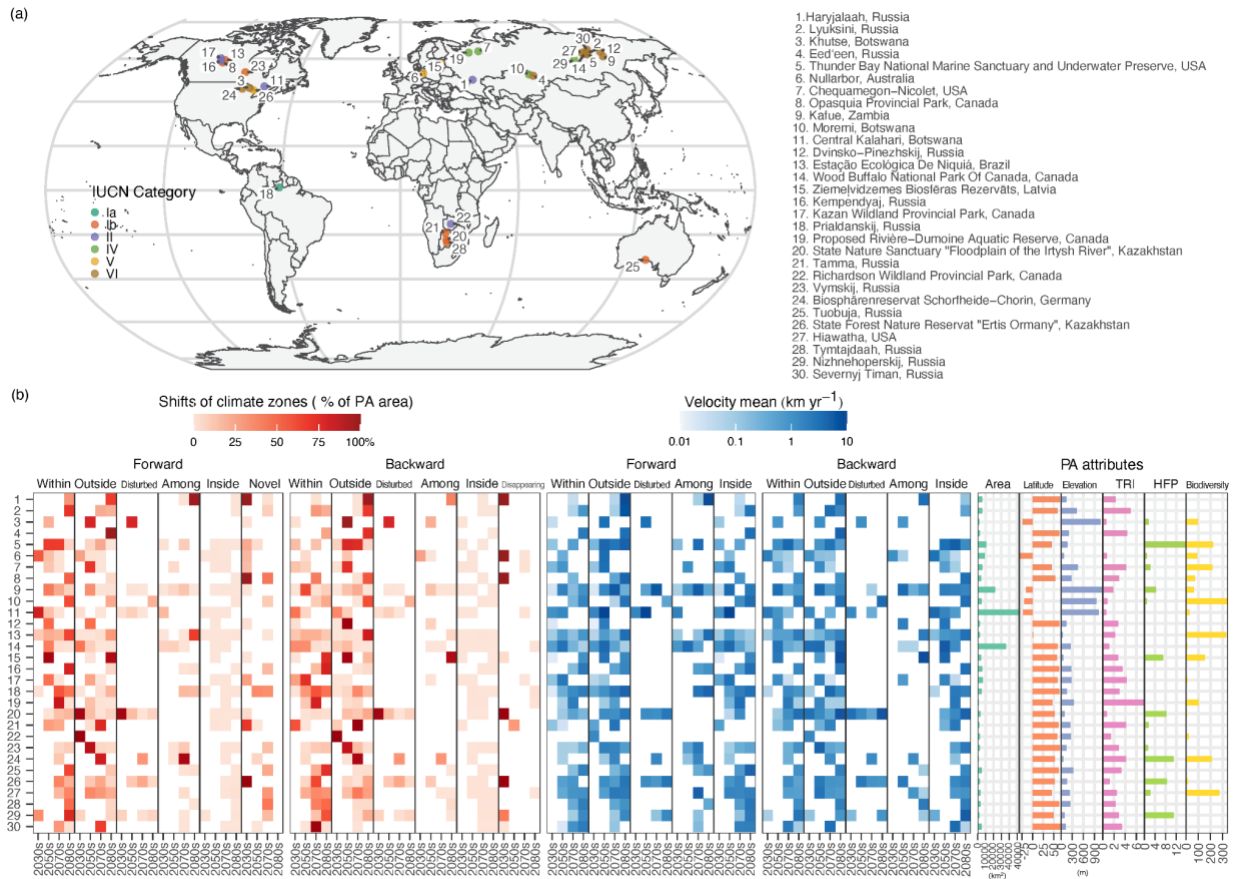
Figure 4-4 PAs exposed to large proportions of climate zone shifts and high climate velocity. (a) Geographic locations, IUCN management categories, countries and names of the 30 terrestrial PAs identified as PAs with extremely high exposure risks. These PAs are expected to experience completely different climate zone distribution and have mean velocities estimated larger than 1km yr^{-1} during this century. (b) Temporal patterns of percent area of climate zone area change (% of PA area), forward and backward climate zone velocity means, and associated attributes of PAs (size, latitude, elevation, terrain ruggedness index, human footprint, and species richness).

We perform an assessment of exposure risks for existing global terrestrial PAs by first examining the spatial patterns of climate shifts based on protection and land use states of the origins and destinations of climate velocities. Developed from the climatic relocation framework (Batllori et al., 2017), the assessment uses climate zone velocities to identify locations where climates, and potentially ranges of species, are redistributing within, among, outside, or inside the existing PA networks, or into unprotected lands with human-dominated land-use, as well as locations facing emergence of novel or disappearing climates.

The redistribution patterns of climates by the end of the century reveal that a small fraction of protected lands will have outgoing (forward) and incoming (backward) climates terminating outside of the current PA networks (7.6% and 8.8% respectively) under the RCP8.5 (Table 4-S4). Meanwhile, for 4.6% and 3.3% of projected lands, outgoing and incoming climates are originating from the surrounding unprotected lands and shifting into the PA boundaries. Additionally, 8.3% of global protected land area will encompass novel climates, with no precedent same climate zone within a 1,000 km search radius, and 6.6% will be exposed to disappearing climates. Climate zone shifts are more likely to occur within the protection limits of PAs (25%) and only a small area percentage (1.4%) shifts among PA networks, when connections between existing PAs can be promoted. The shifting climates may terminate in areas with human dominated land use outside the PA unit, and into surrounding crop, pasture, range, or urban land, posing increasing risks to species extinction and population decline(Newbold et al., 2015). More than three fourths of the global terrestrial PAs, with a coverage of 12.3% of global protected land area, will face threats from potential species movement into unprotected, human modified lands by the end of this century (over 7.3% by mid-century) (Table 4-S8).

The PAs that are expected to have the whole area experiencing relocation of climate zones by the end of this century and their mean velocity estimated to be larger than 1km yr^{-1} are identified (Figure 4-4). Located mainly in northern mid latitudes (50ºN to 60ºN) and southern low latitudes (10ºS to 20ºS) in North America, Europe, Russia, Brazil, Africa, and Australia (Figure 4-4a), these PAs are exposed to varied threats arising from climate relocated outside the PA network into unprotected or degraded land, or disappearing or novel climates, and may have limited opportunity if the relocation is within or among the PAs. We identify distinct temporal and

spatial patterns of different exposure risks for these PAs (Figure 4-4b). The elevations and terrain ruggedness index of the identified vulnerable PAs indicate general low topography complexity within these PAs, meaning they are more likely located in lowlands, or plateau. Moreover, these PAs are mostly biodiversity hotspots and have small sizes (Figure 4-4b).

Correlation analysis between climate zone shifts and PA characteristics suggests increased vulnerability for terrestrial PAs. We find positive correlations of climate zone velocity with elevation and terrain ruggedness (Figure 4-S4), implying that PAs exposed to larger climate zone velocity are more likely to be high elevations with complex topography. Positive correlation between biodiversity and climate zone velocity are found in South America, Africa, and Oceania, indicating higher threats to biodiversity (Figure 4-S4). In addition, the first half of this century showed stronger correlation of climate zone shifts with examined PA characteristics.

4.3.3 Dynamic spatial prioritization for conservation
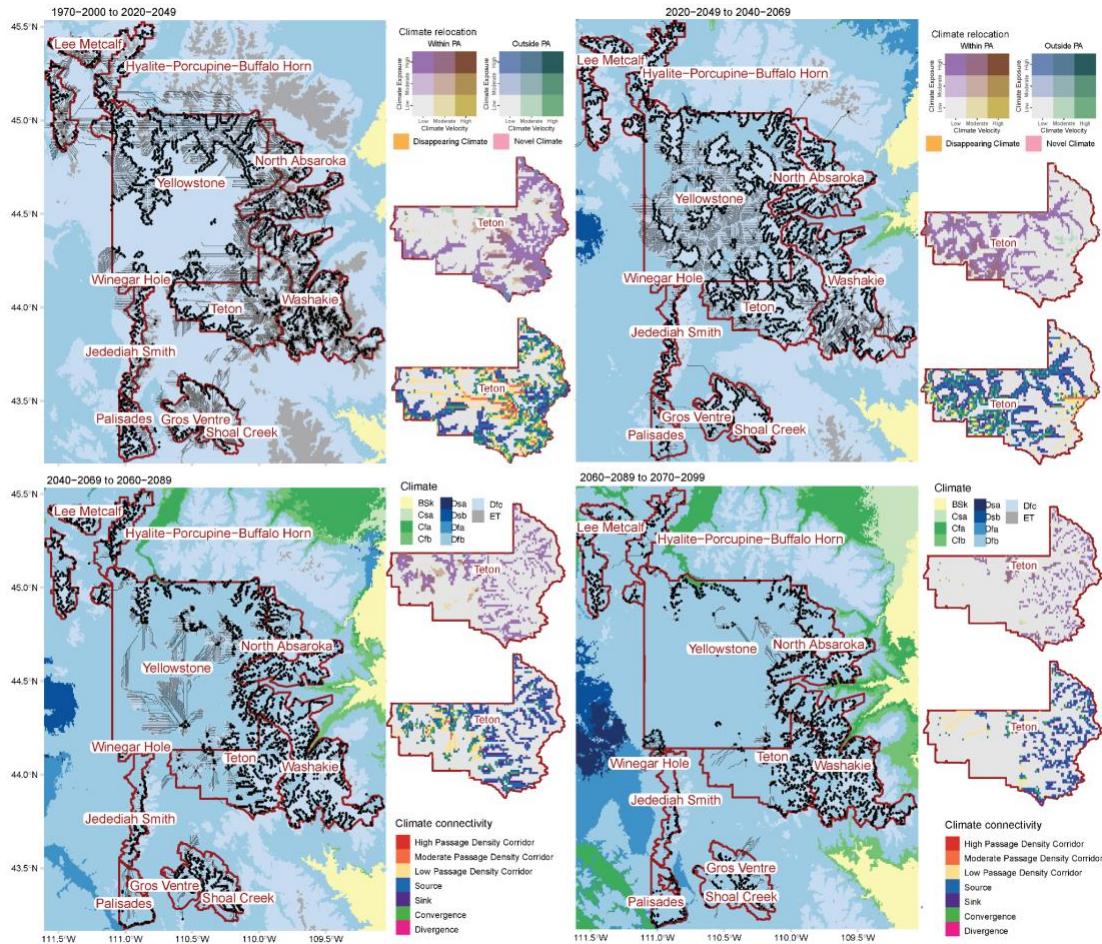
Figure 4-5 Regional case study of the use of climate zone velocity results for conservation prioritization in Yellowstone region. Boundaries of Yellowstone National Park (NP), Teton NP, Jedediah Smith Wilderness, Gros Ventre Wilderness, North Absaroka Wilderness, Washakie Wilderness, Lee Metcalf Wilderness, and other surrounding wilderness areas are outlined in red. Lines show climate zone velocities derived based on topographic paths, with black dots marked as the destinations. Based on 1-km climate zone velocity metric, we categorize the climate relocation patterns (results of Teton NP are shown as an example) using the length of velocity distance, the extent to which velocity path traverses different climate zones (defined as climate exposure index), whether climates are relocated within, among, inside or outside the PA networks (upper maps for results of Teton NP), which is modified from the Batllori's framework (Batllori et al., 2017). We also identify climate connectivity based on the density and percentage of velocities starting in, ending in, and passing through the given cells (lower maps for results of Teton NP). The method is adopted from Burrow's approach of mapping velocity pattern to indicate species distribution shifts (Burrows et al., 2014).

Our results can inform conservation planners to adaptively expand and conserve PAs over multiple time steps, by incorporating climate-induced biological movement and rearrangement of species assemblages in spatial prioritization. To provide a comprehensive example of the use of

climate zone velocity for conservation prioritization, we present a regional case study for Yellowstone region and surrounding wilderness (Figure 4-5). The region covers Yellowstone National Park (NP), Teton NP, and surrounding wilderness areas, including North Absaroka Wilderness, Washakie Wilderness, Lee Metcalf Wilderness, etc. Large proportion of these PAs are projected to transition from polar (ET) and boreal cold summer (Dfc) climate zones to boreal warm summer (Dfb) climate zones over the time frames of the study. Using climate zone velocities, we first assess the spatial relocation patterns of climate velocities across the PA networks to indicate varying threats for biodiversity that may reduce the conservation capacity and undermine the effectiveness of existing PAs. For example, novel and disappearing climates are potentially associated with aggregation and disaggregation of species assemblages (Garcia et al., 2014; Williams et al., 2007; Williams & Jackson, 2007). Climate velocities traversing different climate zones can impose higher exposure risks for sensitive species to track shifting climates (Dobrowski & Parks, 2016), and velocities originating from one PA and terminating in another can be prioritized for corridors linking existing PAs to assist climate-induced species range shifts (Venter, 2014).

Additionally, we identify climate connectivity features to reveal different patterns of species persistence and distribution shifts, and further identify priorities to promote connectivity. For example, sources and sinks of climates may lead to decline of local species richness, and increased local diversity with potential extinction for species with poor tolerance (Burrows et al., 2014). Moreover, results of incoming (backward) climate shifts can indicate potential sources and destinations of species colonization. High passage density can be suggested for biodiversity corridors to advance connections for climate migrants. In general, our projections of climate

shifts and exposure risk assessment can support future dynamic spatial conservation prioritization to ensure climatic connectivity and conservation capacity for global PAs.

4.4 Discussion

Climate change is driving redistribution of species at unprecedented rates, increasingly reducing the effectiveness of the spatially static PAs in conserving future biodiversity, which is concurred in our results and other recent studies (Asamoah et al., 2021; Batllori et al., 2017; Elsen et al., 2020; Hoffmann et al., 2019). We find that under the RCP8.5 scenario which current global warming trajectory is more consistent with, 20% and 38% of global protected land area could experience climatic conditions that correspond to different climate zones in the near-term and long-term future respectively (18% and 20% under RCP2.6, 18% and 26% under RCP4.5, 18% and 30% under RCP6.0). The changing rates of climate zone shifts are broadly consistent with the dynamics projected under emission scenarios, with reduced rates under RCP2.6 and heightened exposure rates under RCP8.5 (Figure 4-S5), which coincides with the relationship between increasing pace of shifting climate zones and global warming found in the previous study (Mahlstein et al., 2013).

We identify additional threats from land use transition and find that 6% of global protected land, mainly in Africa, is projected to undergo extensive human modification under RCP8.5 (1-2% under other scenarios). The human-induced land use degradation, which can lead to habitat loss and fragmentation, and impose dispersal barriers for species, may reinforce the climatic stress on biodiversity. We also identify the displacement of climates into or originating from unprotected surroundings with human dominated land use (crop, pasture, range, or urban land). Our results reveal that climate zones are projected to shift into PA networks with origins in unprotected

surroundings (4.6%, 6.1%, 6.9%, and 9.9% respectively). Moreover, climate zones are

redistributing outside PA networks (3.8%, 4.8%, 5.5%, and 7.6% respectively) and ending in

unprotected and human-dominated areas (Table 4-S4). In addition, we find a small fraction of

protected land area will face novel climate (3.7% under RCP2.6, 4.6% under RCP4.5, 5.1%

under RCP6.0, and 8.3% under RCP8.5) and disappearing climate (3.0%, 3.9%, 4.0%, and 6.6%

respectively), which are both more prevalent in the near future (2020-2049) (Table 4-S8) and for

PAs in northern and southern mid latitudes (Figure 4-2d).

These changes in climate zone distribution can alter the continuity of suitable climatic conditions

available for species to survive. Complementarily, climate zone velocities can indicate the paths

along which the species is required to move to track shifting climates across surrounding

topography. Climate zone velocity can be used not only to imply exposure risks and

opportunities for species range shifts, but also to help identify corridors, climate refugia, thus

guiding spatial prioritization of biodiversity conservation, restoration and connectivity for PA

networks (Brito-Morales et al., 2018; Burrows et al., 2014; Hamann et al., 2015). To enhance the

resilience of the PA networks to the anticipated redistribution of biodiversity, it is critical for

conservation planners to explicitly consider and address the spatiotemporal patterns of climate

shifts over the planning horizon and area. Our exposure risk assessment of the global terrestrial

PAs identifies PAs which will face substantial and rapid shifts in climates and will experience

changing patterns in present-day biodiversity, and thereby need more conservation efforts to

enhance adaptation when climate velocity may exceed the dispersal rates of most species

(Asamoah et al., 2021). These PAs are mostly located in mid latitudes of North America, Europe,

Russia, and Africa, across arid (B) and boreal (D) climate zones. Conversely, PAs exposed to

low climate velocity can provide potential local climate refugia and benefit from establishing

corridors to support species migration and facilitate connectivity (Ackerly et al., 2010; Brito-Morales et al., 2018; Dobrowski et al., 2021).

Based on climate velocity, other approaches quantifying exposure to different climates and other topographic and anthropogenic factors along potential migration pathway (Carroll et al., 2018; Dobrowski & Parks, 2016), assessing climate relocations patterns across PA networks(Batllori et al., 2017), and categorizing features for climate connectivity (Burrows et al., 2014), have been used in previous studies to develop adaptive PA conservation strategies in climate corridor delineation or climate refugia identification. These coarse-filter approaches can be complemented by fine-filter approaches, such as species distribution modeling to predict climatically suitable habitats for individual species, to incorporate more biological information (Jones et al., 2016; Tingley et al., 2014). As shown in the case study for conservation prioritization, our forecasts based on climate velocity are adaptive and can be combined with existing coarse-filter and fine-filter approaches to inform climate adaptation planning and biodiversity conservation prioritization.

To interpret the climate zone velocity results and understand their implications for biodiversity, there are a few issues to clarify. First, the temporal and spatial scales at which the velocity metric is measured are critical and need to be considered to interpret the metric. The study uses 1-km spatial resolution, given the finest available for global climate data and order of species dispersal capabilities. Velocity values may increase substantially with coarsened resolutions and exhibit transient decadal-scale variability (Dobrowski & Parks, 2016; Hamann et al., 2015). Long time frames can ignore fine scale variations and coarse resolution can overlook microrefugia and overestimate exposure risks (Garcia et al., 2014).

Second, velocity is a measure of species exposure to climate change, which is generic across species. The actual effects of climate change on biodiversity also depend on the species intrinsic abilities to address the exposure risk to climate change and other interacting human-induced threats. Altered availability of climatical suitable area, barriers created by human modifications and habitat fragmentation (Bennie et al., 2013; Schloss et al., 2012), varied adaptative and dispersal capacity of species can often result in delays and large variations in biological responses of individual species (I.-C. Chen et al., 2011; Parmesan & Yohe, 2003). Time lags in plant movement can further slow or impede the movements of species that depend on it for habitat (Alexander et al., 2018; Corlett & Westcott, 2013). Moreover, species may not shift their distribution under changing climate but tend to contract into suitable microrefugia within their current range and maintain low-density isolated populations (Lenoir et al., 2017).

Lastly, the climate zones defined by Köppen-Geiger climate classification, used in velocity calculation, have its limitations. Climate zones are distinguished based on thresholds and climate shifts in regions above and below the thresholds cannot be well represented. Another limitation is that other contributing factors such as wind, atmospheric CO2, and solar radiation are not accounted for in the classification (H. E. Beck et al., 2018; Cui, Liang, & Wang, 2021; Mahlstein et al., 2013). Despite these, Köppen-Geiger climate classification is a simple and effective approach to integrate climatic variables and characterize climate zones and demonstrates associations with distribution of biomes (Cui, Liang, & Wang, 2021).

Despite the considerations in coarse-filter climate velocity approach and limitations in climate zone definitions, our study provides a fine-scale quantitative assessment of near, mid and long-term climate change exposure for global terrestrial PAs. Our results highlight the varying spatiotemporal patterns of climate zone shifts and implications for biodiversity conservation over

112

multiple time steps. Shifts in climatic conditions and human-induced land-use degradation could drive large-scale biodiversity changes and undermine the conservation effectiveness of PA networks. To address the ongoing biodiversity crisis and achieve future conservation goals, anticipating climate shifts and climate-induced biological movement is crucial to developing strategic and adaptive PA conservation planning to ensure climatic connectivity and conservation capacity.

4.5 Data and Methods

4.5.1 Climate classification data

We used the 1-km global dataset of historical and future Köppen-Geiger climate classification (KGClim)(Cui, Liang, Wang, et al., 2021) to calculate climate zone velocity for contemporary baseline (1970-2000) and future (2020-2049, 2040-2069, 2060-2089, and 2070-2099) epoches for four RCPs (RCP2.6, 4.5, 6.0 and 8.5) (Table 4-S9). The Köppen-Geiger climate classification scheme used in KGClim dataset followed the classification criteria as described in Kottek et al. (2006) and Rubel and Kottek (2010) which was first presented by Geiger (1961). The classification characterizes climatic conditions based on warmth and aridity and distinguishes 30 climate types in tropical (A), arid (B), temperate (C), boreal (D), and polar (E) climate zones (Table 4-S1).

Baseline (1970-2000) Köppen-Geiger climate classification map was derived based on the 30-year averages of monthly surface air temperature and precipitation from 1-km WorldClim Historical Climate Data V2 (Fick & Hijmans, 2017). WorldClim historical V2 used thin-plate smoothing splines with elevation, distance to the coast and other satellite-derived independent variables to interpolate climate data from 9,000-60,000 weather stations (Fick & Hijmans, 2017).

KGClim future climate classification maps (2020-2049, 2040-2069, 2060-2089, and 2070-2099) were derived based on CCAFS's high-resolution (1-km) bias-corrected downscaled Coupled Model Intercomparison Project Phase 5 (CMIP5) model simulations (Navarro-Racines et al., 2020), which includes a total of 35 GCMs for RCP 2.6, 4.5, 6.0 and 8.5. CCAFS's bias-corrected and downscaled climate projections interpolated anomalies and applied the delta method to baseline climates to correct the model biases (Navarro-Racines et al., 2020), which can effectively reduce the bias effects from the threshold-based climate classification scheme (Hanf et al., 2012).

Climate sensitivity among GCMs could lead to uncertainties in climate projections. GCMs with large model biases exhibit discrepancies in Köppen climates as the Köppen scheme is very sensitive to thresholds. To assess the sensitivity to GCMs, we used model projections from 16 GCMs to estimate climate zone velocity for the randomly selected 100 PAs to show the inter-model variability in the metrics of climate zone shifts (Figure 4-S6). The KGClim dataset (Cui, Liang, Wang, et al., 2021) used in our study selected the highest confidence climate class from an ensemble of future climate maps generated by multiple model projections to develop the future climate classification maps.

4.5.2 Protected area and land use data

We used the World Database on Protected Area (WDPA) (UNEP-WCMC and IUCN, 2021) (https://www.protectedplanet.net/ accessed in June 2021) to delimit the global terrestrial protected areas. WDPA dataset provides a complete and up-to-date source of information on protected areas. First, we removed the PAs with marine coverage and excluded the PAs that are not identified or assigned as IUCN categories I–VI. To facilitate processing, we excluded the large PA in Greenland, Nationalparken I Nord-Og Østgrønland (area coverage=972,000 km²)

114

and retained PA polygons with area larger than 10km^2. We also dissolved overlapping polygons

with the same IUCN category to avoid duplicates. As some PAs consist of multiple polygons, we

used the unique ID WDPAID to identify each PA. Overall, our study included 22,681 terrestrial

PAs, covering 13.5 million km² (10.5% of land surface). The PA coverage of those with IUCN

categories Ia, Ib, II, III and IV, whose main objectives are biodiversity conservation and have

strict management levels, is estimated to be 6.1% of global land, including 14,265 PAs. The

continental PA terrestrial coverage ranges from 5.7% (Asia) to 20.5% (Oceania) and some

countries in Europe, Americas and Oceania have higher PA coverage (Table 4-S11).

To identify the PA attributes that are associated with the PA vulnerability, we examined

correlations between metrics of climate zone shifts with PA characteristics of topographic

heterogeneity, human pressure, and biotic uniqueness. Topographic attributes of PAs, including

elevation and terrain ruggedness, will be extracted from the product of multiple topographic

variables(Amatulli et al., 2018). This product is based on 90m elevation data from the Shuttle

Radar Topography Mission (SRTM) and has a final resolution of 1km. The mean elevation of

PA indicates the geographical location of PAs in highland or lowland regions. The Terrain

Ruggedness Index (TR) is a measure of topographic heterogeneity, which can buffer climate

change effects on ecosystems (Ackerly et al., 2010). The human footprint of a PA will be

calculated using the 1-km human footprint data of 2009 (Venter et al., 2016), which comprises

multiple indicators of human impact on natural systems from in situ and remotely sensed data.

The irreplaceability of PAs is a measure of biotic uniqueness and quantifies the degree of overlap

among the ranges of species (Le Saout et al., 2013). We overlaid the aggregated density maps of

species occurrences from Global Biodiversity Information Facility (GBIF) for bird (n=14,788),

mammal (n=20,867), reptile (n=19,501), and amphibian (n=9,541) species to quantify the species richness for each PA.

The future land use projections that we used to identify threats from human-induced land modifications, are from the Land-Use Harmonization (LUH2) project (Hurtt et al., 2020). LHU2 presents a set of harmonized land use scenarios for future projections at $0.25° \times 0.25°$ resolution(Hurtt et al., 2020). We used the annual gridded fractions of land-use states derived from LUH2 v.2f dataset for 2020-2100 and four scenarios (RCP2.6 from IMAGE, RCP4.5 from MESSAGEix-GLOBIOM, RCP6.0 from GCAM, RCP8.5 from ReMIND-MAgPIE). We considered land use states of managed pasture, rangeland, urban land, and cropland (all functional groups) as human-dominated land use states. Land area undergoing land-use transitions from primary and secondary land to human-dominated land use is identified to estimate the level of human-induced modifications to terrestrial land within each PA.

4.5.3 Climate zone velocity calculation

We developed an analytical measure of climate zone velocity that conforms to climate-analog velocity algorithms (Batllori et al., 2017; Carroll et al., 2018; Dobrowski et al., 2021; Heikkinen et al., 2020). It aims to measure the exposure changes in bioclimatic conditions faced by a species if the climate moves beyond the physiological tolerance of a local population. The climate zone velocity allows calculation of both forward and backward velocities to represent different change directions (Figure 4-1). The forward velocity indicates the distance from past climate locations to the nearest site with the same present climate, reflecting the minimum path that an organism must migrate to maintain constant climate conditions. The backward velocities measure the distance from projected future climate cells back to analogous current climate locations, reflecting the minimum path that a climatically adapted organism would have to

116

migrate to colonize the site. The two forms of velocities can be calculated based on the nearest distance between the climate types as follows,

$$V_A(N)_{forward} = \frac{\left\{ dist(AB) \times \frac{1}{I(kc\left(A_{past}\right)==kc(B_{present}))} \right\}}{Time_{|present-past|}} \quad (1)$$

$$V_A(N)_{backward} = \frac{\left\{ dist(AB) \times \frac{1}{I(kc\left(A_{future}\right)==kc(B_{present}))} \right\}}{Time_{|future-present|}} \quad (2)$$

where $V_A(N)$ is the velocity in site A and N as the searching area of a search radius (=1,000 km). With the recent advances in efficient nearest-neighbor search algorithms(M. Berg et al., 2010), global searches are computationally feasible for high-resolution raster datasets. $Time_{|future-present|}$ is the year number by subtracting the future-time year to the current-time year. $I()$ is the indicator function and returned 1 when the condition inside the parenthesis is satisfied, otherwise returned 0. $dist(AB)$ is the geographic distance between site A and B. $kc\left(A_{future}\right)$ is the Köppen climate type of site A at a future time.

Based on the origins and destinations indicated by climate zone velocity, we incorporated the 1-km topographic surface to generate topographic paths and aggregated the climate zones velocity for four future epochs to represent a continuous trajectory along which climate migrants track the climatic conditions through time and space (Figure 4-S1b). The 1-km elevation data used in our study was from Amatulli et al. (2018), which was derived from the aggregated elevation layers from global 250 m GMTED 2010 (Danielson & Gesch, 2011), and transformed to 1 km spatial grains using median of the values of grid cells within the aggregation window (4 x 4 cells) (Amatulli et al., 2018).

4.5.4 PA exposure risk assessment
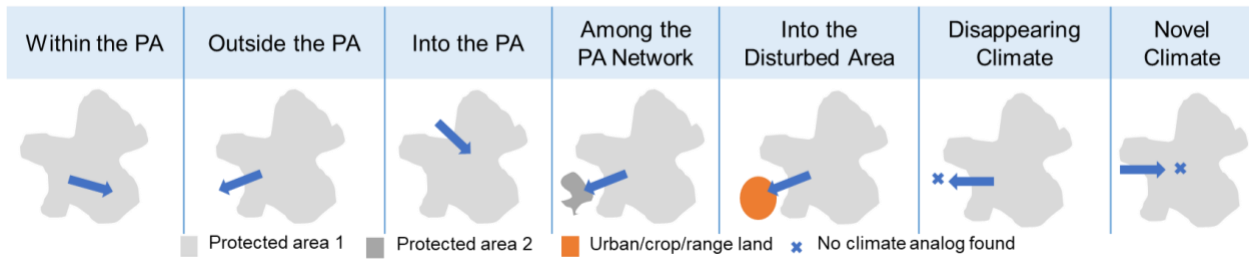
Figure 4-6. Conceptual framework to assess the spatial patterns of climate zone shifts in the global PA networks. For each PA, we assessed the shifts of climate zones based on a) area projected to undergo shifts of climate zones, b) direction and speed by climate zone velocity, and c) spatial patterns of climate zone shifts in the PA network. To interpret these metrics and assess the effects on conservation capacity of current PA networks, we categorized the spatial patterns of climate zone shifts based on whether climates are relocated within, among, outside, inside the PA networks or end in unprotected and human-dominated surroundings, and emergence of novel or disappearing climate zones for the global terrestrial PAs (Figure 4-6) .The framework was modified from the Batllori et al.(Batllori et al., 2017) For each focal cell, we determined the climate zone shift patterns, including within (categorized as "within"), outside (categorized as "outside"), into the given PA, among the PA network, into the disturbed area, disappearing climate, novel climate (categorized as 'Within', 'Outside', 'Inside', 'Among', 'Disturbed', 'Disappearing', and 'Novel' respectively). For each category, we quantified the area change in climate zones and climate zone velocity for each future epochs (2020-2049, 2040-2069, 2060-2089, and 2070-2099) under four RCP scenarios (See Fig. 4b for the 30 terrestrial PAs identified with extremely high exposure risks).

4.6 Supplementary Materials
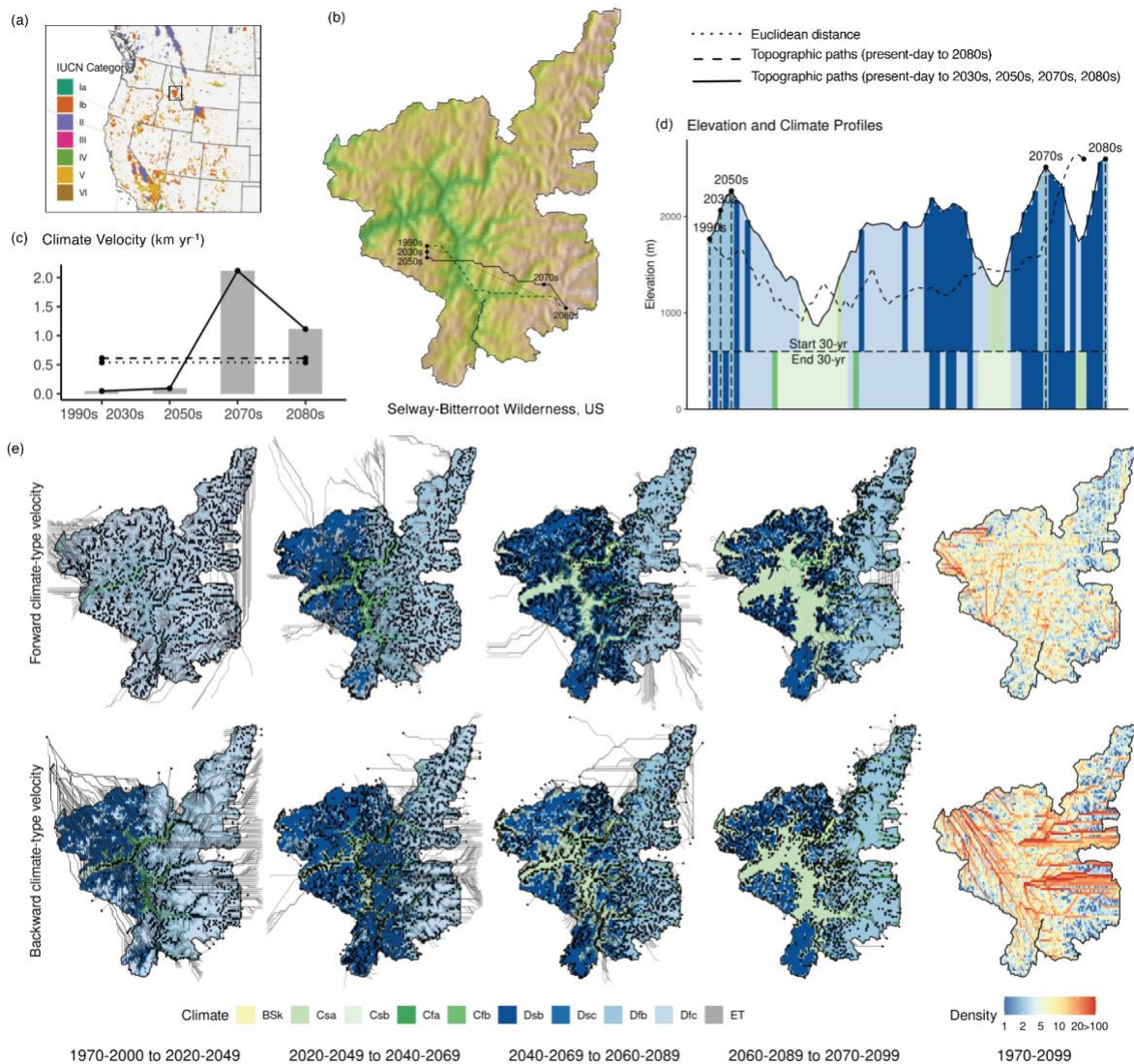
Figure 4-S1 Comparison of velocity algorithms and example results of climate zone velocity. (a) location and IUCN category of the Selway-Bitterroot Wilderness in the United States. (b) Climate velocities derived from three different approaches─dotted line showing climate velocity based on Euclidean distance and one future period, dashed line for climate velocity based on topographic paths, and solid line for climate velocity based on topographic paths and multiple future time frames, which is used in this study. (c) Temporal variations in climate velocities, which are largely overlooked by the first two velocity approaches. (d) Elevation and climate profiles of the climate velocities. The nearest pixel with the same climate class for a mountaintop is often found on an adjacent mountain top. In mountainous regions like this, traditional climate velocities show a general pattern of low values. In summary, Our climate velocity algorithm can benefit from the integrated biological information incorporated in the climate classes, finer temporal scale, and the use of topographic paths to approximate realistic biological movements. (e) Results of one protected area─the Selway-Bitterroot Wilderness. Lines show climate velocities with black dots marked as the trajectory destinations.
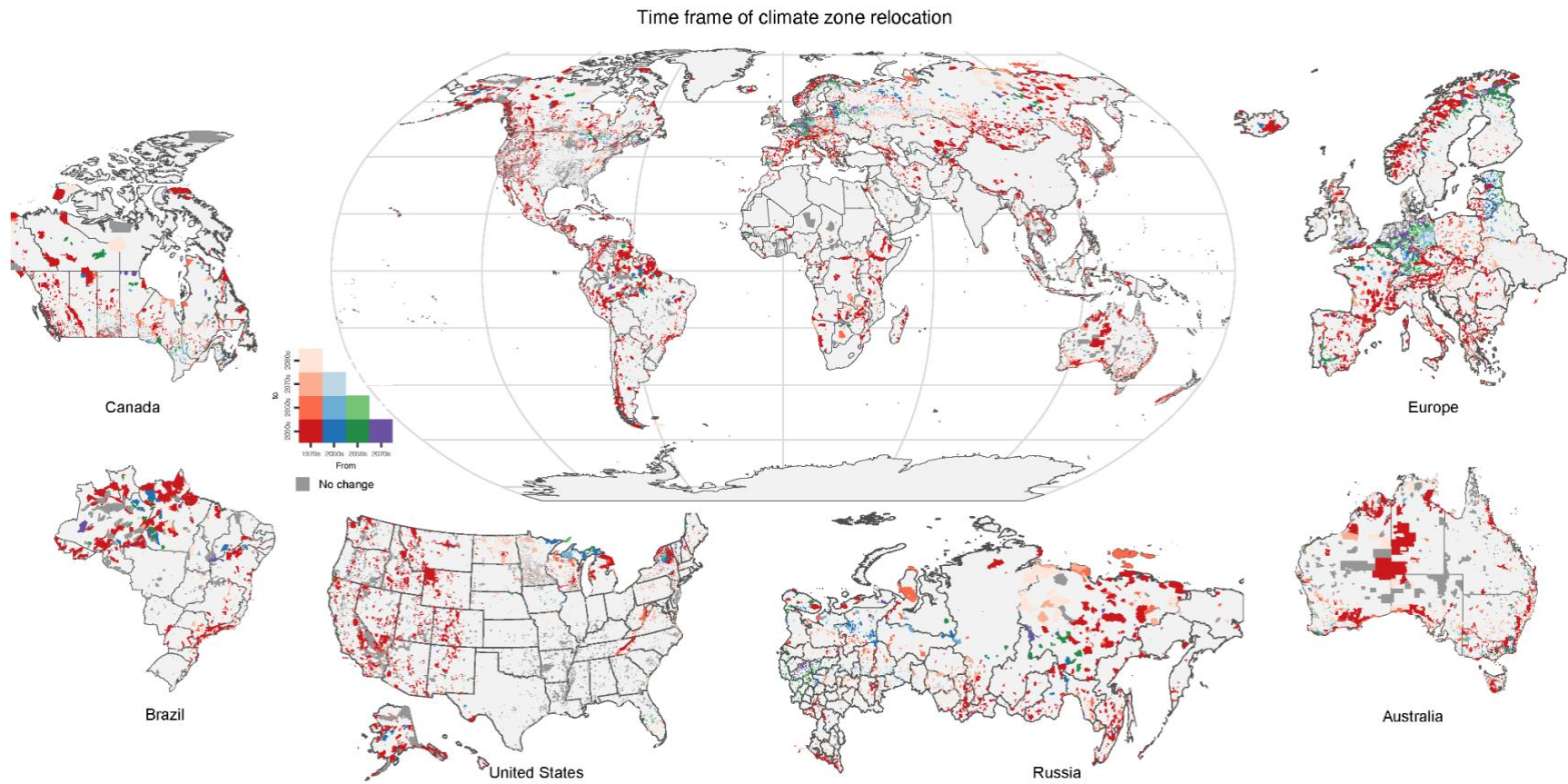
Figure 4-S2 Time frame of projected climate zone shifts within the global terrestrial PAs (RCP8.5). Time frame of the climate zone shifts is estimated with a start 30-year and a end 30-year from periods of 1970-2000 (1980s), 2020-2049 (2030s), 2040-2069 (2050s), 2060-2089 (2070s), and 2070-2099 (2080s). The time frame of climate zone shifts of most of the PAs around the world are expected to cover the whole century.
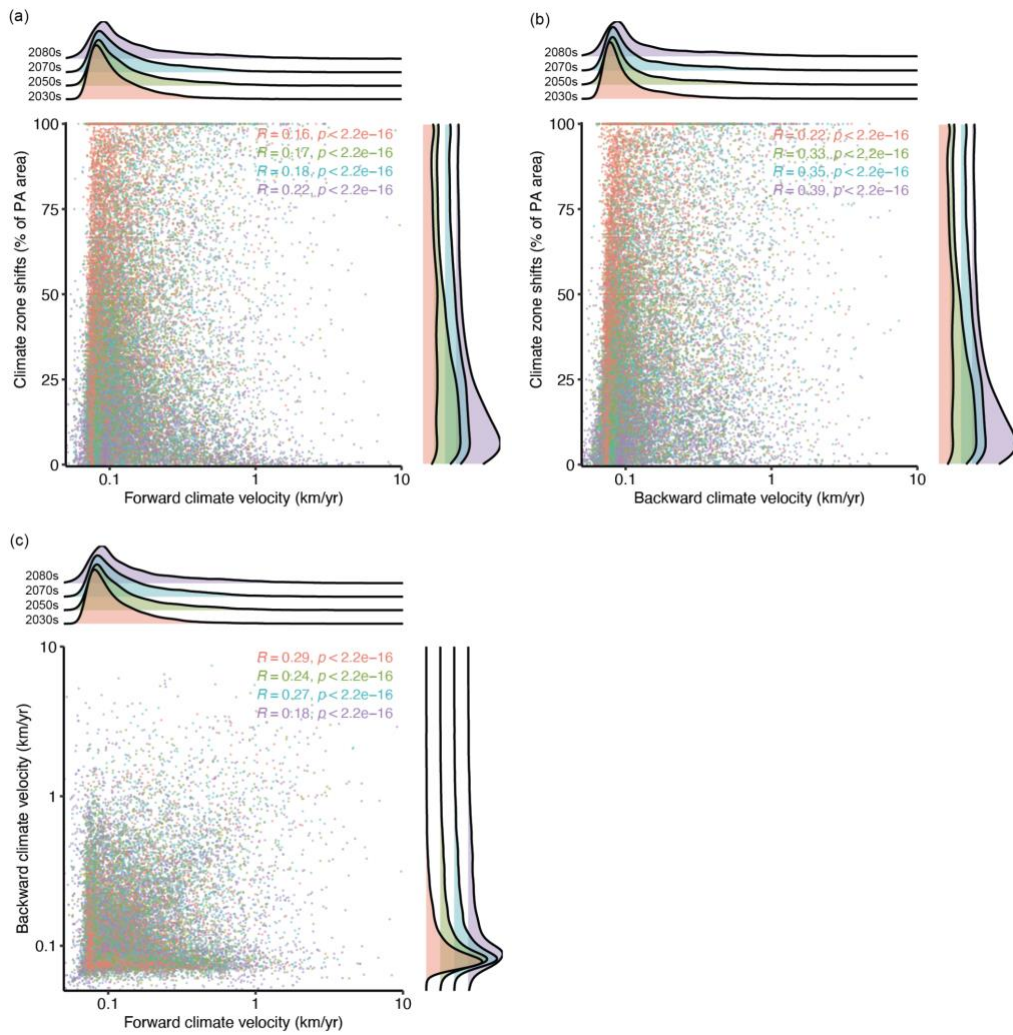
Figure 4-S3 Correlations between climate zone velocity and area percent with projected climate zone shifts (RCP8.5)
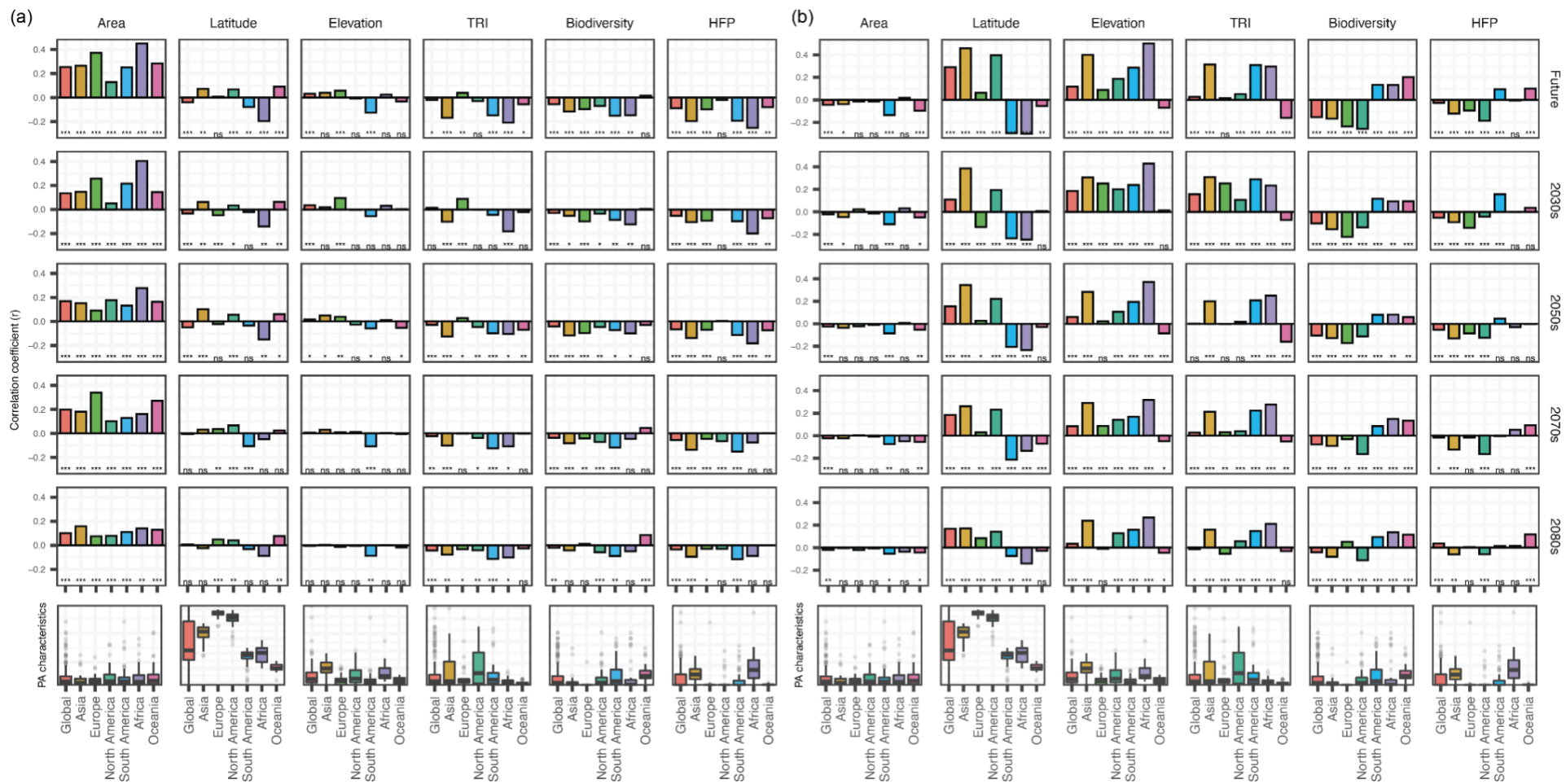
Figure 4-S4 Correlations of PA characteristics with (a) climate zone shifts and (b) climate zone velocity (RCP8.5). Asterisks represent the level of significance based on t-test accounting (*$p \leq 0.05$, **$p \leq 0.01$, ***$p \leq 0.001$, "ns" for non-significant ($p > 0.05$) correlation)
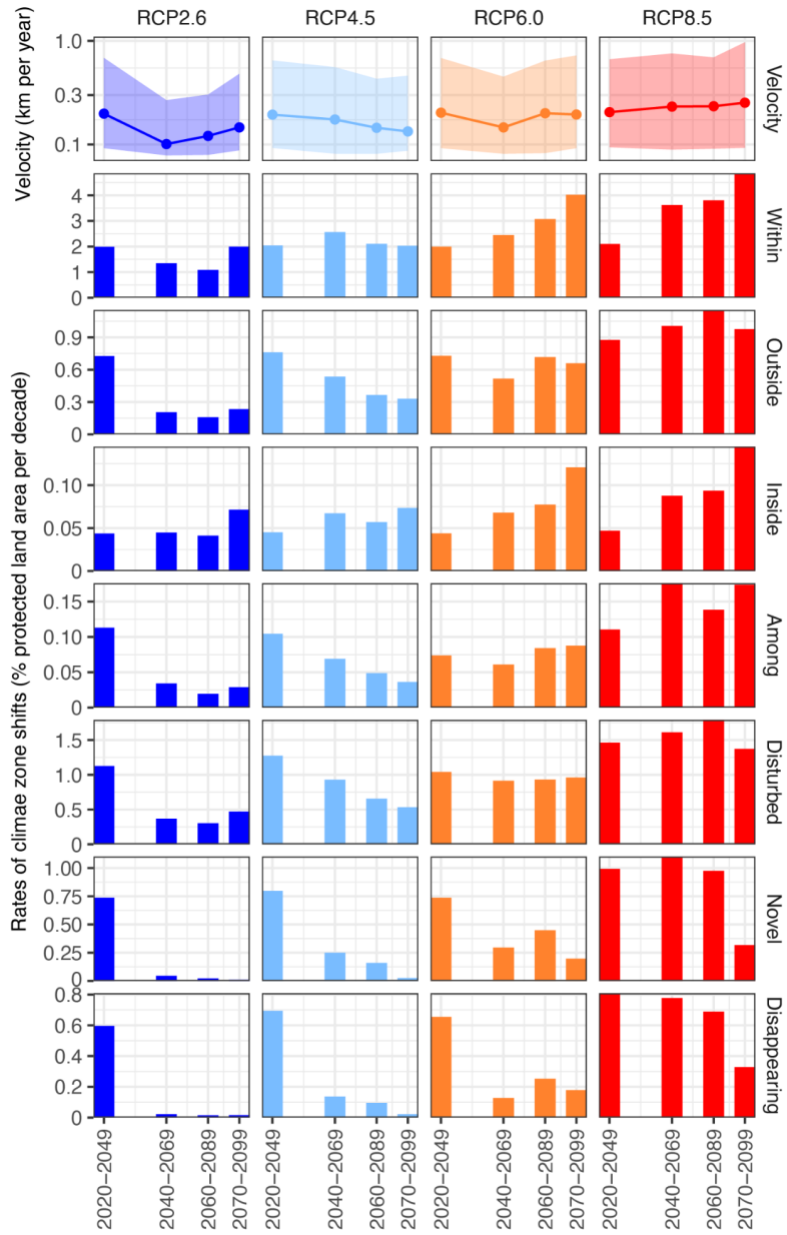
Figure 4-S5 Near-term (2020-2049), mid-term (2040-2069 and 2060-2089) and long-term (2080-2099) climate zone velocity and rates of climate zone shifts.
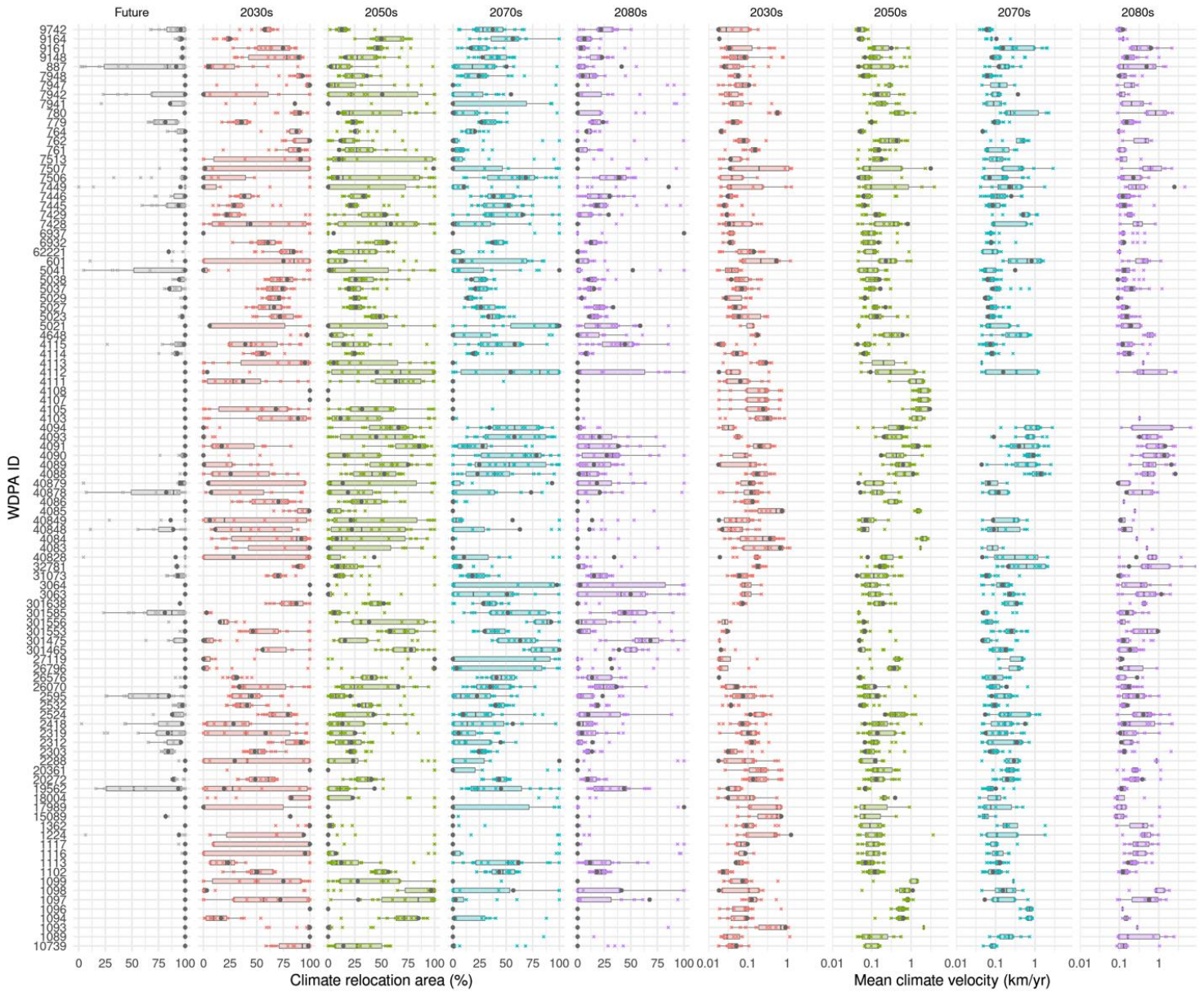
Figure 4-S6 Sensitivity of PA-level climate zone relocation and mean climate velocity to CMIP5 GCMs. X marks indicate the climate zone relocation and mean climate velocity results based on climate classification maps derived from individual GCMs. Black dots indicate the results presented in the main article, which are based on the climate classification maps with the highest confidence level using multiple CMIP5 GCMs. The scenario is RCP8.5 and the 50 PAs are randomly selected.

Table 4-S1 Criteria of the Köppen-Geiger climate classification with temperature in ºC and precipitation in mm.

1st	2nd	3rd	Description	Criterion
A			Tropical	Not (B) & $T_{cold} \geq 18$
	f		- Rainforest	$P_{dry} \geq 60$
	m		- Monsoon	Not (Af) & $P_{dry} \geq 100 - MAP/25$
	w		- Savannah	Not (Af) & $P_{dry} < 100 - MAP/25$
B			Arid	$MAP < 10 \times P_{threshold}$
	W		- Desert	$MAP < 5 \times P_{threshold}$
	S		- Steppe	$MAP \geq 5 \times P_{threshold}$
		h	-- Hot	$MAT \geq 18$
		k	-- Cold	$MAT < 18$
C			Temperate	Not (B) & $T_{hot} > 10$ & $-3 < T_{cold} < 18$
	w		- Dry winter	$P_{wdry} < P_{swet}/10$
	s		- Dry summer	*Not (w)* & $P_{sdry} < 40$ & $P_{sdry} < P_{wwet}/3$
	f		- Without dry season	Not (s) or (w)
		a	-- Hot summer	$T_{hot} \geq 22$
		b	-- Warm summer	Not (a) & $T_{mon10} \geq 4$
		c	-- Cold summer	Not (a or b) & $1 \leq T_{mon10} < 4$
D			Boreal	Not (B) & $T_{hot} > 10$ & $T_{cold} \leq -3$
	w		- Dry winter	$P_{wdry} < P_{swet}/10$
	s		- Dry summer	*Not (w)* & $P_{sdry} < 40$ & $P_{sdry} < P_{wwet}/3$
	f		- Without dry season	Not (s) or (w)
		a	- Hot summer	$T_{hot} \geq 22$
		b	- Warm summer	Not (a) & $T_{mon10} \geq 4$
		c	- Cold summer	Not (a), (b) or (d)
		d	- Very cold winter	Not (a) or (b) & $T_{cold} < -38$
E			Polar	Not (B) & $T_{hot} \leq 10$
	T		- Tundra	$T_{hot} > 0$
	F		- Frost	$T_{hot} \leq 0$

MAT = mean annual air temperature (°C); T_{cold} = the air temperature of the coldest month (°C); T_{hot} = the air temperature of the warmest month (°C); T_{mon10} = the number of months with air temperature >10 °C; MAP = mean annual precipitation (mm y^{-1}); P_{dry} = precipitation in the driest month (mm month^{-1}); P_{sdry} = precipitation in the driest month in summer (mm month^{-1}); P_{wdry} = precipitation in the driest month in winter (mm month^{-1}); P_{swet} = precipitation in the wettest month in summer (mm month^{-1}); P_{wwet} = precipitation in the wettest month in winter (mm month^{-1}); $P_{threshold} = 2 \times MAT$ if >70% of precipitation falls in winter, $P_{threshold} = 2 \times MAT + 28$ if >70% of precipitation falls in summer, otherwise $P_{threshold} = 2 \times MAT + 14$.

Table 4-S2 Recent studies applying local climate velocity or climate analog velocity

Reference	Velocity algorithm	Research topic	Spatial coverage	Res.	Data	Periods	Scenario
Dobrowski et al., 2013	Local climate velocity	Species exposure to climate change	North America	5km	12 CMIP5 GCMs	1981-2010, 2071-2100	RCP8.5
Burrows et al., 2014	Local climate velocity	Climate velocity trajectory and climate connectivity	Global land and ocean	1°	HadISST, CRU, CSIRO ACCESS1.0	1960-2009, 2006-2100	RCP4.5, RCP8.5
Ordonez et al., 2014	Local climate velocity	Species exposure to climate change	US	10km	CMIP5 GCMs	2001-2011, 2041-2051	RCP2.6, RCP6.0, RCP8.5
Batllori et al., 2017	Climate analog velocity	PA exposure to climate change	US PA network	1km	MPI-ESM-LR	1981-2010, 2071-2100	RCP8.5
Carroll et al., 2018	Climate analog velocity	Climate connectivity	North America	5km	15 CMIP5 GCMs	1981-2010, 2071-2100	RCP8.5
Heikkinen et al., 2020	Climate analog velocity	PA exposure to climate change	Finland PA network	50m, 1km	ECA&D, 23 CMIP5 GCMs	1981-2010, 2077-2099	RCP2.6, RCP4.5, RCP8.5

Table 4-S3 Summary of climate zone velocity, percent area of climate zone and human-induced land modifications within global PAs

	Climate zone velocity (Median (IQR)) (km yr-1)								Climate zone and human-dominated land use changes (% of PA)						
	1980s to 2030s		2030s to 2050s		2050s to 2070s		2070s to 2080s		1980s to 2030s	2030s to 2050s		2050s to 2070s		2070s to 2080s	
	Forward	Backward	Forward	Backward	Forward	Backward	Forward	Backward	Climate zone	Climate zone	Land use	Climate zone	Land use	Climate zone	Land use
RCP2.6	0.2 (0.59)	0.2 (0.75)	0.1 (0.19)	0.12 (0.25)	0.12 (0.22)	0.11 (0.21)	0.15 (0.39)	0.13 (0.38)	17.6%	3.3%	0.1%	2.6%	0.3%	2.3%	0.4%
RCP4.5	0.19 (0.55)	0.19 (0.64)	0.17 (0.48)	0.22 (0.76)	0.14 (0.35)	0.16 (0.43)	0.13 (0.37)	0.15 (0.45)	18.3%	6.9%	0.9%	5.4%	0.5%	2.5%	0.2%
RCP6.0	0.2 (0.59)	0.19 (0.7)	0.15 (0.37)	0.16 (0.52)	0.2 (0.56)	0.27 (0.92)	0.19 (0.63)	0.24 (0.93)	17.7%	6.7%	0.9%	8.8%	0.4%	5.0%	0.1%
RCP8.5	0.21 (0.57)	0.21 (0.68)	0.23 (0.67)	0.28 (0.99)	0.23 (0.6)	0.3 (0.92)	0.25 (0.88)	0.31 (1.17)	20.2%	11.8%	1.8%	12.1%	2.4%	6.3%	1.5%
IUCN categories (RCP8.5)															
• I-II	0.19 (0.58)	0.19 (0.58)	0.22 (0.76)	0.22 (0.76)	0.19 (0.5)	0.19 (0.5)	0.19 (0.62)	0.19 (0.62)	22.0%	13.8%	2.2%	13.6%	3.1%	6.8%	1.9%
• III-VI	0.22 (0.56)	0.22 (0.56)	0.24 (0.61)	0.24 (0.61)	0.28 (0.69)	0.28 (0.69)	0.31 (1.11)	0.31 (1.11)	18.9%	10.3%	1.5%	10.9%	1.8%	5.9%	1.2%

Table 4-S4 Summary of velocity within global PAs by RCP scenario, climate zone and species by 2100

| Scenarios | Climate zone velocity (km yr-1) | | | | Climate zone change (% of global PA area) | | | | | | | |
| | Forward | | Backward | | Forward | | | | Backward | | | |
	Mean	Median	Mean	Median	Within	Outside	Inside	Disappearing	Within	Outside	Inside	Novel
RCP2.6	0.45	0.16	0.70	0.16	12.5%	3.8%	4.6%	3.0%	13.1%	4.3%	3.3%	3.7%
RCP4.5	0.50	0.17	0.62	0.19	17.3%	4.8%	6.1%	3.9%	18.1%	5.6%	5.0%	4.6%
RCP6.0	0.57	0.19	0.72	0.21	19.8%	5.5%	6.9%	4.0%	20.8%	6.3%	5.8%	5.1%
RCP8.5	0.64	0.22	0.79	0.25	25.0%	7.6%	9.9%	6.6%	24.6%	8.8%	7.4%	8.3%

Table 4-S5 Summary of velocity, climate zone and land use changes within global PAs by continent/country (RCP8.5)

Continent/ Country	Climate zone velocity (Median (IQR)) (km yr^{-1})								Climate zone and human-dominated land use changes (% of PA area (% of global PA area))						
	1980s to 2030s		2030s to 2050s		2050s to 2070s		2070s to 2080s		1980s to 2030s	2030s to 2050s		2050s to 2070s		2070s to 2080s	
	Forward	Backward	Forward	Backward	Forward	Backward	Forward	Backward	Climate	Climate	Land use	Climate	Land use	Climate	Land use
• Africa	0.37 (0.92)	0.34 (0.9)	0.46 (1.38)	0.41 (1.11)	0.25 (0.53)	0.22 (0.41)	0.31 (0.88)	0.28 (0.69)	15% (3%)	6% (1%)	10% (2%)	5% (1%)	13% (2%)	3% (0%)	8.5% (1.4%)
• Asia	0.12 (0.17)	0.13 (0.39)	0.14 (0.3)	0.14 (0.48)	0.14 (0.34)	0.16 (0.62)	0.17 (0.52)	0.2 (0.81)	19% (2%)	11% (1%)	0.6% (0.1%)	11% (1%)	0.4% (0.1%)	6% (1%)	0.3% (0%)
- Russia	0.47 (1.33)	0.61 (1.47)	0.32 (0.78)	0.44 (1.08)	0.43 (1.15)	0.57 (1.39)	0.53 (2.1)	0.7 (2.23)	39% (4%)	20% (2%)	0% (0%)	22% (3%)	0% (0%)	12% (1%)	0% (0%)
• Europe	0.29 (0.94)	0.32 (1.15)	0.25 (0.63)	0.32 (0.95)	0.29 (0.79)	0.41 (1.12)	0.35 (1.39)	0.48 (1.73)	36% (6%)	20% (3%)	0.1% (0%)	23% (4%)	0.2% (0%)	13% (2%)	0.1% (0%)
• North America	0.15 (0.36)	0.15 (0.44)	0.23 (0.87)	0.36 (1.59)	0.23 (0.59)	0.29 (1.01)	0.19 (0.58)	0.21 (0.9)	30% (5%)	21% (4%)	0.2% (0%)	21% (4%)	0.1% (0%)	9% (2%)	0.1% (0%)
- United States	0.12 (0.2)	0.12 (0.25)	0.15 (0.34)	0.17 (0.54)	0.19 (0.48)	0.24 (1.09)	0.11 (0.28)	0.14 (0.5)	30% (3%)	22% (2%)	0.3% (0%)	23% (2%)	0.1% (0%)	9% (1%)	0% (0%)
- Canada	0.27 (0.82)	0.26 (1.16)	0.61 (1.95)	1.19 (3.1)	0.33 (0.8)	0.4 (1)	0.4 (1.11)	0.45 (1.81)	32% (2%)	25% (2%)	0% (0%)	23% (2%)	0% (0%)	10% (1%)	0% (0%)
• Oceania	0.22 (0.46)	0.34 (0.77)	0.39 (0.93)	0.26 (0.56)	0.25 (0.45)	0.27 (0.6)	0.22 (0.55)	0.21 (0.5)	16% (2%)	7% (1%)	0.2% (0%)	5% (1%)	0.1% (0%)	2% (0%)	0.1% (0%)
• South America	0.17 (0.36)	0.14 (0.27)	0.17 (0.37)	0.16 (0.37)	0.2 (0.43)	0.24 (0.65)	0.22 (0.58)	0.28 (0.84)	10% (2%)	5% (1%)	0.1% (0%)	6% (1%)	0.1% (0%)	4% (1%)	0% (0%)
- Brazil	0.17 (0.22)	0.21 (0.35)	0.24 (0.45)	0.22 (0.46)	0.28 (0.5)	0.35 (0.76)	0.39 (0.93)	0.58 (1.52)	7% (1%)	4% (1%)	0.1% (0%)	5% (1%)	0.2% (0%)	4% (1%)	0.1% (0%)

Table 4-S6 Summary of velocity, climate zone and land use changes within global PAs by IUCN category (RCP8.5)

| IUCN Categories | Climate zone velocity (Median (IQR)) (km yr^{-1}) | | | | | | | | Climate zone and human-dominated land use changes (% of PA area (% of global PA area)) | | | | | | |
| | 1980s to 2030s | | 2030s to 2050s | | 2050s to 2070s | | 2070s to 2080s | | 1980s to 2030s | 2030s to 2050s | | 2050s to 2070s | | 2070s to 2080s | |
	Forward	Backward	Forward	Backward	Forward	Backward	Forward	Backward	Climate	Climate	Land use	Climate	Land use	Climate	Land use
• I-II	0.19 (0.58)	0.19 (0.58)	0.22 (0.76)	0.22 (0.76)	0.19 (0.5)	0.19 (0.5)	0.19 (0.62)	0.19 (0.62)	22% (9%)	14% (6%)	2.2% (0.9%)	14% (6%)	3.1% (1.4%)	7% (3%)	1.9% (0.8%)
- Ia	0.53 (1.67)	0.49 (1.48)	0.2 (0.54)	0.3 (0.78)	0.21 (0.48)	0.48 (1.42)	0.2 (0.5)	0.31 (1.17)	21% (1%)	12% (1%)	0.5% (0%)	14% (1%)	0% (0%)	7% (0%)	0% (0%)
- Ib	0.14 (0.38)	0.18 (0.68)	0.23 (0.77)	0.44 (1.88)	0.18 (0.41)	0.18 (0.63)	0.17 (0.48)	0.2 (0.82)	31% (3%)	22% (2%)	0.2% (0%)	19% (2%)	0% (0%)	9% (1%)	0% (0%)
- II	0.17 (0.43)	0.15 (0.4)	0.22 (0.8)	0.24 (1.01)	0.2 (0.56)	0.24 (0.76)	0.21 (0.76)	0.27 (1.17)	19% (5%)	11% (3%)	1.9% (0.5%)	12% (3%)	0.7% (0.2%)	6% (2%)	0.1% (0%)
• III-VI	0.22 (0.56)	0.22 (0.56)	0.24 (0.61)	0.24 (0.61)	0.28 (0.69)	0.28 (0.69)	0.31 (1.11)	0.31 (1.11)	19% (11%)	10% (6%)	1.5% (0.9%)	11% (6%)	1.8% (1%)	6% (3%)	1.2% (0.7%)
- III	0.1 (0.09)	0.08 (0.1)	0.16 (0.25)	0.12 (0.2)	0.15 (0.25)	0.11 (0.22)	0.2 (0.48)	0.19 (0.4)	16% (0%)	7% (0%)	1.1% (0%)	6% (0%)	0.1% (0%)	3% (0%)	0% (0%)
- IV	0.19 (0.41)	0.23 (0.63)	0.22 (0.5)	0.25 (0.72)	0.27 (0.61)	0.41 (1.26)	0.22 (0.66)	0.37 (1.3)	20% (3%)	15% (2%)	1.4% (0.2%)	16% (2%)	1.2% (0.2%)	7% (1%)	0.4% (0.1%)
- V	0.16 (0.22)	0.15 (0.3)	0.19 (0.42)	0.21 (0.63)	0.19 (0.38)	0.25 (0.68)	0.2 (0.55)	0.22 (0.73)	22% (2%)	14% (1%)	0.8% (0.1%)	15% (2%)	0.4% (0%)	8% (1%)	0.2% (0%)
- VI	0.36 (0.97)	0.41 (1.15)	0.34 (0.88)	0.33 (0.89)	0.41 (1.12)	0.42 (1.06)	0.62 (2.07)	0.5 (1.6)	17% (5%)	7% (2%)	0.1% (0%)	7% (2%)	0% (0%)	5% (1%)	0% (0%)

Table 4-S7 Summary of velocity within global PAs by RCP scenario, climate zone and species

	Climate zone velocity (Median (IQR)) (km yr^{-1})							
	1980s to 2030s		2030s to 2050s		2050s to 2070s		2070s to 2080s	
	Forward	Backward	Forward	Backward	Forward	Backward	Forward	Backward
RCP2.6	0.2 (0.59)	0.2 (0.75)	0.1 (0.19)	0.12 (0.25)	0.12 (0.22)	0.11 (0.21)	0.15 (0.39)	0.13 (0.38)
RCP4.5	0.19 (0.55)	0.19 (0.64)	0.17 (0.48)	0.22 (0.76)	0.14 (0.35)	0.16 (0.43)	0.13 (0.37)	0.15 (0.45)
RCP6.0	0.2 (0.59)	0.19 (0.7)	0.15 (0.37)	0.16 (0.52)	0.2 (0.56)	0.27 (0.92)	0.19 (0.63)	0.24 (0.93)
RCP8.5	0.21 (0.57)	0.21 (0.68)	0.23 (0.67)	0.28 (0.99)	0.23 (0.6)	0.3 (0.92)	0.25 (0.88)	0.31 (1.17)
Major climate zones (RCP8.5)								
• Tropical	0.15 (0.18)	0.19 (0.4)	0.19 (0.34)	0.22 (0.65)	0.24 (0.45)	0.23 (0.56)	0.29 (0.69)	0.22 (0.63)
• Arid	0.25 (0.55)	0.28 (0.68)	0.35 (0.93)	0.27 (0.6)	0.26 (0.53)	0.27 (0.62)	0.34 (0.9)	0.34 (0.92)
• Temperate	0.15 (0.28)	0.1 (0.17)	0.17 (0.44)	0.13 (0.39)	0.16 (0.32)	0.17 (0.53)	0.18 (0.48)	0.19 (0.66)
• Boreal	0.25 (0.71)	0.28 (1.07)	0.29 (0.91)	0.44 (1.47)	0.27 (0.73)	0.41 (1.27)	0.29 (1.23)	0.42 (1.69)
• Polar	0.21 (1)	0.09 (0.06)	0.13 (0.32)	0.08 (0.07)	0.24 (0.89)	0.1 (0.09)	0.1 (0.33)	0.06 (0.08)
Species (RCP8.5)								
• Amphibian	0.14 (0.22)	0.12 (0.23)	0.18 (0.5)	0.17 (0.57)	0.17 (0.38)	0.19 (0.53)	0.19 (0.51)	0.19 (0.63)
• Ave	0.17 (0.38)	0.16 (0.44)	0.21 (0.57)	0.23 (0.84)	0.2 (0.48)	0.24 (0.76)	0.2 (0.59)	0.22 (0.84)
• Mammal	0.15 (0.28)	0.14 (0.33)	0.19 (0.57)	0.2 (0.77)	0.18 (0.41)	0.21 (0.66)	0.19 (0.52)	0.19 (0.65)
• Reptile	0.15 (0.26)	0.15 (0.33)	0.21 (0.56)	0.19 (0.56)	0.18 (0.38)	0.18 (0.49)	0.2 (0.56)	0.19 (0.63)
• Amphibian	0.14 (0.22)	0.12 (0.23)	0.18 (0.5)	0.17 (0.57)	0.17 (0.38)	0.19 (0.53)	0.19 (0.51)	0.19 (0.63)

Table 4-S8 Patterns of forward climate zone velocities in PA networks. Values in parentheses are based on backward velocities.

Scenario	Type	Total area (% of PA area)				PA level (% of PAs)			
		1980s to 2030s	2030s to 2050s	2050s to 2070s	2070s to 2080s	1980s to 2030s	2030s to 2050s	2050s to 2070s	2070s to 2080s
RCP2.6	Within	9.9% (9.8%)	2.7% (2.5%)	2.2% (2.0%)	2.0% (1.8%)	34% (31%)	29% (27%)	27% (25%)	26% (24%)
	Outside	3.6% (3.3%)	0.4% (0.4%)	0.3% (0.3%)	0.2% (0.2%)	33% (32%)	23% (21%)	20% (19%)	18% (17%)
	Inside	4.0% (2.8%)	0.4% (0.5%)	0.3% (0.3%)	0.3% (0.3%)	28% (29%)	20% (22%)	20% (17%)	17% (16%)
	Among	0.6% (0.5%)	0.1% (0.1%)	0% (0.1%)	0% (0%)	11% (11%)	6% (6%)	5% (5%)	4% (5%)
	Disturbed	5.6%	0.7%	0.6%	0.5%	69%	43%	39%	36%
	Novel	3.7%	0.1%	0%	0%	16%	2%	2%	1%
	Disappearing	3.0%	0%	0%	0%	22%	2%	1%	1%
RCP4.5	Within	10.2% (10.1%)	5.1% (4.8%)	4.2% (3.9%)	2.0% (1.9%)	34% (31%)	32% (30%)	31% (30%)	27% (26%)
	Outside	3.8% (3.2%)	1.1% (1.0%)	0.7% (0.7%)	0.3% (0.3%)	33% (32%)	28% (27%)	27% (30%)	20% (25%)
	Inside	4.4% (2.9%)	1.1% (1.2%)	0.8% (0.8%)	0.3% (0.3%)	28% (30%)	25% (27%)	23% (260%)	18% (18%)
	Among	0.5% (0.5%)	0.1% (0.2%)	0.1% (0.1%)	0% (0.1%)	11% (11%)	8% (8%)	7% (7%)	5% (5%)
	Disturbed	6.4%	1.9%	1.3%	0.5%	76%	62%	55%	41%
	Novel	4.0%	0.5%	0.3%	0%	18%	6%	4%	1%
	Disappearing	3.5%	0.3%	0.2%	0%	23%	5%	4%	1%
RCP6.0	Within	10.0% (9.8%)	4.9% (4.7%)	6.1% (5.7%)	4.0% (3.7%)	34% (31%)	31% (31%)	32% (31%)	31% (30%)
	Outside	3.6% (2.9%)	1.0% (0.9%)	1.4% (1.4%)	0.7% (0.6%)	33% (32%)	29% (27%)	30% (30%)	27% (25%)
	Inside	4.1% (2.7%)	1.1% (1.1%)	1.6% (1.5%)	0.7% (0.7%)	28% (29%)	24% (27%)	26% (28%)	24% (25%)
	Among	0.4% (0.3%)	0.1% (0.1%)	0.2% (0.1%)	0.1% (0.1%)	11% (9%)	8% (6%)	9% (7%)	7% (6%)
	Disturbed	5.2%	1.8%	1.9%	1.0%	66%	53%	51%	41%
	Novel	3.7%	0.6%	0.9%	0.2%	16%	6%	8%	3%
	Disappearing	3.3%	0.3%	0.5%	0.2%	22%	5%	7%	4%
RCP8.5	Within	10.5% (11.3%)	7.2% (7.0%)	7.6% (7.8%)	4.9% (4.6%)	34% (31%)	32% (31%)	32% (31%)	32% (30%)
	Outside	4.4% (3.5%)	2.0% (2.0%)	2.3% 2.0%)	1.0% (1.0%)	33% (32%)	31% (30%)	31% (31%)	29% (27%)
	Inside	5.2% (4.6%)	2.2% (2.1%)	2.3% (2.2%)	1.0% (1.0%)	29% (30%)	26% (29%)	26% (29%)	25% (26%)
	Among	0.6% (0.5%)	0.4% (0.3%)	0.3% (0.3%)	0.2% (0.2%)	11% (11%)	10% (10%)	11% (10%)	9% (8%)
	Disturbed	7.3%	3.2%	3.6%	1.4%	77%	67%	67%	59%

Novel	5.0%	2.2%	1.9%	0.3%	20%	13%	13%	5%
Disappearing	4.0%	1.6%	1.4%	0.3%	25%	12%	13%	6%

Table 4-S9 Data description

Data	Name	Reference	Res.	Temporal span	Scenarios
Climate classification maps	Historical and future Köppen-Geiger climate classification maps (KGClim)	Cui et al., 2021	1km	1970-2000 2020-2049 2040-2069 2060-2079 2070-2099	RCP2.6 RCP4.5 RCP6.0 RCP8.5
Land use	Land-Use Harmonizaltion2 (LUH2) v2f	Hurtt et al., 2020	0.25o	2020-2100	RCP2.6 RCP4.5 RCP6.0 RCP8.5
Terrestrial protected areas	World Database on Protected Area (WDPA)	UNEP-WCMC and IUCN, 2021	Polygon	Present	
Elevation and terrain ruggedness	Global 1km topography	Amatulli et al., 2018	1km	Present	
Human footprint	Global terrestrial Human Footprint maps for 1993 and 2009	Venter et al., 2016	1km	1993-2009	
Biodiversity	Species occurrence records from Global Biodiversity Information Facility (GBIF)	GBIF, 2021	Point	1970-2020	

Table 4-S10 CMIP5 GCMs used to conduct sensitivity analysis

Model	Institute
BCC-CSM1.1	Beijing Climate Center, China Meteorological Administration
BCC-CSM1.1(m)	Beijing Climate Center, China Meteorological Administration
CCCMA-CanESM2	Canadian Centre for Climate Modeling and Analysis
CESM1-CAM5	National Science Foundation, Department of Energy, National Center for Atmospheric Research
CSIRO-Mk3.6.0	Queensland Climate Change Centre of Excellence and Commonwealth Scientific and Industrial Research Organization
FIO-ESM	The First Institute of Oceanography, State Oceanic Administration, China
GFDL-CM3	NOAA Geophysical Fluid Dynamics Laboratory
GFDL-ESM2G	NOAA Geophysical Fluid Dynamics Laboratory
GISS-E2R	NASA Goddard Institute for Space Studies USA
IPSL-CM5A-LR	Institut Pierre Simon Laplace
MIROC-MIROC5	University of Tokyo, National Institute for Environmental Studies and Japan Agency for Marine-Earth Science and Technology
MOHC-HadGEM2-ES	UK Met Office Hadley Centre
MRI-CGCM3	Meteorological Research Institute
NCAR-CCSM4	US National Centre for Atmospheric Research
NCC-NorESM1-M	Norwegian Climate Centre
NIMR-HadGEM2-AO	National Institute of Meteorological Research and Korea Meteorological Administration

Table 4-S11 PA terrestrial coverage and numbers by continents, country, and IUCN categories

	PA coverage (% of land)	Number of PAs
Continent/Country		
• Africa	7.9%	1,037
• Asia	5.7%	2,841
- Russia	9.6%	1,922
• Europe	10.4%	7,481
• North America	10.6%	6,951
- United States	13.5%	4,698
- Canada	9.7%	1,471
• Oceania	20.5%	2,563
• South America	17.9%	1,834
- Brazil	19.6%	779
IUCN Category		
• Ia	0.6%	1,390
• Ib	1.0%	2,062
• II	3.0%	3,589
• III	0.1%	1,355
• IV	1.5%	5,869
• V	1.1%	6,125
• VI	3.2%	2,324

Chapter 5: Conclusion

5.1 Major findings

This dissertation identified the spatiotemporal patterns of global climate zone shifts and potential biodiversity redistribution using a suite of fine-scale velocity metrics, which were developed based on the new 1-km climate classification dataset (KGClim) and species distribution model (SDM) predictions. Moreover, this dissertation demonstrated the use of velocity metrics for assessment of species exposure to climate change and assessment of vulnerability of protected areas (PAs), and highlighted incorporation of climate zone shifts and biodiversity redistribution into conservation planning to enhance the effectiveness of global PAs and develop strategic and adaptive PA conservation approaches.

Chapter 2 provided a comprehensive insight into the changes in global Köppen climate zones. This chapter summarized the advancements and limitations of climate zone definitions and assessed the available climate classification map products. Recent detection and assessment studies on observed and projected climate zone changes were assessed and summarized. Previous findings show that the recent accelerated global warming since the 1980s has led to large-scale shifts in macro climatic conditions over approximately 5.3–5.7% (7.9–8.5 million km2) of the total land area. During the 21st century, 13–20% (19.6–29.8 million km2) of the total land area is projected to undergo climate zone changes under the high-emission RCP8.5 scenario. The arid and hot climates in the tropics and subtropics are expected to expand worldwide into the large areas of the middle and high latitudes, which is potentially linked to the intensification of the global hydrologic cycle. Driven by increased warming in the Arctic, high-

latitude climates are projected to shift poleward, leading to a significant area shrinkage. However, due to the large model uncertainties, the detectability of significant climate zone changes through observations and projections, the rate and time of the changes, and their causes remain unclear. This chapter identified the research gaps and proposed directions for future research.

Chapter 3 developed a series of 1 km Köppen–Geiger climate classification maps (KGClim) for six historical periods in 1979–2013 and four future periods in 2020–2099 under RCP2.6, 4.5, 6.0, and 8.5, to fulfill the need for improved historical and future global climate maps with long-term temporal coverage and accurate depiction of fine-grained bioclimatic conditions. The historical maps were derived from multiple downscaled observational datasets, and the future maps were derived from an ensemble of bias-corrected downscaled CMIP5 projections. In addition to climate classification maps, the dataset includes 12 bioclimatic variables at 1 km resolution, providing detailed descriptions of annual averages, seasonality, and stressful conditions of climates. The new maps offer higher classification accuracy than existing datasets and demonstrate the ability to capture recent and future projected changes in distribution of climate zones. On regional and continental scales, the new maps show accurate depictions of topographic features and correspond closely with vegetation distribution. This KGClim dataset can be used in conjunction with SDMs to promote biodiversity conservation and to analyze and identify recent and future changes in climate zones on a global or regional scale. The dataset is publicly available via http://glass.umd.edu/KGClim.

Chapter 4 presented a new velocity measure with fine spatial scale (1-km) based on Köppen-Geiger climate classes to assess exposure risks of global PAs and examine patterns of climate zone shifts for four future periods (2020-2049, 2040-2069, 2060-2089, 2070-2099) based on four

RCPs (RCP2.6, RCP4.5, RCP6.0 and RCP8.5) with a baseline period of 1971-2000. The research identified the PAs projected to undergo shifts of climate zones of great magnitude and quantified additional threats from human-induced land modifications for global PAs. Lastly, this research presented a case study to integrate climate shifts in PA prioritization scheme to inform future climate adaptation planning and biodiversity conservation. Based on the results, 38% of global protected land in more than three fourths of global terrestrial PAs could undergo climate zone shifts at accelerating rates during the remainder of this century under RCP8.5. Moreover, protected lands are experiencing heightened climate change exposure from novel (8.3% of global protected land) and disappearing (6.6%) climates, shifts of climates outside PA networks (7.6%), and transition to human dominated land use (5.7%). PAs located across arid (B) and boreal (D) climate zones, in mid latitudes of North America, Europe, Russia, and Africa, and those with strict management categories (IUCN category I-II), are facing more rapid and substantial changes. Relationships with PA attributes suggest increased vulnerability over small, high elevation PAs with complex topography and high species richness. The findings of climate zone shifts, and exposure assessment of PAs can inform climate adaptation planning and biodiversity conservation prioritization.

5.2 Future research

Consideration of habitat and climatic heterogeneity within PAs is critical in conservation planning under climate change (Ackerly et al., 2010; Hannah et al., 2007). PAs have demonstrated their importance in reducing habitat loss and environmental degradation (Geldmann et al., 2013; J. E. M. Watson et al., 2018), and enhancing species diversity within their boundaries(Gray et al., 2016). This dissertation was focused on the change patterns of

availability and positions of climatic conditions and species habitat within or near PAs, ignoring the potential conservation value of unprotected lands, which may harbor high levels of biodiversity and provide climatically suitable areas for species (Elsen, Ramesh, et al., 2018). Moreover, large biases have been identified in the locations of current global PAs towards 1) protection of land with rare climates (Elsen et al., 2020), 2) high elevations (Elsen, Monahan, et al., 2018), and areas of low influence from human settlements and infrastructure (Joppa & Pfaff, 2009). The close alignment with existing biodiversity patterns with inadequate consideration of future changes (Lawler et al., 2015; Loucks et al., 2008; Myers et al., 2000) could further diminish the capacity of PA networks in protecting future biodiversity. Future research can include assessment of biodiversity exposure for unprotected lands to promote understanding how biased and static distribution of PAs can influence the PA biodiversity conservation capacity, and how establishing new PAs or expanding existing PAs can act to reduce climate exposure, which can provide insight into promising strategies for climate adaptation.

Moreover, PAs are established not only to conserve landscapes and protect endangered species, but also to provide livelihood for local communities and bolster national economies (J. E. M. Watson et al., 2014). This dissertation provided insight into the importance of PAs in mitigating effects of climate change on species but there are numerous factors that need to be considered for PA conservation planning in reality (Virkkala et al., 2013). Governmental policies play an important role in facilitating the creation, financing, and management of PAs in order to meet national and international conservation objectives, and countries provide the standard in assessments of conservation values and performance of PAs (Loucks et al., 2008; J. E. M. Watson et al., 2014). Large differences have been documented in protection status across countries, including their PA coverage, protection evenness, and progress towards Aichi

Biodiversity Targets. PAs in some countries in Africa, Asia, and South America may not be effectively and equitably managed, climatically and ecologically representative or well connected. For example, some small countries with limited climate availability may be threatened by faster rates of climate change and lose intact habitat or face habitat fragmentation as a result of increasing human activities. National assessments of biodiversity exposure provide a direction for future research, which can focus on the national threatened species, provide a more detailed discussion about national political commitment, and consider the social and environmental agendas, to better inform policy makers and biologists to conserve species, local ecosystems and community. One of the countries of interest is China given the urgent need in China to conserve and restore the diverse ecosystems and species, as well as to mitigate the ongoing loss of ecosystem services and biodiversity (Ouyang et al., 2016). The principal PAs in China are nature reserves, the majority of which were established opportunistically, without a clear planning framework (Wu et al., 2011). There is an urgent need for assessment of PA exposure and effectiveness in China to inform design of PA networks and enhance conservation management in China.

This dissertation focused on velocity measures to assess species exposure to climate change, which have limitations because the actual effects of climate change on biodiversity also depend on the species intrinsic abilities to address the exposure risk to climate change and other interacting human-induced threats. Complex interactions exist between the velocity of climate change, species range shifts, the degree of human pressures, and species dispersal and adaptive capacities (Elsen et al., 2020). For example, altered availability of climatically suitable area, barriers created by human modifications and habitat fragmentation (Bennie et al., 2013; Schloss et al., 2012), varied adaptative and dispersal capacity of species can often result in delays and

large variations in biological responses of individual species (I.-C. Chen et al., 2011; Parmesan & Yohe, 2003). Moreover, species may not shift their distribution under changing climate but instead tend to contract into suitable microrefugia within their current range and maintain low-density isolated populations (Lenoir et al., 2017). These complex interactions need to be taken into account to improve predictions of biodiversity redistribution and advance understanding of its consequences on ecosystems and human well-being under climate change. Future research can incorporate datasets of species traits (Kattge et al., 2011; Kissling et al., 2014; Oliveira et al., 2017) in SDMs, to make it more informative in determining species vulnerability.

Bibliography

Ackerly, D. D., Loarie, S. R., Cornwell, W. K., Weiss, S. B., Hamilton, H., Branciforte, R., & Kraft, N. J. B. (2010). The geography of climate change: Implications for conservation biogeography. *Diversity and Distributions*, *16*(3), 476–487. https://doi.org/10.1111/j.1472-4642.2010.00654.x

Alexander, J. M., Chalmandrier, L., Lenoir, J., Burgess, T. I., Essl, F., Haider, S., Kueffer, C., McDougall, K., Milbau, A., Nuñez, M. A., Pauchard, A., Rabitsch, W., Rew, L. J., Sanders, N. J., & Pellissier, L. (2018). Lags in the response of mountain plant communities to climate change. *Global Change Biology*, *24*(2), 563–579. https://doi.org/10.1111/gcb.13976

Amatulli, G., Domisch, S., Tuanmu, M.-N., Parmentier, B., Ranipeta, A., Malczyk, J., & Jetz, W. (2018). A suite of global, cross-scale topographic variables for environmental and biodiversity modeling. *Scientific Data*, *5*, 180040. https://doi.org/10.1038/sdata.2018.40

Arafeh-Dalmau, N., Brito-Morales, I., Schoeman, D. S., Possingham, H. P., Klein, C. J., & Richardson, A. J. (2021). Incorporating climate velocity into the design of climate-smart networks of marine protected areas. *Methods in Ecology and Evolution*, *12*(10), 1969–1983. https://doi.org/10.1111/2041-210X.13675

Asamoah, E. F., Beaumont, L. J., & Maina, J. M. (2021). Climate and land-use changes reduce the benefits of terrestrial protected areas. *Nature Climate Change*, *11*(12), 1105–1110. https://doi.org/10.1038/s41558-021-01223-2

Bacon, S. J., Aebi, A., Calanca, P., Bacher, S., & Essl, F. (2014). Quarantine arthropod invasions in Europe. *Diversity and Distributions*, *20*(1), 84–94. https://doi.org/10.1111/ddi.12149

Batllori, E., Parisien, M.-A., Parks, S. A., Moritz, M. A., & Miller, C. (2017). Potential relocation of climatic environments suggests high rates of climate displacement within the North American protection network. *Global Change Biology*, *23*(8), 3219–3230. https://doi.org/10.1111/gcb.13663

Beaumont, L. J., Pitman, A., Perkins, S., Zimmermann, N. E., Yoccoz, N. G., & Thuiller, W. (2011). Impacts of climate change on the world's most exceptional ecoregions. *Proceedings of the National Academy of Sciences of the United States of America*, *108*(6), 2306–2311. https://doi.org/10.1073/pnas.1007217108

Beck, C., Grieser, J., Kottek, M., Rubel, F., & Rudolf, B. (2005). *Characterizing global climate change by means of Köppen climate classification*. https://www.dwd.de/DE/leistungen/klimastatusbericht/publikationen/ksb2005_pdf/10_2005.pdf?__blob=publicationFile&v=1

Beck, C., Grieser, J., Rudolf, B., & Schneider, U. (2005). *A new monthly precipitation climatology for the global land areas for the period 1951 to 2000*. *7*, 07154.

Beck, H. E., Zimmermann, N. E., McVicar, T. R., Vergopolan, N., Berg, A., & Wood, E. F. (2018). Present and future Köppen-Geiger climate classification maps at 1-km resolution. *Scientific Data*, *5*, 180214. https://doi.org/10.1038/sdata.2018.214

Belda, M., Holtanová, E., Halenka, T., & Kalvová, J. (2014). Climate classification revisited. *Climate Research*, *59*(1), 1–13. https://doi.org/10.3354/cr01204

Belda, M., Holtanová, E., Halenka, T., Kalvová, J., & Hlávka, Z. (2015). Evaluation of CMIP5 present climate

simulations using the Köppen-Trewartha climate classification. *Climate Research*, *64*(3), 201–212. https://doi.org/10.3354/cr01316

Belda, M., Holtanová, E., Kalvová, J., & Halenka, T. (2016). Global warming-induced changes in climate zones based on CMIP5 projections. *Climate Research*, *71*(1), 17–31. https://doi.org/10.3354/cr01418

Bennie, J., Hodgson, J. A., Lawson, C. R., Holloway, C. T. R., Roy, D. B., Brereton, T., Thomas, C. D., & Wilson, R. J. (2013). Range expansion through fragmented landscapes under a variable climate. *Ecology Letters*, *16*(7), 921–929. https://doi.org/10.1111/ele.12129

Berg, A., Noblet-Ducoudré, N., Sultan, B., Lengaigne, M., & Guimberteau, M. (2013). Projections of climate change impacts on potential C4 crop productivity over tropical regions. *Agricultural and Forest Meteorology*, *170*, 89–102. https://doi.org/10.1016/j.agrformet.2011.12.003

Berg, M., Meyer, U., Arya, S., da Fonseca, G. D., & Mount, D. M. (Eds.). (2010). *A Unified Approach to Approximate Proximity Searching*. Springer Berlin Heidelberg.

Bockheim, J. G., Gennadiyev, A. N., Hammer, R. D., & Tandarich, J. P. (2005). Historical development of key concepts in pedology. *Geoderma*, *124*(1–2), 23–36. https://doi.org/10.1016/j.geoderma.2004.03.004

Brito-Morales, I., García Molinos, J., Schoeman, D. S., Burrows, M. T., Poloczanska, E. S., Brown, C. J., Ferrier, S., Harwood, T. D., Klein, C. J., McDonald-Madden, E., Moore, P. J., Pandolfi, J. M., Watson, J. E. M., Wenger, A. S., & Richardson, A. J. (2018). Climate Velocity Can Inform Conservation in a Warming World. *Trends in Ecology & Evolution*, *33*(6), 441–457. https://doi.org/10.1016/j.tree.2018.03.009

Brugger, K., & Rubel, F. (2013). Characterizing the species composition of European Culicoides vectors by means of the Köppen-Geiger climate classification. *Parasites & Vectors*, *6*(1), 333. https://doi.org/10.1186/1756-3305-6-333

Bunkers, M. J., Miller, J. R., & Degaetano, A. T. (1996). Definition of Climate Regions in the Northern Plains Using an Objective Cluster Modification Technique. *Journal of Climate*, *9*(1), 130–146. https://doi.org/10.1175/1520-0442(1996)009<0130:DOCRIT>2.0.CO;2

Burrows, M. T., Schoeman, D. S., Buckley, L. B., Moore, P., Poloczanska, E. S., Brander, K. M., Brown, C., Bruno, J. F., Duarte, C. M., Halpern, B. S., Holding, J., Kappel, C. V., Kiessling, W., O'Connor, M. I., Pandolfi, J. M., Parmesan, C., Schwing, F. B., Sydeman, W. J., & Richardson, A. J. (2011). The pace of shifting climate in marine and terrestrial ecosystems. *Science (New York, N.Y.)*, *334*(6056), 652–655. https://doi.org/10.1126/science.1210288

Burrows, M. T., Schoeman, D. S., Richardson, A. J., Molinos, J. G., Hoffmann, A., Buckley, L. B., Moore, P. J., Brown, C. J., Bruno, J. F., Duarte, C. M., Halpern, B. S., Hoegh-Guldberg, O., Kappel, C. V., Kiessling, W., O'Connor, M. I., Pandolfi, J. M., Parmesan, C., Sydeman, W. J., Ferrier, S., … Poloczanska, E. S. (2014). Geographical limits to species-range shifts are suggested by climate velocity. *Nature*, *507*(7493), 492–495. https://doi.org/10.1038/nature12976

Carroll, C., Lawler, J. J., Roberts, D. R., & Hamann, A. (2015). Biotic and Climatic Velocity Identify Contrasting Areas of Vulnerability to Climate Change. *PloS One*, *10*(10), e0140486. https://doi.org/10.1371/journal.pone.0140486

Carroll, C., Parks, S. A., Dobrowski, S. Z., & Roberts, D. R. (2018). Climatic, topographic, and anthropogenic factors determine connectivity between current and future climate analogs in North America. *Global Change Biology*, *24*(11), 5318–5331. https://doi.org/10.1111/gcb.14373

Carroll, C., Roberts, D. R., Michalak, J. L., Lawler, J. J., Nielsen, S. E., Stralberg, D., Hamann, A., McRae, B. H., & Wang, T. (2017). Scale-dependent complementarity of climatic velocity and environmental diversity for identifying priority areas for conservation under climate change. *Global Change Biology*, *23*(11), 4508–4520. https://doi.org/10.1111/gcb.13679

Castro, M., Gallardo, C., Jylha, K., & Tuomenvirta, H. (2007). The use of a climate-type classification for assessing climate change effects in Europe from an ensemble of nine regional climate models. *Climatic Change*, *81*(S1), 329–341. https://doi.org/10.1007/s10584-006-9224-1

Chan, D., & Wu, Q. (2015). Significant anthropogenic-induced changes of climate classes since 1950. *Scientific Reports*, *5*, 13487. https://doi.org/10.1038/srep13487

Chen, D., & Chen, H. W. (2013). Using the Köppen classification to quantify climate variation and change. *Environmental Development*, *6*, 69–79. https://doi.org/10.1016/j.envdev.2013.03.007

Chen, I.-C., Hill, J. K., Ohlemüller, R., Roy, D. B., & Thomas, C. D. (2011). Rapid range shifts of species associated with high levels of climate warming. *Science (New York, N.Y.)*, *333*(6045), 1024–1026. https://doi.org/10.1126/science.1206432

Chen, M., Xie, P., Janowiak, J. E., & Arkin, P. A. (2002). Global land precipitation. *Journal of Hydrometeorology*, *3*(3), 249–266.

Chen, T., Zhang, H., Chen, X., Hagan, D. F., Wang, G., Gao, Z., & Shi, T. (2017). Robust drying and wetting trends found in regions over China based on Köppen climate classifications. *Journal of Geophysical Research: Atmospheres*, *122*(8), 4228–4237. https://doi.org/10.1002/2016JD026168

Convention on Biological Diversity. (n.d.). *First draft of the post-2020 global biodiversity framework*. 12. https://doi.org/2021

Corlett, R. T., & Westcott, D. A. (2013). Will plant movements keep up with climate change? *Trends in Ecology & Evolution*, *28*(8), 482–488. https://doi.org/10.1016/j.tree.2013.04.003

Cui, D., Liang, S., & Wang, D. (2021). Observed and projected changes in global climate zones based on Köppen climate classification. *WIREs Climate Change*, *14*(5), 484. https://doi.org/10.1002/wcc.701

Cui, D., Liang, S., Wang, D., & Liu, Z. (2021). A 1 km global dataset of historical (1979–2013) and future (2020–2100) Köppen–Geiger climate classification and bioclimatic variables. *Earth System Science Data*, *13*(11), 5087–5114. https://doi.org/10.5194/essd-13-5087-2021

Daly, C. (2006). Guidelines for assessing the suitability of spatial climate data sets. *International Journal of Climatology*, *26*(6), 707–721.

Danielson, J. J., & Gesch, D. B. (2011). *Global Multi-resolution Terrain Elevation Data 2010 (GMTED2010)*. 34.

Degaetano, A. T. (1996). Delineation of Mesoscale Climate Zones in the Northeastern United States Using a Novel Approach to Cluster Analysis. *Journal of Climate*, *9*(8), 1765–1782. https://doi.org/10.1175/1520-0442(1996)009<1765:DOMCZI>2.0.CO;2

Dobrowski, S. Z. (2011). A climatic basis for microrefugia. *Global Change Biology*, *17*(2), 1022–1035. https://doi.org/10.1111/j.1365-2486.2010.02263.x

Dobrowski, S. Z., Abatzoglou, J., Swanson, A. K., Greenberg, J. A., Mynsberge, A. R., Holden, Z. A., & Schwartz, M. K. (2013). The climate velocity of the contiguous United States during the 20th century. *Global Change Biology*, *19*(1), 241–251. https://doi.org/10.1111/gcb.12026

Dobrowski, S. Z., Littlefield, C. E., Lyons, D. S., Hollenberg, C., Carroll, C., Parks, S. A., Abatzoglou, J. T., Hegewisch, K., & Gage, J. (2021). Protected-area targets could be undermined by climate change-driven shifts in ecoregions and biomes. *Communications Earth & Environment*, *2*(1), 472. https://doi.org/10.1038/s43247-021-00270-z

Dobrowski, S. Z., & Parks, S. A. (2016). Climate change velocity underestimates climate change exposure in mountainous regions. *Nature Communications*, *7*(1), 1–8.

Elguindi, N., Grundstein, A., Bernardes, S., Turuncoglu, U., & Feddema, J. (2014). Assessment of CMIP5 global model simulations and climate change projections for the 21 st century using a modified Thornthwaite climate classification. *Climatic Change*, *122*(4), 523–538. https://doi.org/10.1007/s10584-013-1020-0

Elsen, P. R., Monahan, W. B., Dougherty, E. R., & Merenlender, A. M. (2020). Keeping pace with climate change in global terrestrial protected areas. *Science Advances*, *6*(25), eaay0814. https://doi.org/10.1126/sciadv.aay0814

Elsen, P. R., Monahan, W. B., & Merenlender, A. M. (2018). Global patterns of protection of elevational gradients in mountain ranges. *Proceedings of the National Academy of Sciences*, *115*(23), 6004–6009. https://doi.org/10.1073/pnas.1720141115

Elsen, P. R., Ramesh, K., & Wilcove, D. S. (2018). Conserving Himalayan birds in highly seasonal forested and agricultural landscapes. *Conservation Biology*, *32*(6), 1313–1324. https://doi.org/10.1111/cobi.13145

Essenwanger, O. M., & Landsberg, H. E. (2001). *General Climatology. 1C, Classification of climate* (Vol. 1C). Elsevier. http://catalogue.bnf.fr/ark:/12148/cb38803905s

Fan, Y., & Dool, H. van den. (2008). A global monthly land surface air temperature analysis for 1948–present. *Journal of Geophysical Research*, *113*(D1), 161. https://doi.org/10.1029/2007JD008470

FAO. (2001). *FRA 2000*.

Farr, T. G., Rosen, P. A., Caro, E., Crippen, R., Duren, R., Hensley, S., Kobrick, M., Paller, M., Rodriguez, E., Roth, L., Seal, D., Shaffer, S., Shimada, J., Umland, J., Werner, M., Oskin, M., Burbank, D., & Alsdorf, D. (2007). The Shuttle Radar Topography Mission. *Reviews of Geophysics*, *45*(2), 1485. https://doi.org/10.1029/2005RG000183

Feng, S., Ho, C.-H., Hu, Q., Oglesby, R. J., Jeong, S.-J., & Kim, B.-M. (2012). Evaluating observed and projected future climate changes for the Arctic using the Köppen-Trewartha climate classification. *Climate Dynamics*, *38*(7–8), 1359–1373. https://doi.org/10.1007/s00382-011-1020-6

Feng, S., Hu, Q., Huang, W., Ho, C.-H., Li, R., & Tang, Z. (2014). Projected climate regime shift under future global warming from multi-model, multi-scenario CMIP5 simulations. *Global and Planetary Change*, *112*, 41–52. https://doi.org/10.1016/j.gloplacha.2013.11.002

Fick, S. E., & Hijmans, R. J. (2017). WorldClim 2. *International Journal of Climatology*, *37*(12), 4302–4315. https://doi.org/10.1002/joc.5086

Fovell, R. G., & Fovell, M.-Y. C. (1993). Climate Zones of the Conterminous United States Defined Using Cluster Analysis. *Journal of Climate*, *6*(11), 2103–2135. https://doi.org/10.1175/1520-0442(1993)006<2103:CZOTCU>2.0.CO;2

Fraedrich, K., Gerstengarbe, F. W., & Wnerner, P. C. (2001). Climate Shifts during the Last Century. *Climatic*

Change, *50*, 405–417.

Franklin, J., Davis, F. W., Ikegami, M., Syphard, A. D., Flint, L. E., Flint, A. L., & Hannah, L. (2013). Modeling plant species distributions under future climates. *Global Change Biology*, *19*(2), 473–483. https://doi.org/10.1111/gcb.12051

Fuller, R. A., McDonald-Madden, E., Wilson, K. A., Carwardine, J., Grantham, H. S., Watson, J. E. M., Klein, C. J., Green, D. C., & Possingham, H. P. (2010). Replacing underperforming protected areas achieves better conservation outcomes. *Nature*, *466*(7304), 365–367. https://doi.org/10.1038/nature09180

Funk, C., Verdin, A., Michaelsen, J., Peterson, P., Pedreros, D., & Husak, G. (2015). A global satellite-assisted precipitation climatology. *Earth System Science Data*, *7*(2), 275–287. https://doi.org/10.5194/essd-7-275-2015

Garcia, R. A., Cabeza, M., Rahbek, C., & Araújo, M. B. (2014). Multiple dimensions of climate change and their implications for biodiversity. *Science (New York, N.Y.)*, *344*(6183), 1247579. https://doi.org/10.1126/science.1247579

Geiger, R. (1961). Überarbeitete Neuausgabe von Geiger, R. *Köppen-Geiger/Klima Der Erde.(Wandkarte 1: 16 Mill.)-Klett-Perthes, Gotha.*

Geldmann, J., Barnes, M., Coad, L., Craigie, I. D., Hockings, M., & Burgess, N. D. (2013). Effectiveness of terrestrial protected areas in reducing habitat loss and population declines. *Biological Conservation*, *161*, 230–238. https://doi.org/10.1016/j.biocon.2013.02.018

Giorgi, F. (2006). Climate change hot-spots. *Geophysical Research Letters*, *33*(8), 89. https://doi.org/10.1029/2006GL025734

Gnanadesikan, A., & Stouffer, R. J. (2006). Diagnosing atmosphere-ocean general circulation model errors relevant to the terrestrial biosphere using the Köppen climate classification. *Geophysical Research Letters*, *33*(22), 643. https://doi.org/10.1029/2006GL028098

Gray, C. L., Hill, S. L. L., Newbold, T., Hudson, L. N., Börger, L., Contu, S., Hoskins, A. J., Ferrier, S., Purvis, A., & Scharlemann, J. P. W. (2016). Local biodiversity is higher inside than outside terrestrial protected areas worldwide. *Nature Communications*, *7*, 12306. https://doi.org/10.1038/ncomms12306

Grieser, J., Gommes, R., Cofield, S., & Bernardi, M. (2006). New gridded maps of Koeppen's climate classification. *Data, Methodology and Gridded Data Available at: Http://Www. Fao. Org/Nr/Climpag/Globgrids/KC_classification_en. Asp. Methodology Also Downloadable from Http://Www. Juergen-Grieser. de/Downloads/Koeppen-Climatology/Koeppen_Climatology. Pdf (Accessed September 2015).*

Hamann, A., Roberts, D. R., Barber, Q. E., Carroll, C., & Nielsen, S. E. (2015). Velocity of climate change algorithms for guiding conservation and management. *Global Change Biology*, *21*(2), 997–1004. https://doi.org/10.1111/gcb.12736

Hanf, F., Körper, J., Spangehl, T., & Cubasch, U. (2012). Shifts of climate zones in multi-model climate change experiments using the Köppen climate classification. *Meteorologische Zeitschrift*, *21*(2), 111–123. https://doi.org/10.1127/0941-2948/2012/0344

Hannah, L., Midgley, G., Andelman, S., Araújo, M., Hughes, G., Martinez-Meyer, E., Pearson, R., & Williams, P. (2007). Protected area needs in a changing climate. *Frontiers in Ecology and the Environment*, *5*(3), 131–138. https://doi.org/10.1890/1540-9295(2007)5[131:PANIAC]2.0.CO;2

Hansen, M. C., Potapov, P. V., Moore, R., Hancher, M., Turubanova, S. A., Tyukavina, A., Thau, D., Stehman, S. V., Goetz, S. J., Loveland, T. R., Kommareddy, A., Egorov, A., Chini, L., Justice, C. O., & Townshend, J. R. G. (2013). High-resolution global maps of 21st-century forest cover change. *Science (New York, N.Y.)*, *342*(6160), 850–853. https://doi.org/10.1126/science.1244693

Harris, I., Jones, P. D., Osborn, T. J., & Lister, D. H. (2014). Updated high-resolution grids of monthly climatic observations—The CRU TS3.10 Dataset. *International Journal of Climatology*, *34*(3), 623–642. https://doi.org/10.1002/joc.3711

Hartmann, D. L., A.M.G. Klein Tank, M. Rusticucci, L.V. Alexander, S. Brönnimann, Y. Charabi, F.J. Dentener, E.J. Dlugokencky, D.R. Easterling, A. Kaplan, B.J. Soden, P.W. Thorne, M. Wild, & P.M. Zhai. (2013). *Observations: Atmosphere and Surface*. Cambridge University Press.

Hay, L. E., Wilby, R. L., & Leavesley, G. H. (2000). A COMPARISON OF DELTA CHANGE AND DOWNSCALED GCM SCENARIOS FOR THREE MOUNTAINOUS BASINS IN THE UNITED STATES1. *JAWRA Journal of the American Water Resources Association*, *36*(2), 387–397. https://doi.org/10.1111/j.1752-1688.2000.tb04276.x

Heikkinen, R. K., Leikola, N., Aalto, J., Aapala, K., Kuusela, S., Luoto, M., & Virkkala, R. (2020). Fine-grained climate velocities reveal vulnerability of protected areas to climate change. *Scientific Reports*, *10*(1), 1678. https://doi.org/10.1038/s41598-020-58638-8

Heikkinen, R. K., Luoto, M., Araújo, M. B., Virkkala, R., Thuiller, W., & Sykes, M. T. (2016). Methods and uncertainties in bioclimatic envelope modelling under climate change. *Progress in Physical Geography: Earth and Environment*, *30*(6), 751–777. https://doi.org/10.1177/0309133306071957

Hijmans, R. J., Cameron, S. E., Parra, J. L., Jones, P. G., & Jarvis, A. (2005). Very high resolution interpolated climate surfaces for global land areas. *International Journal of Climatology*, *25*(15), 1965–1978. https://doi.org/10.1002/joc.1276

Hitch, A. T., & Leberg, P. L. (2007). Breeding Distributions of North American Bird Species Moving North as a Result of Climate Change. *Conservation Biology*, *21*(2), 534–539. https://doi.org/10.1111/j.1523-1739.2006.00609.x

Ho, C. K., Stephenson, D. B., Collins, M., Ferro, C. A. T., & Brown, S. J. (2012). Calibration Strategies. *Bulletin of the American Meteorological Society*, *93*(1), 21–26. https://doi.org/10.1175/2011BAMS3110.1

Hoffman, F. M., Hargrove, W. W., Erickson, D. J., & Oglesby, R. J. (2005). Using Clustered Climate Regimes to Analyze and Compare Predictions from Fully Coupled General Circulation Models. *Earth Interactions*, *9*(10), 1–27. https://doi.org/10.1175/EI110.1

Hoffmann, S., Irl, S. D. H., & Beierkuhnlein, C. (2019). Predicted climate shifts within terrestrial protected areas worldwide. *Nature Communications*, *10*(1), 4787. https://doi.org/10.1038/s41467-019-12603-w

Holdridge, L. R. (1947). Determination of World Plant Formations From Simple Climatic Data. *Science (New York, N.Y.)*, *105*(2727), 367–368. https://doi.org/10.1126/science.105.2727.367

Hurtt, G. C., Chini, L., Sahajpal, R., Frolking, S., Bodirsky, B. L., Calvin, K., Doelman, J. C., Fisk, J., Fujimori, S., Klein Goldewijk, K., Hasegawa, T., Havlik, P., Heinimann, A., Humpenöder, F., Jungclaus, J., Kaplan, J. O., Kennedy, J., Krisztin, T., Lawrence, D., … Zhang, X. (2020). Harmonization of global land use change and management for the period 850–2100 (LUH2) for CMIP6. *Geoscientific Model Development*, *13*(11), 5425–5464. https://doi.org/10.5194/gmd-13-5425-

2020

IPCC. (2018). Summary for Policymakers. In P. Z. V. Masson-Delmotte H. O. Pörtner, D. Roberts, J. Skea, P. R. Shukla, A. Pirani, W. Moufouma-Okia, C. Péan, R. Pidcock, S. Connors, J. B. R. Matthews, Y. Chen, X. Zhou, M. I. Gomis, E. Lonnoy, T. Maycock, M. Tignor, T. Waterfield (Ed.), *Global warming of 1.5°C.An IPCC Special Report on the impacts of global warming of 1.5°C above pre-industrial levels and related global greenhouse gas emission pathways, in the context of strengthening the global response to the threat of climate change, sustainable development, and efforts to eradicate poverty* (pp. 45–64). https://doi.org/10.1553/aar14s45

James, P. E. (1966). *A geography of man*.

Jiménez, M. A., Jaksic, F. M., Armesto, J. J., Gaxiola, A., Meserve, P. L., Kelt, D. A., & Gutiérrez, J. R. (2011). Extreme climatic events change the dynamics and invasibility of semi-arid annual plant communities. *Ecology Letters*, *14*(12), 1227–1235. https://doi.org/10.1111/j.1461-0248.2011.01693.x

Jones, K. R., Venter, O., Fuller, R. A., Allan, J. R., Maxwell, S. L., Negret, P. J., & Watson, J. E. M. (2018). One-third of global protected land is under intense human pressure. *Science (New York, N.Y.)*, *360*(6390), 788–791. https://doi.org/10.1126/science.aap9565

Jones, K. R., Watson, J. E. M., Possingham, H. P., & Klein, C. J. (2016). Incorporating climate change into spatial conservation prioritisation. *Biological Conservation*, *194*, 121–130. https://doi.org/10.1016/j.biocon.2015.12.008

Joppa, L. N., & Pfaff, A. (2009). High and Far: Biases in the Location of Protected Areas. *PLoS ONE*, *4*(12), e8273. https://doi.org/10.1371/journal.pone.0008273

Kalvová, J., Halenka, T., Bezpalcová, K., & Nemešová, I. (2003). Köppen Climate Types in Observed and Simulated Climates. *Studia Geophysica et Geodaetica*, *47*(1), 185–202. https://doi.org/10.1023/A:1022263908716

Karger, D. N., Conrad, O., Böhner, J., Kawohl, T., Kreft, H., Soria-Auza, R. W., Zimmermann, N. E., Linder, H. P., & Kessler, M. (2017). Climatologies at high resolution for the earth's land surface areas. *Scientific Data*, *4*, 170122. https://doi.org/10.1038/sdata.2017.122

Kattge, J., Díaz, S., Lavorel, S., Prentice, I. C., Leadley, P., Bönisch, G., Garnier, E., Westoby, M., Reich, P. B., Wright, I. J., Cornelissen, J. H. C., Violle, C., Harrison, S. P., Van BODEGOM, P. M., Reichstein, M., Enquist, B. J., Soudzilovskaia, N. A., Ackerly, D. D., Anand, M., … Wirth, C. (2011). TRY - a global database of plant traits: TRY - A GLOBAL DATABASE OF PLANT TRAITS. *Global Change Biology*, *17*(9), 2905–2935. https://doi.org/10.1111/j.1365-2486.2011.02451.x

Kim, K., Park, J., Baik, J., & Choi, M. (2017). Evaluation of topographical and seasonal feature using GPM IMERG and TRMM 3B42 over Far-East Asia. *Atmospheric Research*, *187*, 95–105. https://doi.org/10.1016/j.atmosres.2016.12.007

Kissling, W. D., Dalby, L., Fløjgaard, C., Lenoir, J., Sandel, B., Sandom, C., Trøjelsgaard, K., & Svenning, J. (2014). Establishing macroecological trait datasets: Digitalization, extrapolation, and validation of diet preferences in terrestrial mammals worldwide. *Ecology and Evolution*, *4*(14), 2913–2930. https://doi.org/10.1002/ece3.1136

Kleidon, A., Fraedrich, K., & Heimann, M. (2000). A Green Planet Versus a Desert World: Estimating the Maximum Effect of Vegetation on the Land Surface Climate. *Climatic Change*, *44*(4), 471–493. https://doi.org/10.1023/A:1005559518889

Köppen, W. P. (1923). *Die klimate der erde*. Walter de Gruyter.

Köppen, W. P. (1931). *Grundriss der klimakunde*.

Köppen, W. P. (1936). *Das geographische System der Klimate*. Borntraeger.

Kottek, M., Grieser, J., Beck, C., Rudolf, B., & Rubel, F. (2006). World Map of the Köppen-Geiger climate classification updated. *Meteorologische Zeitschrift*, *15*(3), 259–263. https://doi.org/10.1127/0941-2948/2006/0130

Kreft, H., & Jetz, W. (2007). Global patterns and determinants of vascular plant diversity. *Proceedings of the National Academy of Sciences*, *104*(14), 5925–5930. https://doi.org/10.1073/pnas.0608361104

Kriticos, D. J., Webber, B. L., Leriche, A., Ota, N., Macadam, I., Bathols, J., & Scott, J. K. (2012). CliMond: Global high-resolution historical and future scenario climate surfaces for bioclimatic modelling. *Methods in Ecology and Evolution*, *3*(1), 53–64. https://doi.org/10.1111/j.2041-210X.2011.00134.x

Larson, P. R., & Lohrengel, C. F. (2011). A New Tool for Climatic Analysis Using the Köppen Climate Classification. *Journal of Geography*, *110*(3), 120–130. https://doi.org/10.1080/00221341.2011.537672

Lawler, J. J., Ackerly, D. D., Albano, C. M., Anderson, M. G., Dobrowski, S. Z., Gill, J. L., Heller, N. E., Pressey, R. L., Sanderson, E. W., & Weiss, S. B. (2015). The theory behind, and the challenges of, conserving nature's stage in a time of rapid change: Conserving Nature's Stage in a Time of Rapid Change. *Conservation Biology*, *29*(3), 618–629. https://doi.org/10.1111/cobi.12505

Le Saout, S., Hoffmann, M., Shi, Y., Hughes, A., Bernard, C., Brooks, T. M., Bertzky, B., Butchart, S. H. M., Stuart, S. N., Badman, T., & Rodrigues, A. S. L. (2013). Conservation. Protected areas and effective biodiversity conservation. *Science (New York, N.Y.)*, *342*(6160), 803–805. https://doi.org/10.1126/science.1239268

Leemans, R., Cramer, W., & van Minnen, J. G. (1996). Prediction of global biome distribution using bioclimatic equilibrium models. *SCOPE-SCIENTIFIC COMMITTEE ON PROBLEMS OF THE ENVIRONMENT INTERNATIONAL COUNCIL OF SCIENTIFIC UNIONS*, *56*, 413–440.

Lenoir, J., Bertrand, R., Comte, L., Bourgeaud, L., Hattab, T., Murienne, J., & Grenouillet, G. (2020). Species better track climate warming in the oceans than on land. *Nature Ecology & Evolution*, *4*(8), 1044–1059. https://doi.org/10.1038/s41559-020-1198-2

Lenoir, J., Hattab, T., & Pierre, G. (2017). Climatic microrefugia under anthropogenic climate change. *Ecography*, *40*(2), 253–266. https://doi.org/10.1111/ecog.02788

Loarie, S. R., Duffy, P. B., Hamilton, H., Asner, G. P., Field, C. B., & Ackerly, D. D. (2009). The velocity of climate change. *Nature*, *462*(7276), 1052–1055. https://doi.org/10.1038/nature08649

Lohmann, U., Sausen, R., Bengtsson, L., Cubasch, U., Perlwitz, J., & Roeckner, E. (1993). The Köppen climate classification as a diagnostic tool for general circulation models. *Climate Research*, *3*, 177–193. https://doi.org/10.3354/cr003177

Loucks, C., Ricketts, T. H., Naidoo, R., Lamoreux, J., & Hoekstra, J. (2008). Explaining the global pattern of protected area coverage: Relative importance of vertebrate biodiversity, human activities and agricultural suitability. *Journal of Biogeography*, *35*(8), 1337–1348. https://doi.org/10.1111/j.1365-2699.2008.01899.x

Luoto, M., Virkkala, R., & Heikkinen, R. K. (2007). The role of land cover in bioclimatic models depends on

spatial resolution. *Global Ecology and Biogeography*, *16*(1), 34–42. https://doi.org/10.1111/j.1466-8238.2006.00262.x

Mahlstein, I., Daniel, J. S., & Solomon, S. (2013). Pace of shifts in climate regions increases with global temperature. *Nature Climate Change*, *3*(8), 739–743. https://doi.org/10.1038/nclimate1876

Mahlstein, I., & Knutti, R. (2010). Regional climate change patterns identified by cluster analysis. *Climate Dynamics*, *35*(4), 587–600. https://doi.org/10.1007/s00382-009-0654-0

Manabe, S., & Holloway, J. L. (1975). The seasonal variation of the hydrologic cycle as simulated by a global model of the atmosphere. *Journal of Geophysical Research*, *80*(12), 1617–1649. https://doi.org/10.1029/JC080i012p01617

McGuire, J. L., Lawler, J. J., McRae, B. H., Nuñez, T. A., & Theobald, D. M. (2016). Achieving climate connectivity in a fragmented landscape. *Proceedings of the National Academy of Sciences of the United States of America*, *113*(26), 7195–7200. https://doi.org/10.1073/pnas.1602817113

Menne, M. J., Durre, I., Vose, R. S., Gleason, B. E., & Houston, T. G. (2012). *An Overview of the Global Historical Climatology Network-Daily Database*. https://doi.org/10.1175/jtech-d-11-00103.1

Merilä, J., & Hendry, A. P. (2014). Climate change, adaptation, and phenotypic plasticity: The problem and the evidence. *Evolutionary Applications*, *7*(1), 1–14. https://doi.org/10.1111/eva.12137

Metzger, M. J., Bunce, R. G. H., Jongman, R. H. G., Sayre, R., Trabucco, A., Zomer, R., & Sykes, M. (2013). A high-resolution bioclimate map of the world. *Global Ecology and Biogeography*, *22*(5), 630–638. https://doi.org/10.1111/geb.12022

Miró, J. J., Caselles, V., & Estrela, M. J. (2017). Multiple imputation of rainfall missing data in the Iberian Mediterranean context. *Atmospheric Research*, *197*, 313–330. https://doi.org/10.1016/j.atmosres.2017.07.016

Mitchell, T. D., Carter, T. R., Jones, P., & Hulme, M. (2004). A Comprehensive Set of High-Resolution Grids of Monthly Climate for Europe and the Globe. *Tyndall Centre Working Paper*, *55*.

Mitchell, T. D., & Jones, P. D. (2005). An improved method of constructing a database of monthly climate observations and associated high-resolution grids. *International Journal of Climatology*, *25*(6), 693–712. https://doi.org/10.1002/joc.1181

Myers, N., Mittermeier, R. A., Mittermeier, C. G., da Fonseca, G. A. B., & Kent, J. (2000). Biodiversity hotspots for conservation priorities. *Nature*, *403*(6772), 853–858. https://doi.org/10.1038/35002501

National Climatic Data Center, NESDIS, NOAA, & U.S. Department of Commerce. (2015). *Global Surface Summary of the Day—GSOD*. https://data.nodc.noaa.gov/cgi-bin/iso?id=gov.noaa.ncdc:C00516#

Navarro-Racines, C., Tarapues, J., Thornton, P., Jarvis, A., & Ramirez-Villegas, J. (2020). High-resolution and bias-corrected CMIP5 projections for climate change impact assessments. *Scientific Data*, *7*(1), 7. https://doi.org/10.1038/s41597-019-0343-8

Netzel, P., & Stepinski, T. (2016). On Using a Clustering Approach for Global Climate Classification. *Journal of Climate*, *29*(9), 3387–3401. https://doi.org/10.1175/JCLI-D-15-0640.1

New, M., Hulme, M., & Jones, P. (2000). Representing Twentieth-Century Space–Time Climate Variability. Part II. *Journal of Climate*, *13*(13), 2217–2238. https://doi.org/10.1175/1520-0442(2000)013<2217:RTCSTC>2.0.CO;2

Newbold, T., Hudson, L. N., Hill, S. L. L., Contu, S., Lysenko, I., Senior, R. A., Börger, L., Bennett, D. J., Choimes, A., Collen, B., Day, J., Palma, A., Díaz, S., Echeverria-Londoño, S., Edgar, M. J., Feldman, A., Garon, M., Harrison, M. L. K., Alhusseini, T., … Purvis, A. (2015). Global effects of land use on local terrestrial biodiversity. *Nature*, *520*(7545), 45–50. https://doi.org/10.1038/nature14324

OECD. (2019). *The post-2020 biodiversity framework: Targets, indicators and measurability implications at global and national level*.

Oliveira, B. F., São-Pedro, V. A., Santos-Barrera, G., Penone, C., & Costa, G. C. (2017). AmphiBIO, a global database for amphibian ecological traits. *Scientific Data*, *4*(1), 170123. https://doi.org/10.1038/sdata.2017.123

Ordonez, A., Martinuzzi, S., Radeloff, V. C., & Williams, J. W. (2014). Combined speeds of climate and land-use change of the conterminous US until 2050. *Nature Climate Change*, *4*(9), 811–816. https://doi.org/10.1038/nclimate2337

Ordonez, A., & Williams, J. W. (2013). Projected climate reshuffling based on multivariate climate-availability, climate-analog, and climate-velocity analyses. *Climatic Change*, *119*(3–4), 659–675. https://doi.org/10.1007/s10584-013-0752-1

Ouyang, Z., Zheng, H., Xiao, Y., Polasky, S., Liu, J., Xu, W., Wang, Q., Zhang, L., Xiao, Y., Rao, E., Jiang, L., Lu, F., Wang, X., Yang, G., Gong, S., Wu, B., Zeng, Y., Yang, W., & Daily, G. C. (2016). Improvements in ecosystem services from investments in natural capital. *Science*, *352*(6292), 1455–1459. https://doi.org/10.1126/science.aaf2295

Parks, S. A., Carroll, C., Dobrowski, S. Z., & Allred, B. W. (2020). Human land uses reduce climate connectivity across North America. *Global Change Biology*, *26*(5), 2944–2955. https://doi.org/10.1111/gcb.15009

Parmesan, C. (2006). Ecological and Evolutionary Responses to Recent Climate Change. *Annual Review of Ecology, Evolution, and Systematics*, *37*(1), 637–669. https://doi.org/10.1146/annurev.ecolsys.37.091305.110100

Parmesan, C., & Yohe, G. (2003). A globally coherent fingerprint of climate change impacts across natural systems. *Nature*, *421*(6918), 37–42. https://doi.org/10.1038/nature01286

Pearson, R. G., & Dawson, T. P. (2003). Predicting the impacts of climate change on the distribution of species. *Global Ecology and Biogeography*, *12*(5), 361–371. https://doi.org/10.1046/j.1466-822X.2003.00042.x

Pecl, G. T., Araújo, M. B., Bell, J. D., Blanchard, J., Bonebrake, T. C., Chen, I.-C., Clark, T. D., Colwell, R. K., Danielsen, F., Evengård, B., Falconi, L., Ferrier, S., Frusher, S., Garcia, R. A., Griffis, R. B., Hobday, A. J., Janion-Scheepers, C., Jarzyna, M. A., Jennings, S., … Williams, S. E. (2017). Biodiversity redistribution under climate change. *Science (New York, N.Y.)*, *355*(6332). https://doi.org/10.1126/science.aai9214

Peel, M. C., Finlayson, B. L., & McMahon, T. A. (2007). Updated world map of the Köppen-Geiger climate classification. *Hydrology and Earth System Sciences*, *11*(5), 1633–1644. https://doi.org/10.5194/hess-11-1633-2007

Peel, M. C., McMahon, T. A., Finlayson, B. L., & Watson, F. G. R. (2001). Identification and explanation of continental differences in the variability of annual runoff. *Journal of Hydrology*, *250*(1–4), 224–240. https://doi.org/10.1016/S0022-1694(01)00438-3

Peña-Angulo, D., Trigo, R. M., Cortesi, N., & González-Hidalgo, J. C. (2016). The influence of weather types on the monthly average maximum and minimum temperatures in the Iberian Peninsula. *Atmospheric Research*, *178–179*, 217–230. https://doi.org/10.1016/j.atmosres.2016.03.022

Peterson, T. C., & Vose, R. S. (1997). An Overview of the Global Historical Climatology Network Temperature Database. *Bulletin of the American Meteorological Society*, *78*(12), 2837–2849. https://doi.org/10.1175/1520-0477(1997)078<2837:AOOTGH>2.0.CO;2

Phillips, T. J., & Bonfils, C. J. W. (2015). Köppen bioclimatic evaluation of CMIP historical climate simulations. *Environmental Research Letters*, *10*(6), 064005. https://doi.org/10.1088/1748-9326/10/6/064005

Pinsky, M. L., Worm, B., Fogarty, M. J., Sarmiento, J. L., & Levin, S. A. (2013). Marine taxa track local climate velocities. *Science (New York, N.Y.)*, *341*(6151), 1239–1242. https://doi.org/10.1126/science.1239352

Poulter, B., Ciais, P., Hodson, E., Lischke, H., Maignan, F., Plummer, S., & Zimmermann, N. E. (2011). Plant functional type mapping for earth system models. *Geoscientific Model Development*, *4*(4), 993–1010. https://doi.org/10.5194/gmd-4-993-2011

Roderfeld, H., Blyth, E., Dankers, R., Huse, G., Slagstad, D., Ellingsen, I., Wolf, A., & Lange, M. A. (2008). Potential impact of climate change on ecosystems of the Barents Sea Region. *Climatic Change*, *87*(1–2), 283–303. https://doi.org/10.1007/s10584-007-9350-4

Rohli, R. V., Andrew, J. T., Reynolds, S. J., Shaw, C., & Vázquez, J. R. (2015). Globally Extended Köppen–Geiger climate classification and temporal shifts in terrestrial climatic types. *Physical Geography*, *36*(2), 142–157. https://doi.org/10.1080/02723646.2015.1016382

Rohli, R. V., Joyner, T. A., Reynolds, S. J., & Ballinger, T. J. (2015). Overlap of global Köppen–Geiger climates, biomes, and soil orders. *Physical Geography*, *36*(2), 158–175. https://doi.org/10.1080/02723646.2015.1016384

Rubel, F., Brugger, K., Haslinger, K., & Auer, I. (2017). The climate of the European Alps. *Meteorologische Zeitschrift*, *26*(2), 115–125. https://doi.org/10.1127/metz/2016/0816

Rubel, F., & Kottek, M. (2010). Observed and projected climate shifts 1901-2100 depicted by world maps of the Köppen-Geiger climate classification. *Meteorologische Zeitschrift*, *19*(2), 135–141. https://doi.org/10.1127/0941-2948/2010/0430

Rubel, F., & Kottek, M. (2011). Comments on. *Meteorologische Zeitschrift*, *20*(3), 361–365. https://doi.org/10.1127/0941-2948/2011/0285

Sanderson, M. (1999). The Classification of Climates from Pythagoras to Koeppen. *Bulletin of the American Meteorological Society*, *80*(4), 669–673. https://doi.org/10.1175/1520-0477(1999)080<0669:TCOCFP>2.0.CO;2

Scheffers, B. R., Meester, L., Bridge, T. C. L., Hoffmann, A. A., Pandolfi, J. M., Corlett, R. T., Butchart, S. H. M., Pearce-Kelly, P., Kovacs, K. M., Dudgeon, D., Pacifici, M., Rondinini, C., Foden, W. B., Martin, T. G., Mora, C., Bickford, D., & Watson, J. E. M. (2016). The broad footprint of climate change from genes to biomes to people. *Science (New York, N.Y.)*, *354*(6313). https://doi.org/10.1126/science.aaf7671

Schloss, C. A., Nuñez, T. A., & Lawler, J. J. (2012). Dispersal will limit ability of mammals to track climate change in the Western Hemisphere. *Proceedings of the National Academy of Sciences*, *109*(22), 8606–

8611. https://doi.org/10.1073/pnas.1116791109

Schwalm, C. R., Glendon, S., & Duffy, P. B. (2020). RCP8.5 tracks cumulative CO2 emissions. *Proceedings of the National Academy of Sciences of the United States of America*, *117*(33), 19656–19657. https://doi.org/10.1073/pnas.2007117117

Serra, C., Martínez, M. D., Lana, X., & Burgueño, A. (2014). European dry spell regimes (1951–2000). *Atmospheric Research*, *144*, 151–174. https://doi.org/10.1016/j.atmosres.2013.05.022

Sharifi, E., Steinacker, R., & Saghafian, B. (2018). Multi time-scale evaluation of high-resolution satellite-based precipitation products over northeast of Austria. *Atmospheric Research*, *206*, 46–63. https://doi.org/10.1016/j.atmosres.2018.02.020

Stooksbury, D. E., & Michaels, P. J. (1991). Cluster analysis of Southeastern U.S. climate stations. *Theoretical and Applied Climatology*, *44*(3–4), 143–150. https://doi.org/10.1007/BF00868169

Sun, Q., Miao, C., Duan, Q., Ashouri, H., Sorooshian, S., & Hsu, K.-L. (2018). A Review of Global Precipitation Data Sets. *Reviews of Geophysics*, *56*(1), 79–107. https://doi.org/10.1002/2017RG000574

Tang, L., & Hossain, F. (2012). Investigating the similarity of satellite rainfall error metrics as a function of Köppen climate classification. *Atmospheric Research*, *104–105*, 182–192. https://doi.org/10.1016/j.atmosres.2011.10.006

Tapiador, F. J., Moreno, R., & Navarro, A. (2019). Consensus in climate classifications for present climate and global warming scenarios. *Atmospheric Research*, *216*, 26–36. https://doi.org/10.1016/j.atmosres.2018.09.017

Tarkan, A. S., & Vilizzi, L. (2015). Patterns, latitudinal clines and countergradient variation in the growth of roach Rutilus rutilus (Cyprinidae) in its Eurasian area of distribution. *Reviews in Fish Biology and Fisheries*, *25*(4), 587–602. https://doi.org/10.1007/s11160-015-9398-6

Taylor, K. E., Stouffer, R. J., & Meehl, G. A. (2012). An Overview of CMIP5 and the Experiment Design. *Bulletin of the American Meteorological Society*, *93*(4), 485–498. https://doi.org/10.1175/BAMS-D-11-00094.1

Tererai, F., & Wood, A. R. (2014). On the present and potential distribution of Ageratina adenophora (Asteraceae) in South Africa. *South African Journal of Botany*, *95*, 152–158. https://doi.org/10.1016/j.sajb.2014.09.001

Thornthwaite, C. W. (1931). The Climates of North America. *Geographical Review*, *21*(4), 633. https://doi.org/10.2307/209372

Thuiller, W., Lavorel, S., Araújo, M. B., Sykes, M. T., & Prentice, I. C. (2005). Climate change threats to plant diversity in Europe. *Proceedings of the National Academy of Sciences of the United States of America*, *102*(23), 8245–8250. https://doi.org/10.1073/pnas.0409902102

Tingley, M. W., Darling, E. S., & Wilcove, D. S. (2014). Fine- and coarse-filter conservation strategies in a time of climate change. *Annals of the New York Academy of Sciences*, *1322*, 92–109. https://doi.org/10.1111/nyas.12484

Trewartha, G. T. (1954). *An introduction to climate*. McGRAW-HILL BOOK COMPANY, INC. NEW YORK TORONTO LONDON.

Unal, Y., Kindap, T., & Karaca, M. (2003). Redefining the climate zones of Turkey using cluster analysis.

International Journal of Climatology, *23*(9), 1045–1055. https://doi.org/10.1002/joc.910

UNEP-WCMC and IUCN. (2021). *Protected Planet: The World Database on Protected Areas (WDPA)/The Global Database on Protected Areas Management Effectiveness (GD-PAME)*. www.protectedplanet.net

van Vuuren, D. P., Edmonds, J., Kainuma, M., Riahi, K., Thomson, A., Hibbard, K., Hurtt, G. C., Kram, T., Krey, V., Lamarque, J.-F., Masui, T., Meinshausen, M., Nakicenovic, N., Smith, S. J., & Rose, S. K. (2011). The representative concentration pathways: An overview. *Climatic Change*, *109*(1–2), 5–31. https://doi.org/10.1007/s10584-011-0148-z

Venter, O. (2014). Corridors of carbon and biodiversity. *Nature Climate Change*, *4*(2), 91–92. https://doi.org/10.1038/nclimate2115

Venter, O., Magrach, A., Outram, N., Klein, C. J., Possingham, H. P., Di Marco, M., & Watson, J. E. M. (2018). Bias in protected-area location and its effects on long-term aspirations of biodiversity conventions: Protected Areas Missing Biodiversity. *Conservation Biology*, *32*(1), 127–134. https://doi.org/10.1111/cobi.12970

Venter, O., Sanderson, E. W., Magrach, A., Allan, J. R., Beher, J., Jones, K. R., Possingham, H. P., Laurance, W. F., Wood, P., Fekete, B. M., Levy, M. A., & Watson, J. E. M. (2016). Global terrestrial Human Footprint maps for 1993 and 2009. *Scientific Data*, *3*, 160067. https://doi.org/10.1038/sdata.2016.67

Virkkala, R., Heikkinen, R. K., Fronzek, S., Kujala, H., & Leikola, N. (2013). Does the protected area network preserve bird species of conservation concern in a rapidly changing climate? *Biodiversity and Conservation*, *22*(2), 459–482. https://doi.org/10.1007/s10531-012-0423-y

Visconti, P., Butchart, S. H. M., Brooks, T. M., Langhammer, P. F., Marnewick, D., Vergara, S., Yanosky, A., & Watson, J. E. M. (2019). Protected area targets post-2020. *Science (New York, N.Y.)*, *364*(6437), 239–241. https://doi.org/10.1126/science.aav6886

Walter, S. D., & Elwood, J. M. (1975). A test for seasonality of events with a variable population at risk. *Journal of Epidemiology & Community Health*, *29*(1), 18–21. https://doi.org/10.1136/jech.29.1.18

Wang, M., & Overland, J. E. (2004). Detecting Arctic Climate Change Using Kppen Climate Classification. *Climatic Change*, *67*(1), 43–62. https://doi.org/10.1007/s10584-004-4786-2

Ward, M., Saura, S., Williams, B., Ramírez-Delgado, J. P., Arafeh-Dalmau, N., Allan, J. R., Venter, O., Dubois, G., & Watson, J. E. M. (2020). Just ten percent of the global terrestrial protected area network is structurally connected via intact land. *Nature Communications*, *11*(1), 4563. https://doi.org/10.1038/s41467-020-18457-x

Watson, J. E. M., Dudley, N., Segan, D. B., & Hockings, M. (2014). The performance and potential of protected areas. *Nature*, *515*(7525), 67–73. https://doi.org/10.1038/nature13947

Watson, J. E. M., Evans, T., Venter, O., Williams, B., Tulloch, A., Stewart, C., Thompson, I., Ray, J. C., Murray, K., Salazar, A., McAlpine, C., Potapov, P., Walston, J., Robinson, J. G., Painter, M., Wilkie, D., Filardi, C., Laurance, W. F., Houghton, R. A., … Lindenmayer, D. (2018). The exceptional value of intact forest ecosystems. *Nature Ecology & Evolution*, *2*(4), 599–610. https://doi.org/10.1038/s41559-018-0490-x

Watson, J. E. M., Iwamura, T., & Butt, N. (2013). Mapping vulnerability and conservation adaptation strategies under climate change. *Nature Climate Change*, *3*(11), 989–994. https://doi.org/10.1038/nclimate2007

Watson, J., Keith, D., Strassburg, B., Venter, O., Williams, B., & Nicholson, E. (2022). *Set a global target for ecosystems*. *578*. https://media.nature.com/original/magazine-assets/d41586-020-00446-1/d41586-020-00446-1.pdf

Webber, B. L., Yates, C. J., Le Maitre, D. C., Scott, J. K., Kriticos, D. J., Ota, N., McNeill, A., Le Roux, J. J., & Midgley, G. F. (2011). Modelling horses for novel climate courses. *Diversity and Distributions*, *17*(5), 978–1000. https://doi.org/10.1111/j.1472-4642.2011.00811.x

Weigel, A. P., Liniger, M. A., & Appenzeller, C. (2008). Can multi-model combination really enhance the prediction skill of probabilistic ensemble forecasts? *Quarterly Journal of the Royal Meteorological Society*, *134*(630), 241–260. https://doi.org/10.1002/qj.210

Wen, G., Xiao, H., Yang, H., Bi, Y., & Xu, W. (2017). Characteristics of summer and winter precipitation over northern China. *Atmospheric Research*, *197*, 390–406. https://doi.org/10.1016/j.atmosres.2017.07.023

Wessely, J., Hülber, K., Gattringer, A., Kuttner, M., Moser, D., Rabitsch, W., Schindler, S., Dullinger, S., & Essl, F. (2017). Habitat-based conservation strategies cannot compensate for climate-change-induced range loss. *Nature Climate Change*, *7*(11), 823–827. https://doi.org/10.1038/nclimate3414

Williams, J. W., & Jackson, S. T. (2007). Novel climates, no-analog communities, and ecological surprises. *Frontiers in Ecology and the Environment*, *5*(9), 475–482. https://doi.org/10.1890/070037

Williams, J. W., Jackson, S. T., & Kutzbach, J. E. (2007). Projected distributions of novel and disappearing climates by 2100 AD. *Proceedings of the National Academy of Sciences of the United States of America*, *104*(14), 5738–5742. https://doi.org/10.1073/pnas.0606292104

Willmott, C. J., & Matsuura, K. (2001). *Terrestrial Air Temperature and Precipitation: Monthly and Annual Time Series (1950—1999)*. http://climate.geog.udel.edu/~climate/html_pages/README.ghcn_ts2.html.

Woodward, F. I., Lomas, M. R., & Kelly, C. K. (2004). Global climate and the distribution of plant biomes. *Philosophical Transactions of the Royal Society of London. Series B: Biological Sciences*, *359*(1450), 1465–1476. https://doi.org/10.1098/rstb.2004.1525

Wu, R., Zhang, S., Yu, D. W., Zhao, P., Li, X., Wang, L., Yu, Q., Ma, J., Chen, A., & Long, Y. (2011). Effectiveness of China's nature reserves in representing ecological diversity. *Frontiers in Ecology and the Environment*, *9*(7), 383–389. https://doi.org/10.1890/100093

Yoo, J., & Rohli, R. V. (2016). Global distribution of Köppen–Geiger climate types during the Last Glacial Maximum, Mid-Holocene, and present. *Palaeogeography, Palaeoclimatology, Palaeoecology*, *446*, 326–337. https://doi.org/10.1016/j.palaeo.2015.12.010

Zhang, X., Xiong, Z., Zhang, X., Shi, Y., Liu, J., Shao, Q., & Yan, X. (2016). Using multi-model ensembles to improve the simulated effects of land use/cover change on temperature. *Climate Dynamics*, *46*(3–4), 765–778. https://doi.org/10.1007/s00382-015-2611-4

Zhang, X., & Yan, X. (2014). Spatiotemporal change in geographical distribution of global climate types in the context of climate warming. *Climate Dynamics*, *43*(3–4), 595–605. https://doi.org/10.1007/s00382-013-2019-y

Zhang, X., Yan, X., & Chen, Z. (2017). Geographic distribution of global climate zones under future scenarios. *International Journal of Climatology*, *37*(12), 4327–4334. https://doi.org/10.1002/joc.5089

Zhou, G., & Wang, Y. (2000). Global change and climate-vegetation classification. *Chinese Science Bulletin*,

45(7), 577–585. https://doi.org/10.1007/BF02886031

Zscheischler, J., Mahecha, M. D., & Harmeling, S. (2012). Climate Classifications. *Procedia Computer Science*, *9*, 897–906. https://doi.org/10.1016/j.procs.2012.04.096